INTERNATIONAL IBERIAN
NANOTECHNOLOGY
LABORATORY

Microfabrication process of magnetic sensors based on magnetic tunnel junctions

E. Paz, T. Boehnert, M. Gonzalez Debs, R. Ferreira and P. Freitas

Elvira Paz

Nanoelectronics Engineering / Spintronics

www.inl.int

- **Intergovernmental Organization**

+300
Researchers

+100
Students

Multidisciplinary:

- Chemist
- Pharmaceutic
- Biologist
- Physicist
- Electronic
- Engineers

1000 m^2 Nanofabrication Clean Room

- A clean room environment is required in order to achieve **high yield and good reproducibilit**y of small scale devices

- Thin Film Deposition and Material Growth
- Optical and E-Beam Lithography
- Etching, Ashing, and Micromachining
- Metrology, Inspection and Wafer-Scale Device Testing
- Advanced Packaging, Annealing, and Back-End Processes

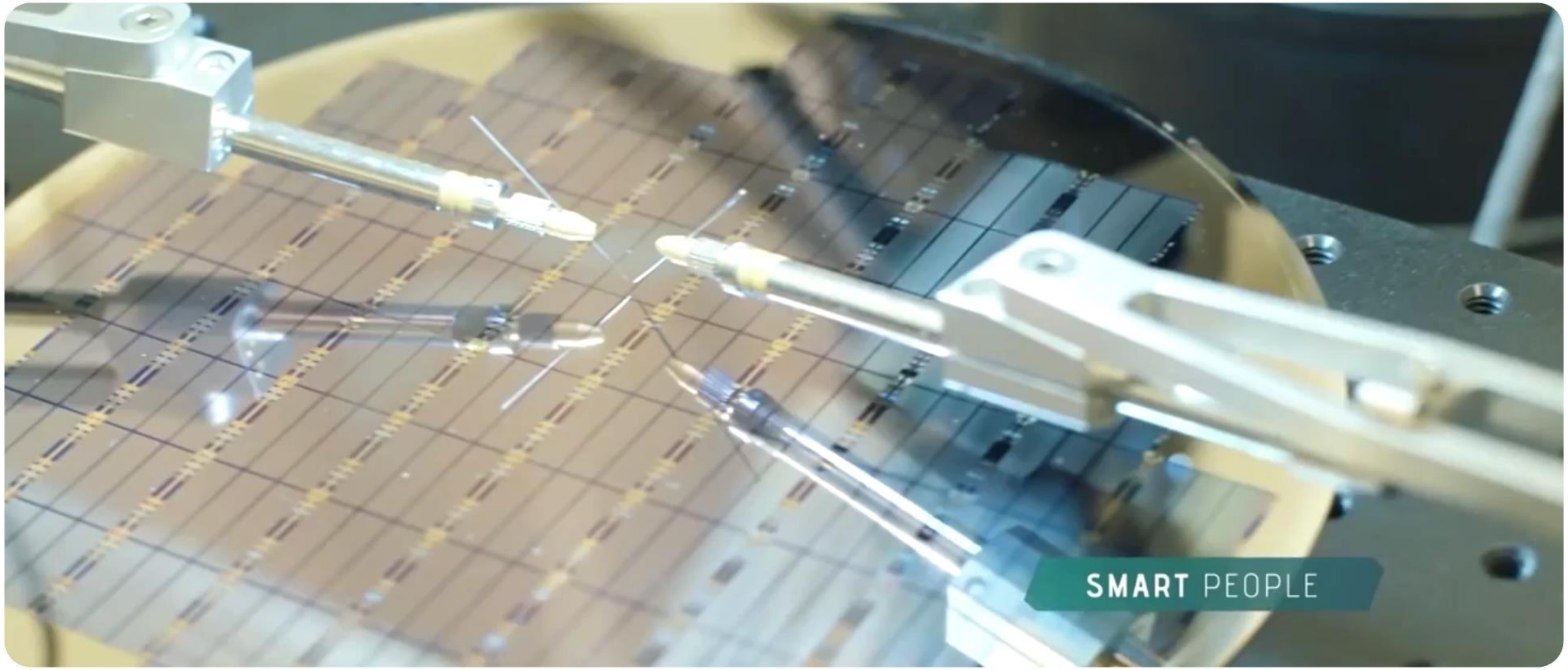

Outline

- Part I – Fabrication techniques
- Part II – Introduction to spintronics
- Part III – MTJ stack deposition and microfabrication
- Part IV – MTJ stack linearization
- Part V – Noise

Part I
Fabrication techniques

Thin Film Deposition and Material Growth

Deposition

- DC and RF magnetron sputtering
- Plasma Enhanced Chemical Vapour Deposition (PECVD)

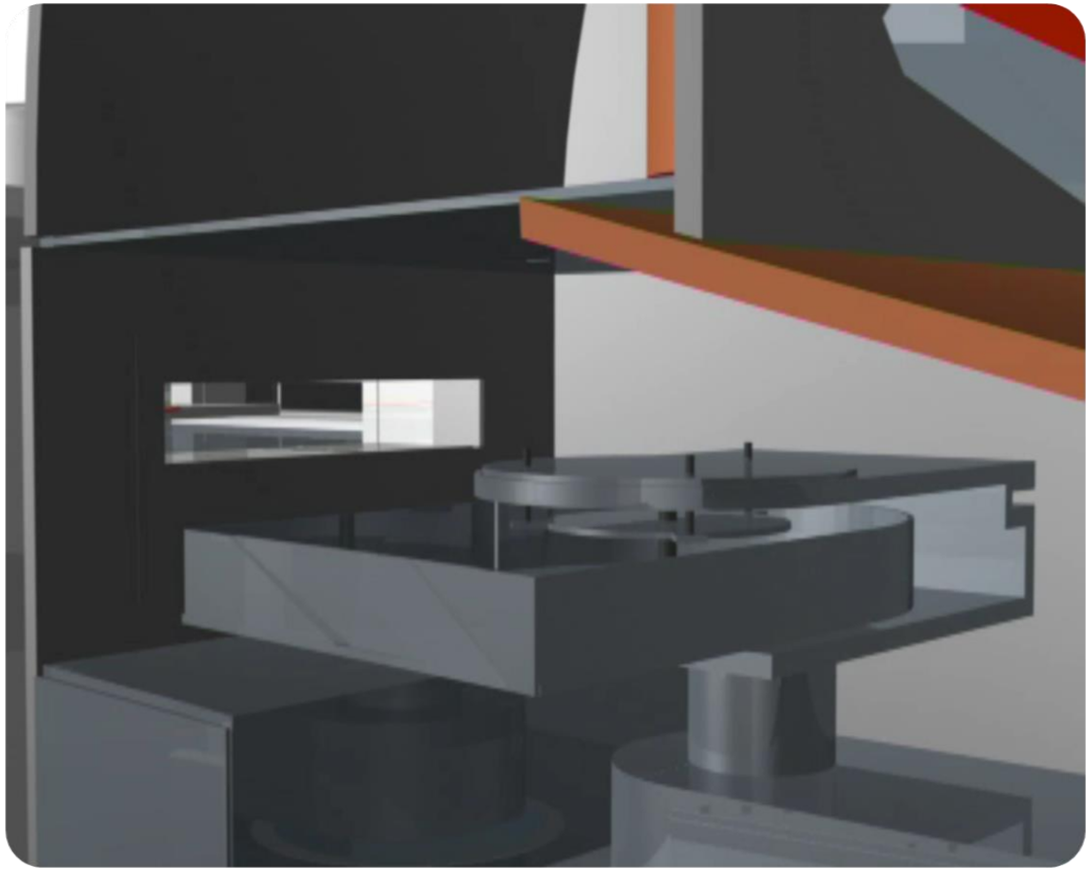

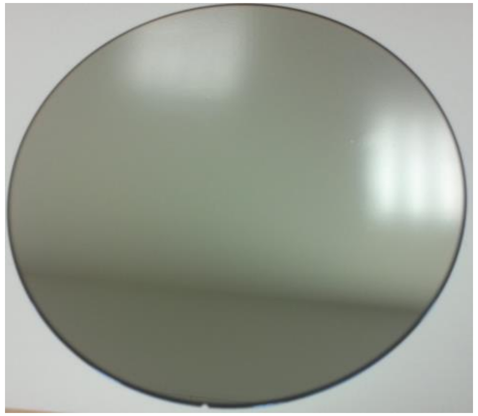

Cap	
Ru	7nm
Ta	10nm
IrMn	5.5 nm
Ru	0.5 nm
NiFe	16 nm
Ta	0.21nm
CoFeB	2.6nm
MgO	~ 1.2nm
CoFeB	2.6nm
Ru	0.85nm
CoFe	2.0nm
IrMn	20 nm
Ru	5nm
Ta	5nm
Ru	15nm
Ta	5nm
Ru	15nm
Ta	5nm

- Yellow filters to protect the resist of white light

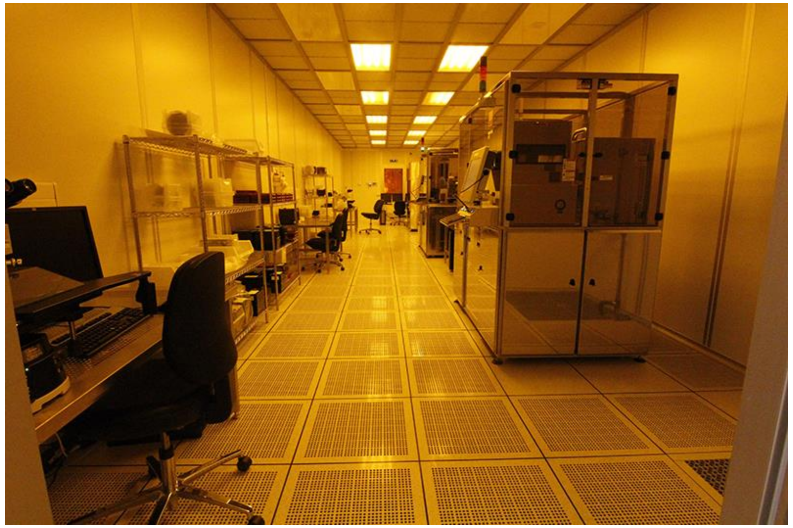

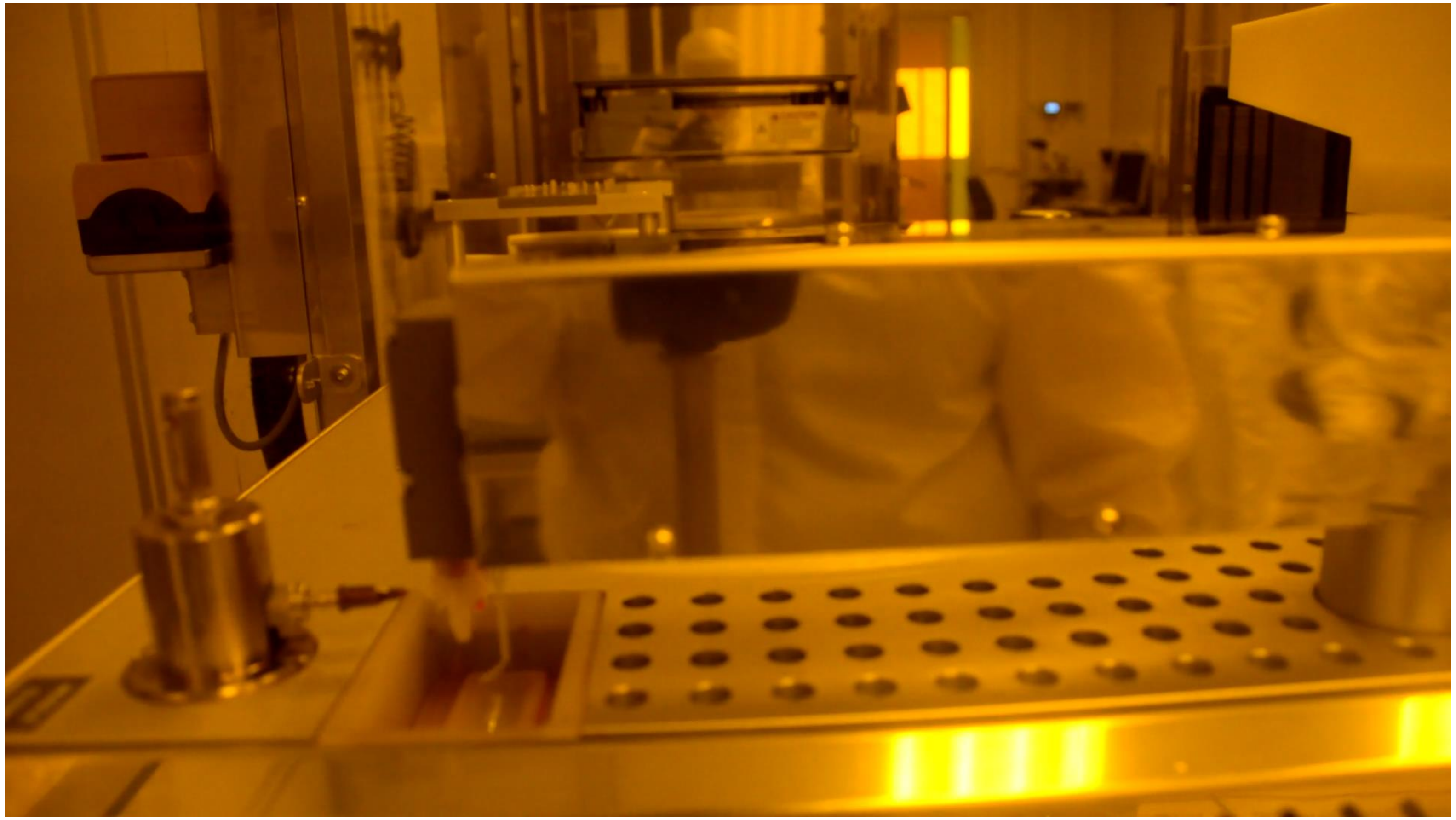

- Volume
- Rotation speed
- Number of rotations
- Temperature for curing

Lithography

Mask Aligner

- 6″ Mask aligner with mercury lamp

- Masks fabricated in the DWL
- Minimum feature size 3 μm

- 8″ Mask aligner with LED lamp

Lithography

Direct Laser Writer

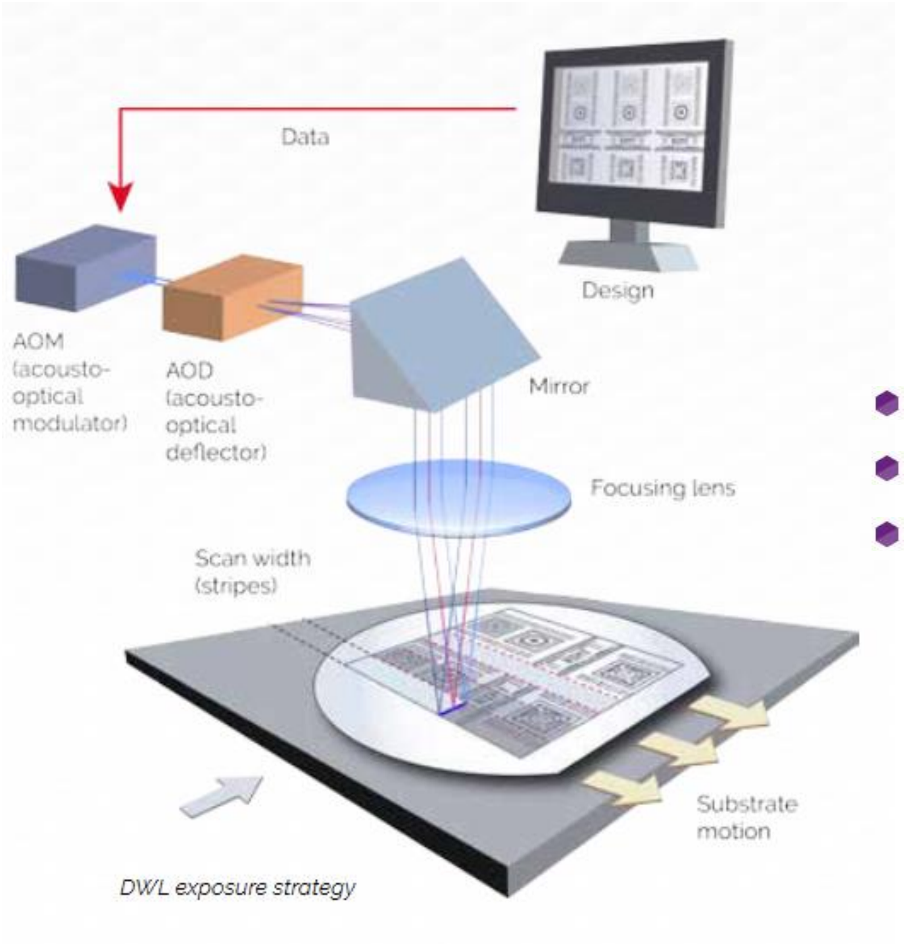

- Diode laser with 405 nm
- Minimum feature size 1 μm
- Grey scale

Lithography

Electron Beam

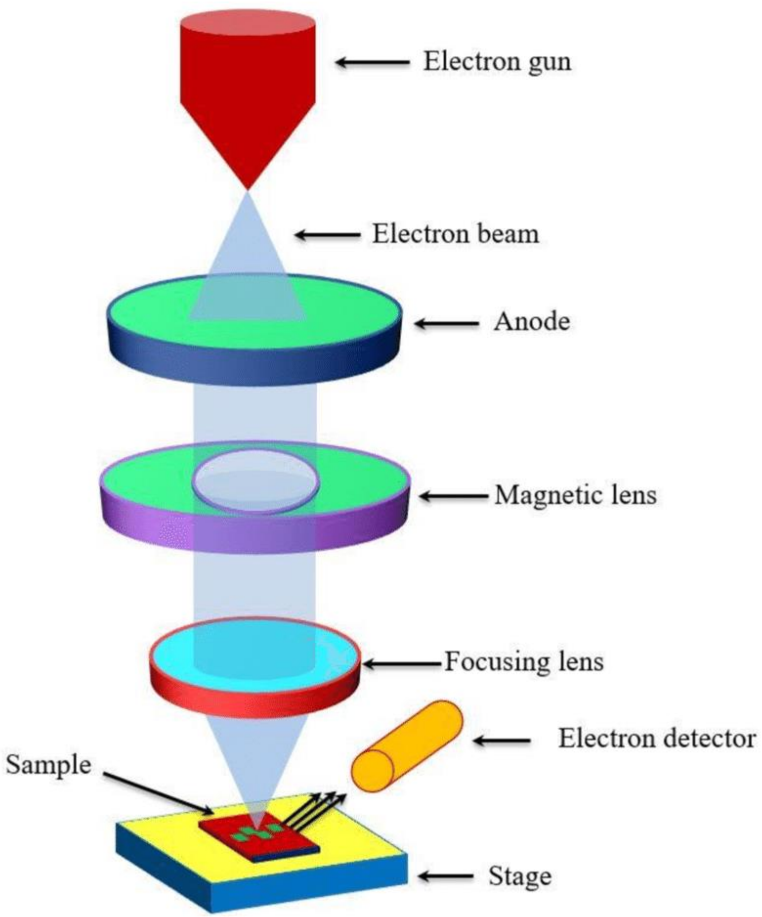

- 100 kV Electron Beam
- Minimum feature below 10 nm

Lithography

Develop

- Volume
- Rotation speed
- Time
- Post exposure bake

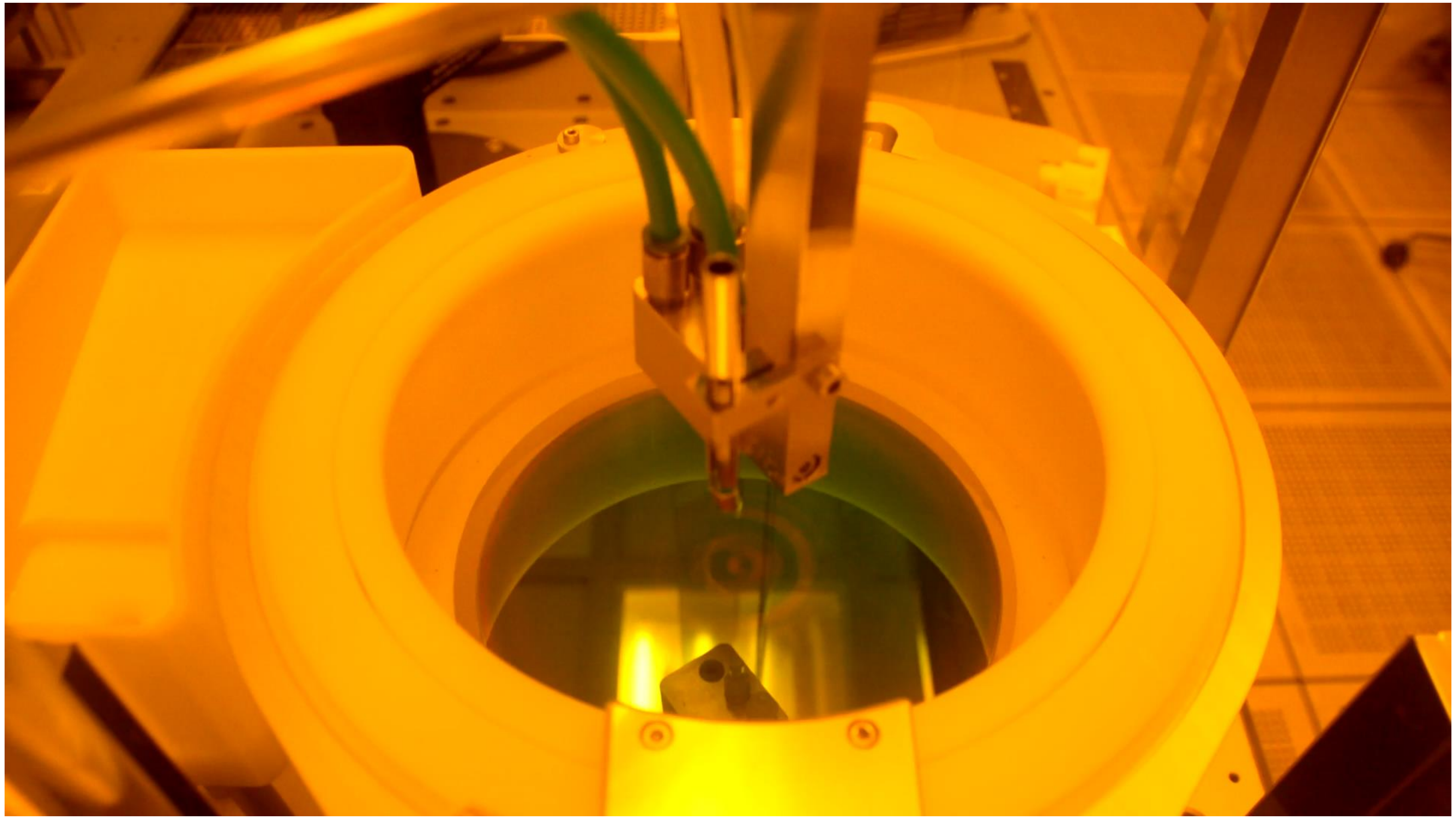

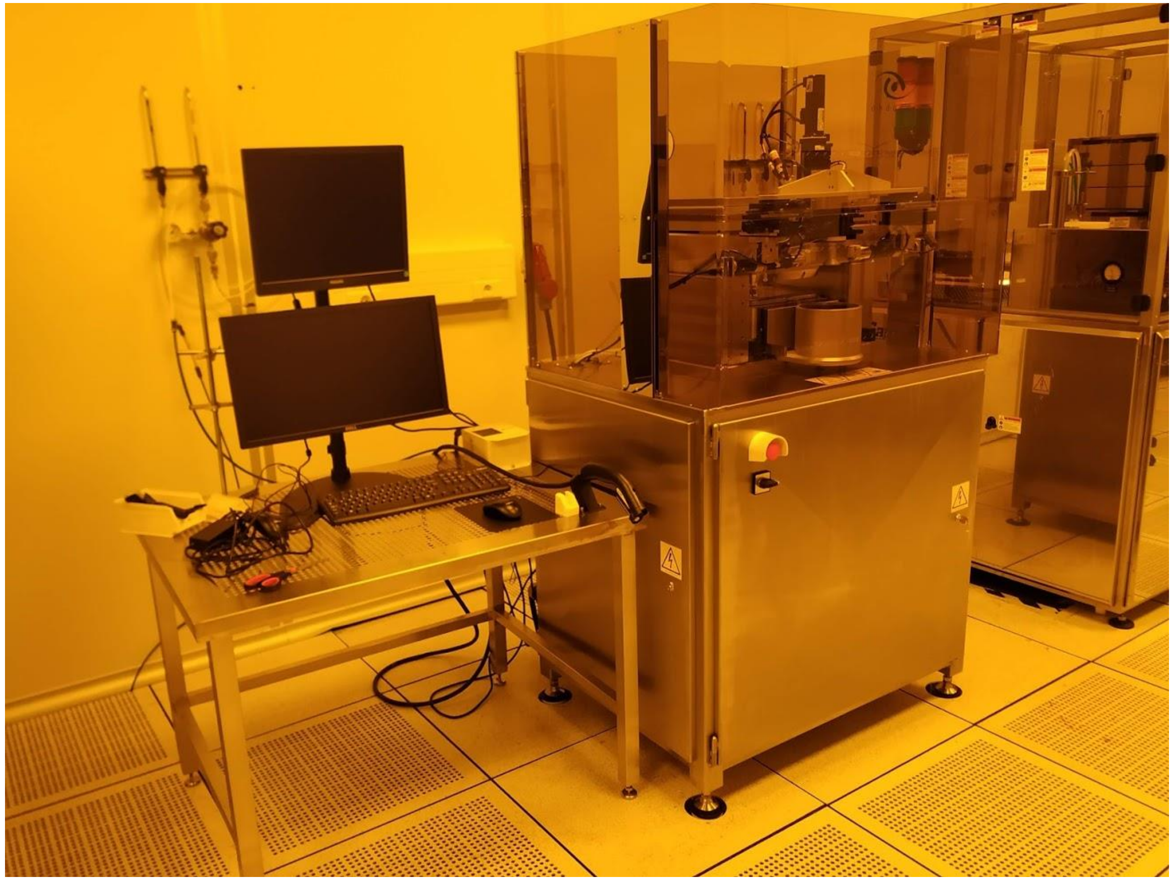

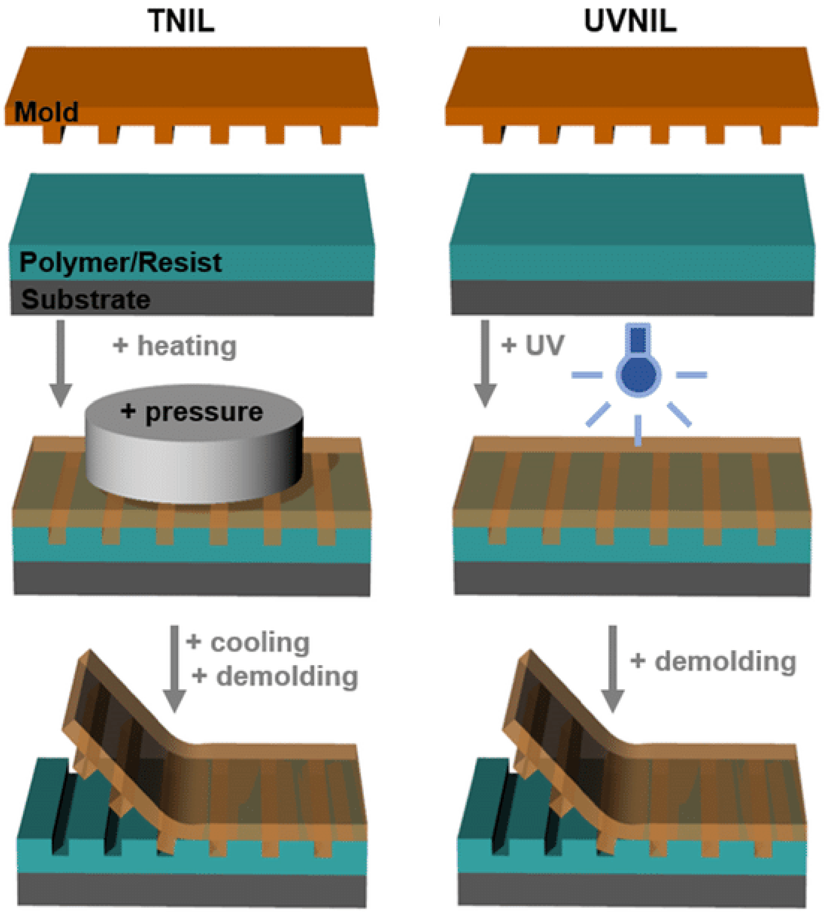

Molds review: Journal of Nanoscience **2016** 657129

Etching

Ion beam and Reactive etching

- **Ion beam etching**

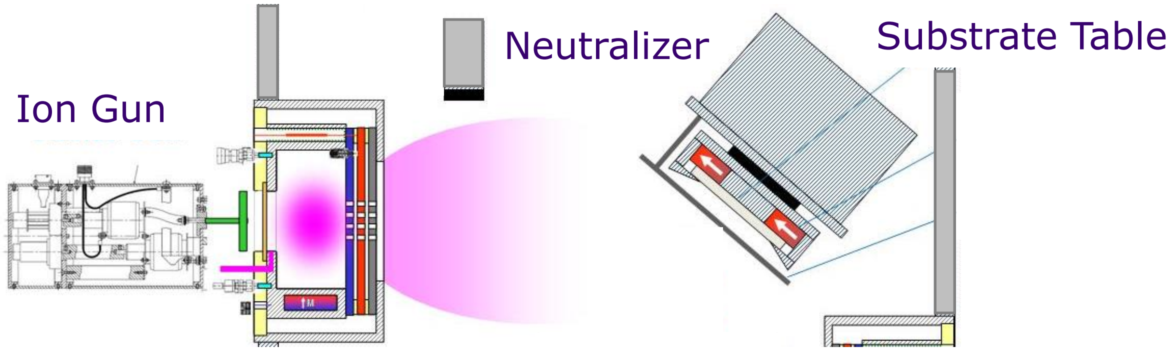

Secondary Ion Mass Spectroscopy (SIMS)

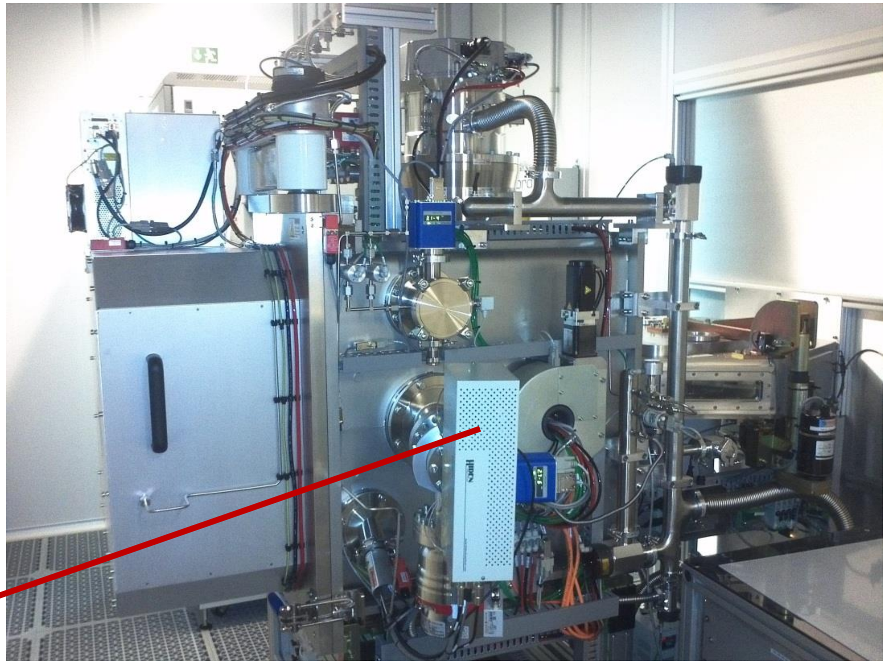

- **Reactive Ion Etching:**
  - anisotropic etching of silicon oxide, silicon nitride, polysilicon, and other materials such as amorphous Si, using a plasma source and fluorine chemistry
  - anisotropic etching of Si trenches with high aspect ratios and through wafer vias. For that, it uses a switched process by alternated cycles of SF6 plasma etching and C4F8 plasma for polymeric deposition.

Part II
Introduction to spintronics

Elvira Paz
www.inl.int

The Nobel Prize in Physics 2007

Albert Fert

Prize share: 1/2

Peter Grünberg

Prize share: 1/2

The Nobel Prize in Physics 2007 was awarded jointly to Albert Fert and Peter Grünberg "for the discovery of Giant Magnetoresistance."

Giant Magnetoresistance Effect

GMR – Physical origin

Antiparallel magnetizations

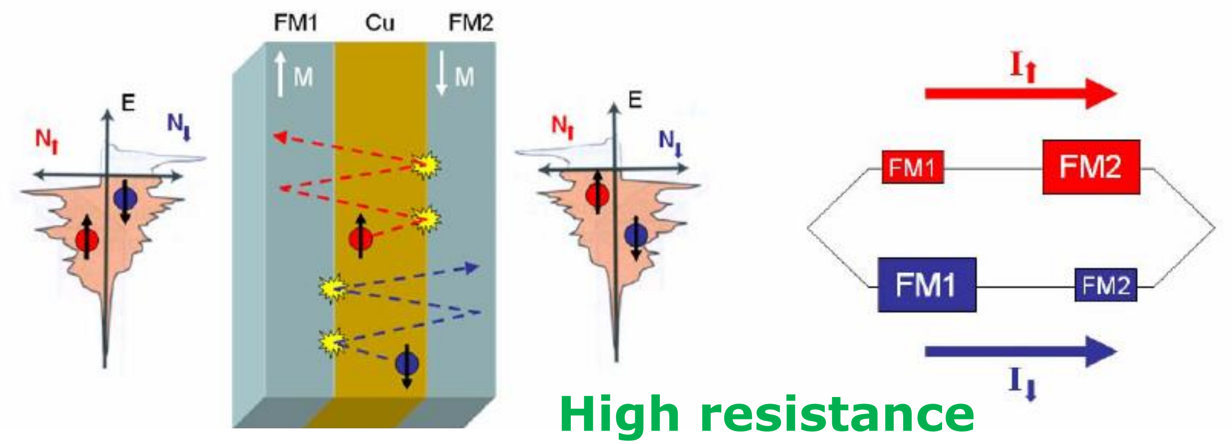

High resistance

Parallel magnetizations

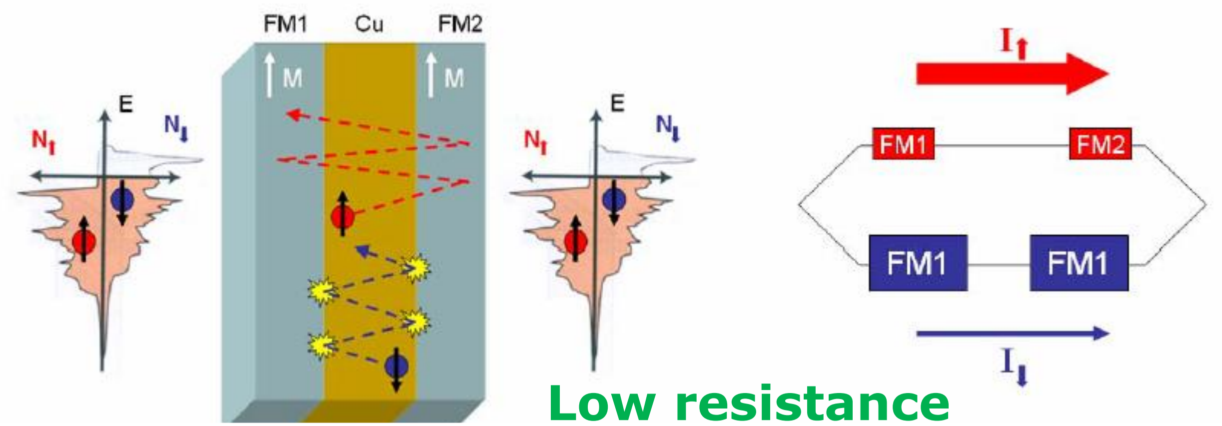

Low resistance

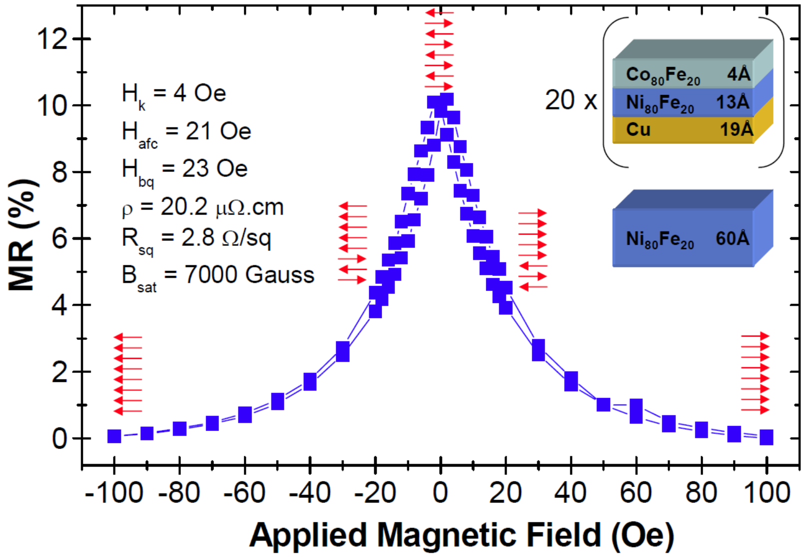

Julíère Model

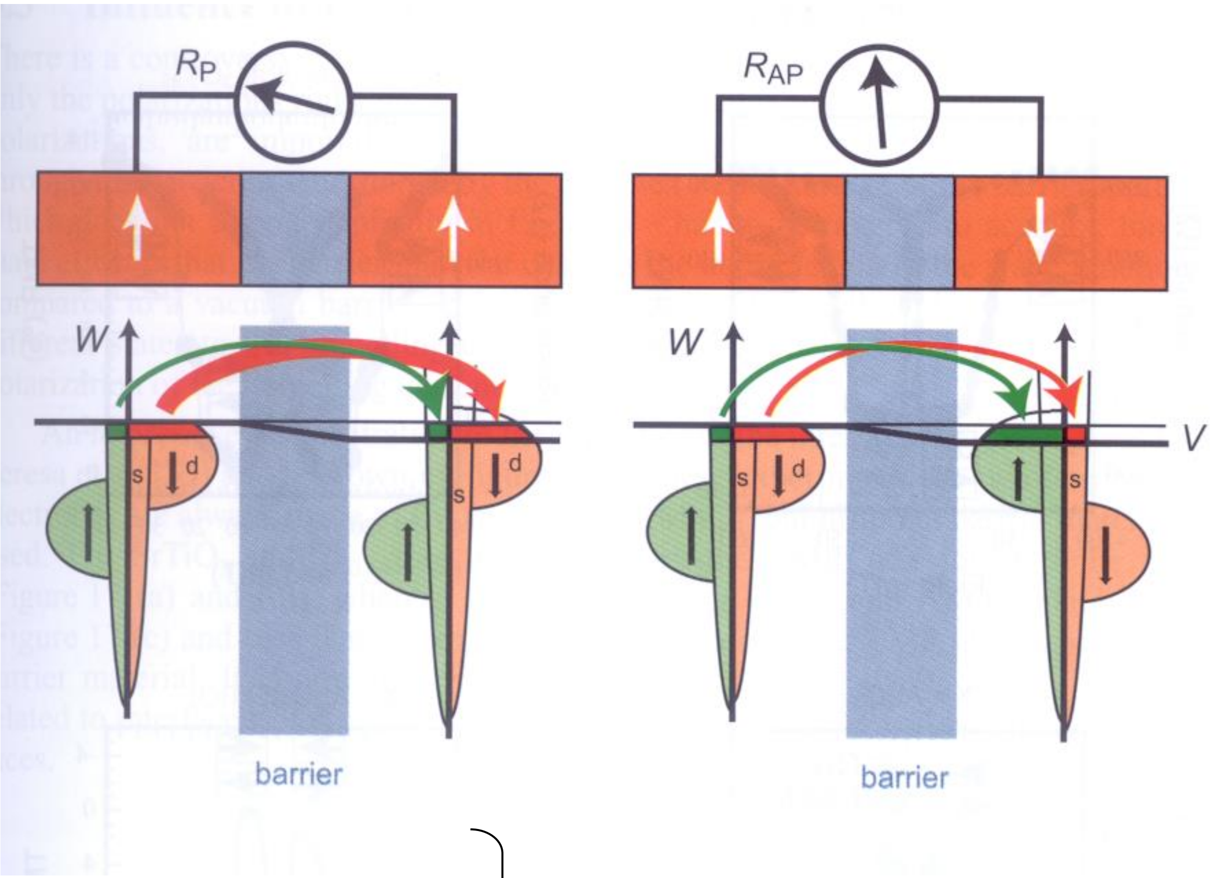

- Spin is conserved during tunneling
- Probability of Tunneling proportional to density of states product in initial and final ferromagnet

$$TMR = \frac{R_{AP} - R_P}{R_P} \text{ x } 100$$

Tunnelling Magnetoresistance Effect (TMR)

Coherent tunnelling effect

Amorphous Barrier

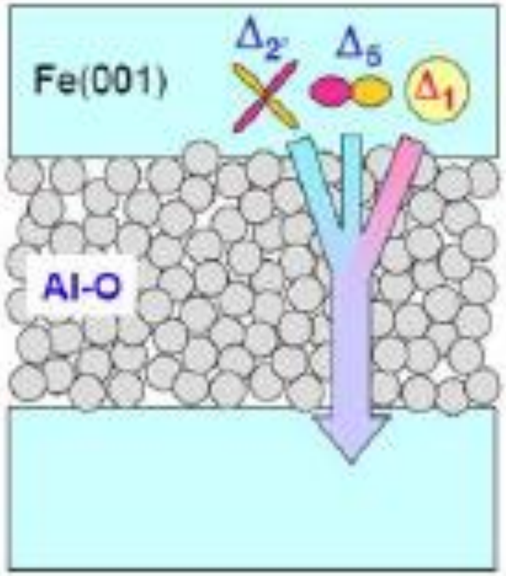

TMR<40%

Crystalline Barrier

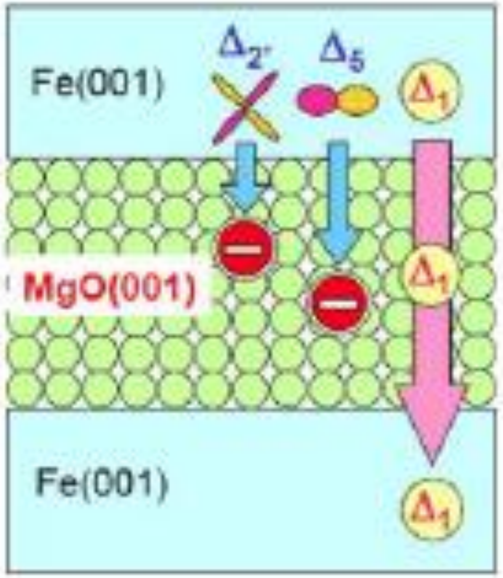

TMR>200%

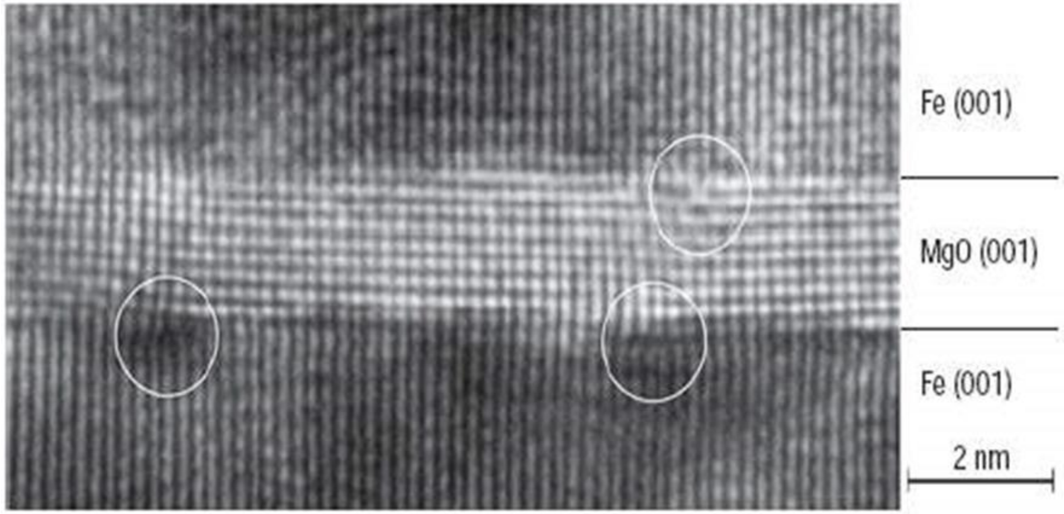

Yuasa et al, Fe/MgO/Fe
Nature Mat. 2005
$\Delta R/R = (R_{AP}-R_P)/ R_P \approx$ **200%** at RT

Magnetoresistive devices

Stack optimization

Magnetic Sensors

Cap	Ru	7nm
	CuN	50nm
	Ta	10nm
Free Layer	NiFe	16nm
	Ta	0.21nm
	CoFeB	2.6nm
Tunnel Barrier	MgO	~ 1nm
Reference Layer (SAF)	CoFeB	2.6nm
	Ru	0.85nm
	CoFe	2.0nm
Pinning Layer	IrMn	7.5nm
Buffer	Ru	5nm
	Ta	5nm
	CuN	50nm
	Ta	5nm
	CuN	50nm
	Ta	5nm

Ru	7nm
Ta	10nm
IrMn	5.5 nm
Ru	0.5 nm
NiFe	16 nm
Ta	0.21nm
CoFeB	2.6nm
MgO	~ 1.2nm
CoFeB	2.6nm
Ru	0.85nm
CoFe	2.0nm
IrMn	20 nm
Ru	5nm
Ta	5nm
Ru	15nm
Ta	5nm
Ru	15nm
Ta	5nm

Non-volatile Memory

Ru	7nm
CuN	150nm
Ta	10nm
CoFeB	2.2nm
MgO	~ 0.8nm
CoFeB	2.6nm
Ru	0.85nm
CoFe	2.0nm
IrMn	7.5nm
Ru	5nm
Ta	5nm
CuN	50nm
Ta	5nm
CuN	50nm
Ta	5nm

Spin Transfer Nano-Oscillator

Ru	7nm
CuN	30nm
Ta	10nm
IrMn	6.0nm
CoFe	2.0nm
Ru	0.85nm
CoFeB	2.6nm
MgO	~ 0.9nm
CoFeB	1.5nm
MgO	~ 0.8nm
CoFeB	2.6nm
Ru	0.85nm
CoFe	2.0nm
IrMn	20nm
Ru	5nm
Ta	5nm
CuN	50nm
Ta	5nm
CuN	50nm
Ta	5nm

Vortex

Ru	7nm
CuN	50nm
Ta	10nm
NiFe	6nm
Ta	0.21nm
CoFeB	2.6nm
MgO	~ 0.8nm
CoFeB	2.6nm
Ru	0.85nm
CoFe	2.0nm
IrMn	7.5nm
Ru	5nm
Ta	5nm
CuN	50nm
Ta	5nm
CuN	50nm
Ta	5nm

Ferromagnetism

Exchange interaction

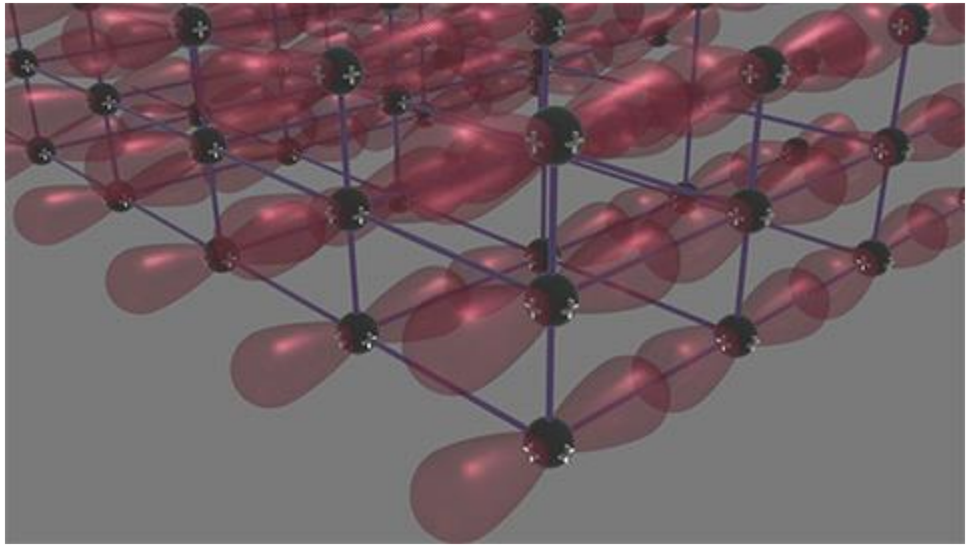

Heisenberg exchange $E_H = -\sum_{i,j} J_{ij} \mathbf{S}_i \cdot \mathbf{S}_j$

$J_1 > 0$ **ferromagnetic**

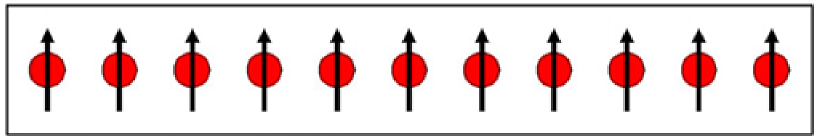

$J_1 < 0$ **antiferromagnetic**

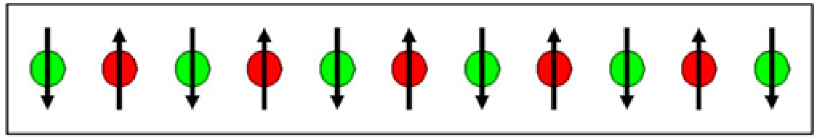

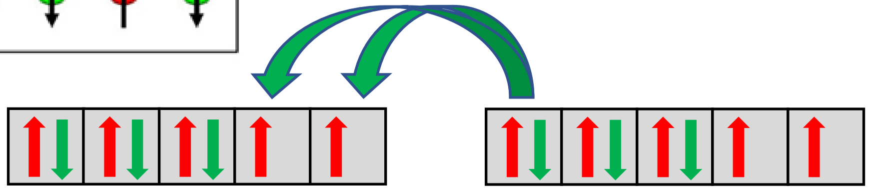

Nearly filled or nearly empty orbitals tend to have J>0

Conditions for ferromagnetism:

- Non-compensated spin moments
- Positive Exchange Interaction

26	27	28
Fe	Co	Ni
55.85	58.93	58.70

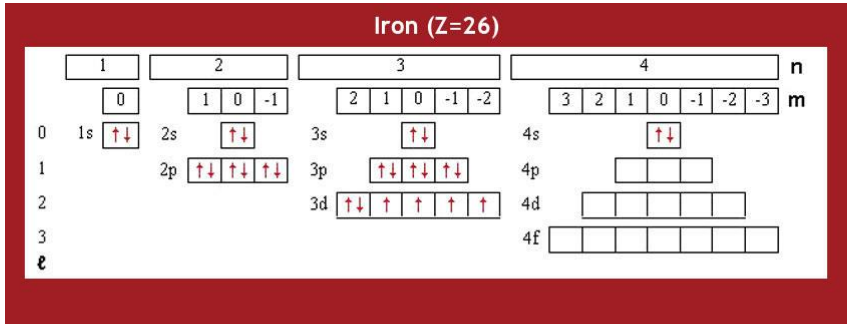

Magnetic domain growth under a magnetic field

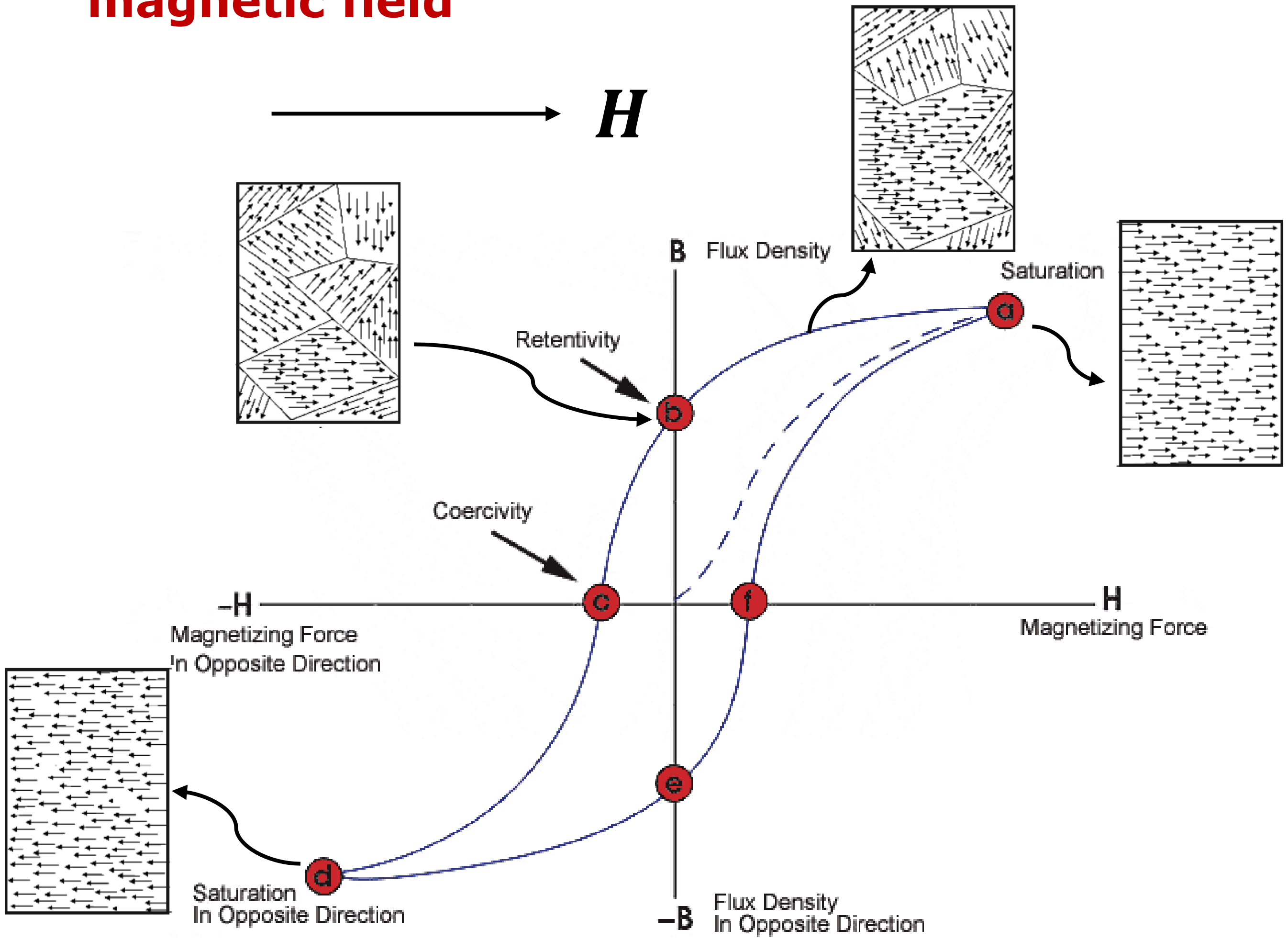

- **Retentivity** - A measure of the residual flux density corresponding to the saturation induction of a magnetic material.
- **Residual Magnetism** or **Residual Flux** - the magnetic flux density that remains in a material when the magnetizing force is zero. Note that residual magnetism and retentivity are the same when the material has been magnetized to the saturation point. However, the level of residual magnetism may be lower than the retentivity value when the magnetizing force did not reach the saturation level.
- **Coercive Force** - The amount of reverse magnetic field which must be applied to a magnetic material to make the magnetic flux return to zero. (The value of **H** at points c and f on the hysteresis curve.)

Exchange Bias

Granular Model

Ideal Interface

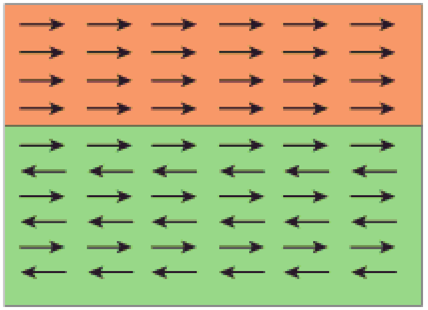

Mauri Model

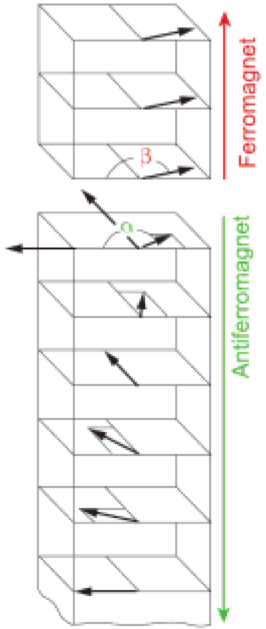

Roughness model

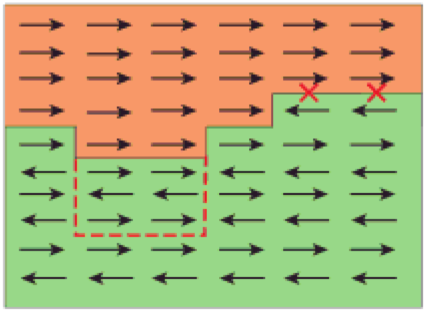

- Exchange anisotropy at an ideal interface. All interface spins of the antiferromagnet are uncompensated and act in the same way on the ferromagnet. Here we assume ferromagnetic coupling across the interface

- When the exchange coupling is stronger than the anisotropy, noncollinear (see angles α and β) configurations are likely. A domain wall in the antiferromagnet is formed when the ferromagnetic film is magnetized to the right. Only one spin sublattice of the antiferromagnet is shown

- At real surfaces with roughness the nearest neighbour exchange couplings cannot all be fulfilled simultaneoustly. Therefore frustration (red crosses) and domain walls (dashed line) occur and the number of uncompensated spins at the interface is reduced, here from 6 (ideal interface) to 2 (rough interface)

Heisenberg exchange $E_H = -\sum_{i,j} J_{ij} \mathbf{S}_i \cdot \mathbf{S}_j$

$J_1 > 0$ **ferromagnetic**

$J_1 < 0$ **antiferromagnetic**

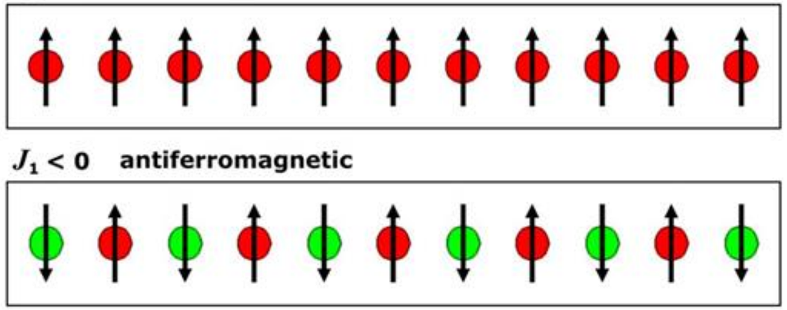

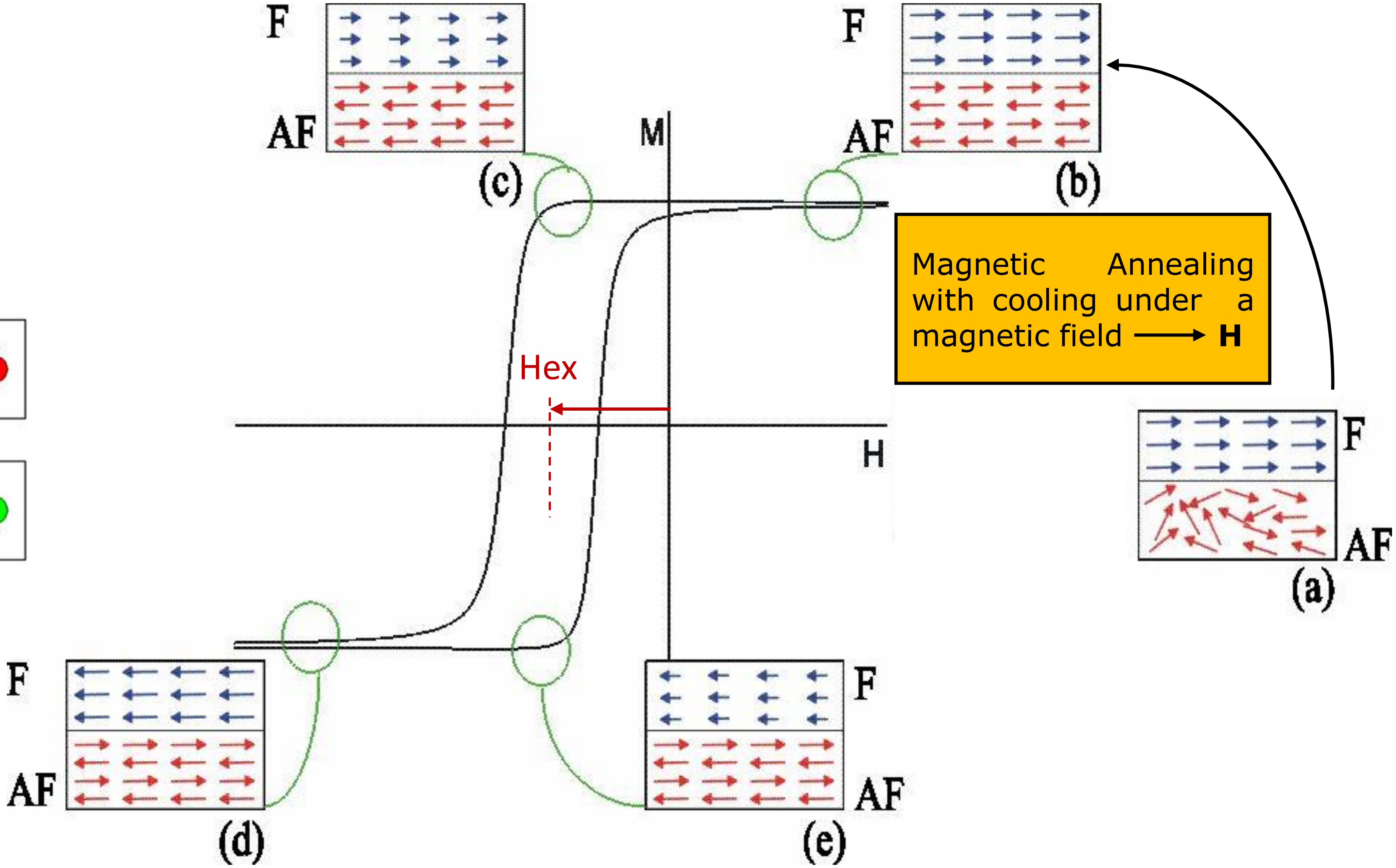

Magnetic impurity in a conducting medium induces spatial fluctuations of spin polarization of s-electrons about the impurity

- the oscillatory term of wave number $2k_F$ falls off like r^{-3} at large distances

- the second impurity placed in the vicinity experiences interaction with the first impurity
- depending on the distance between impurities the interactions may be ferromagnetic or antiferromagnetic

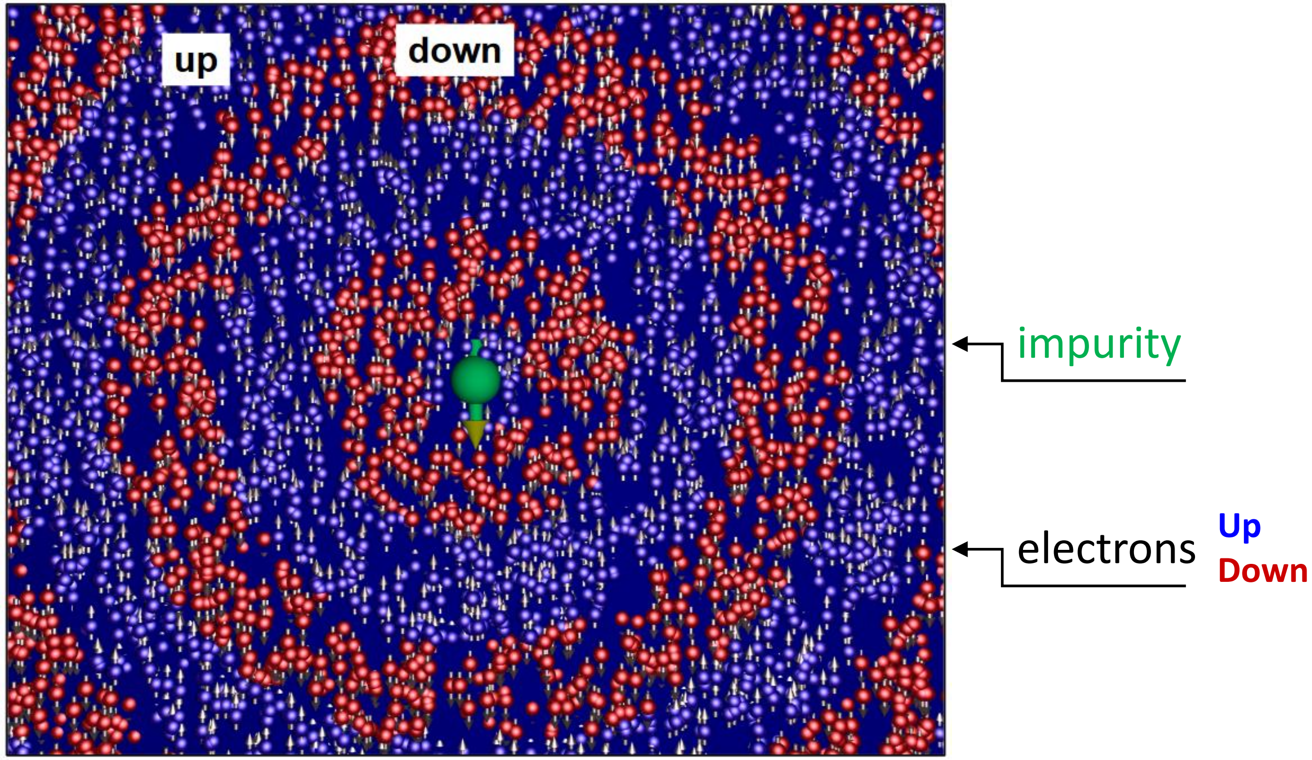

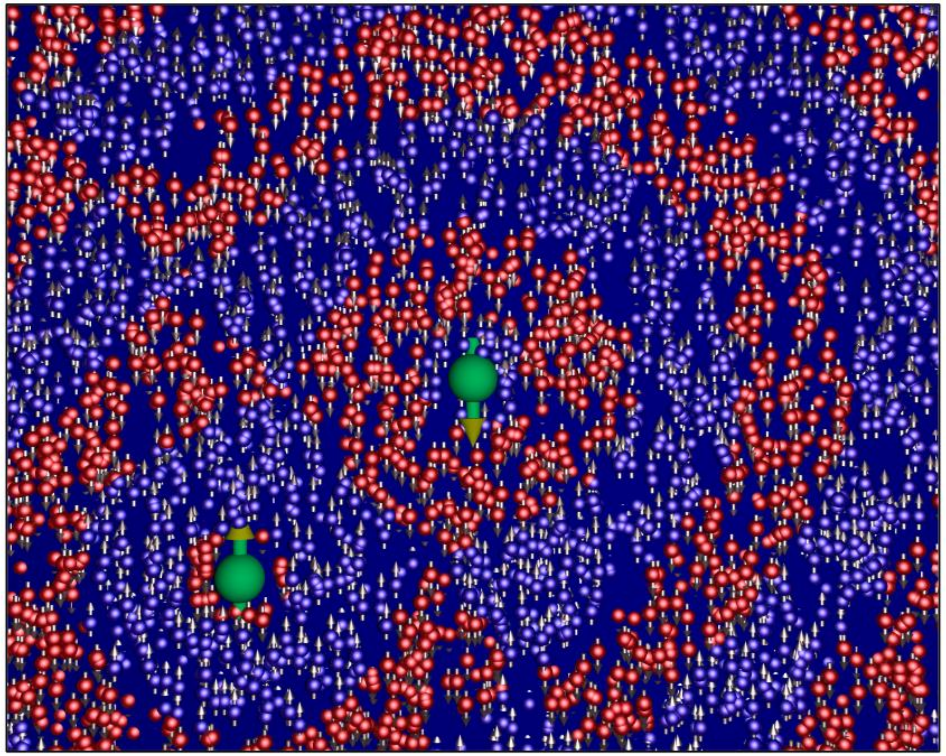

Ruderman-Kittel-Kasuya-Yoshida Interaction

It refers to a coupling mechanism magnetic moments in a metal by means of an interaction through the conduction electrons.

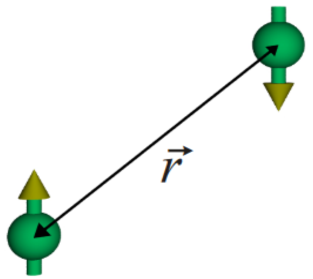

$$J_{RKKY} \ \alpha \ \frac{1}{r^3} \cos(2kFr)$$

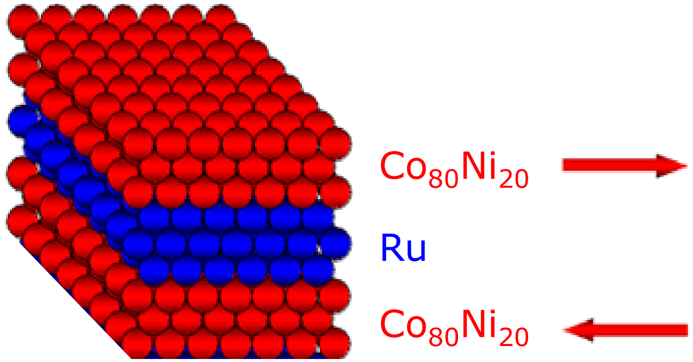

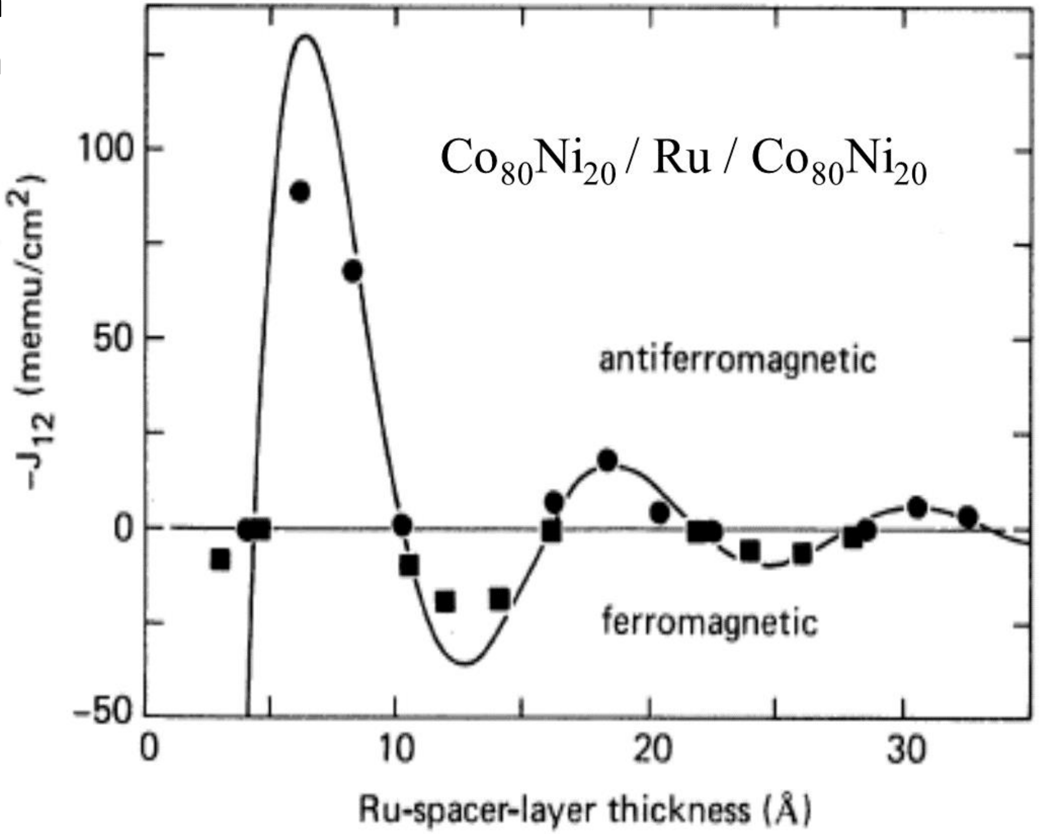

VSM – Vibrating Sample Magnetometer

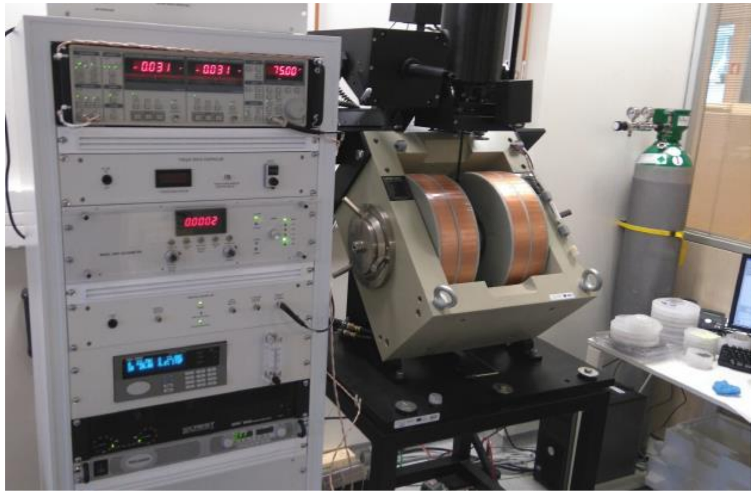

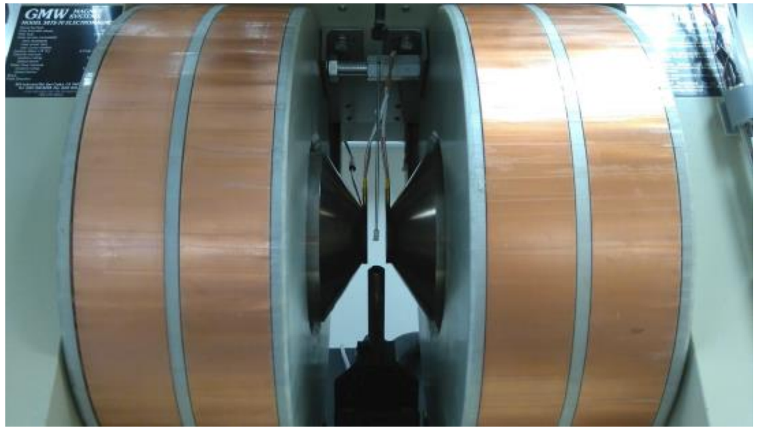

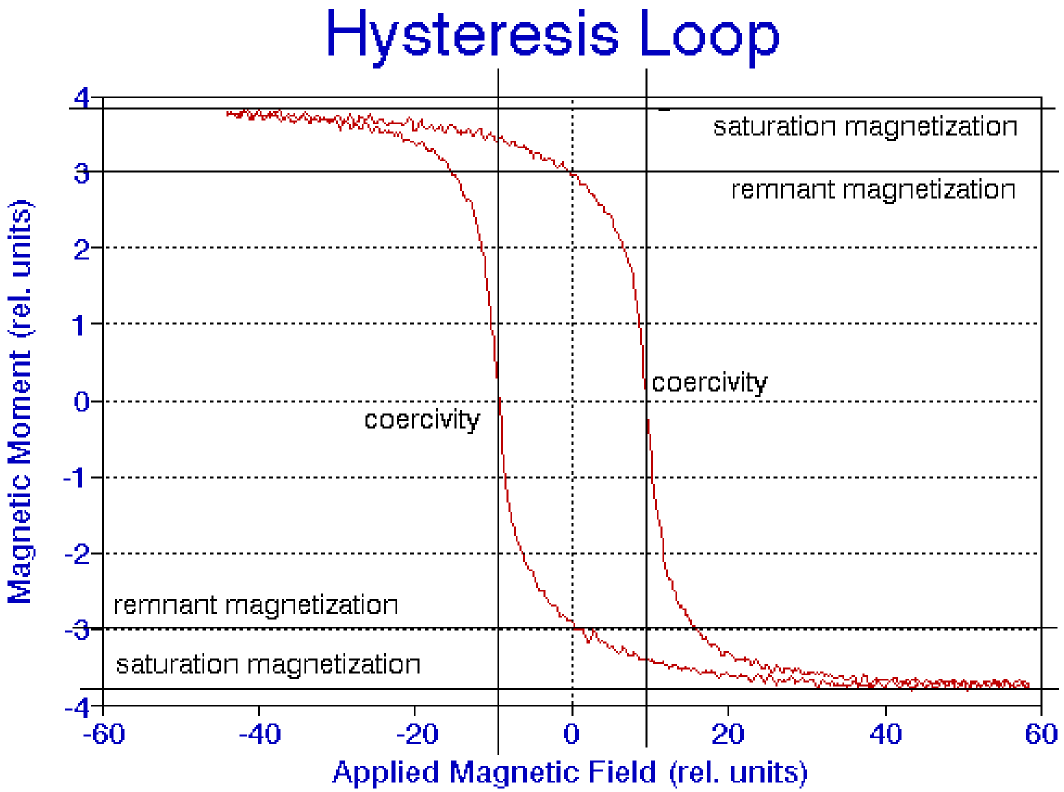

Magnetoresistive devices

Magnetic sensors

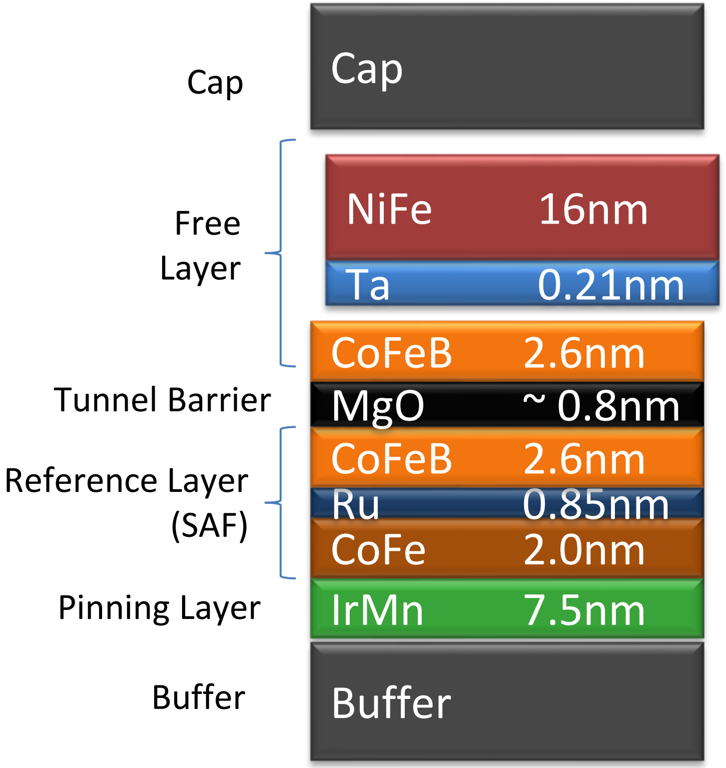

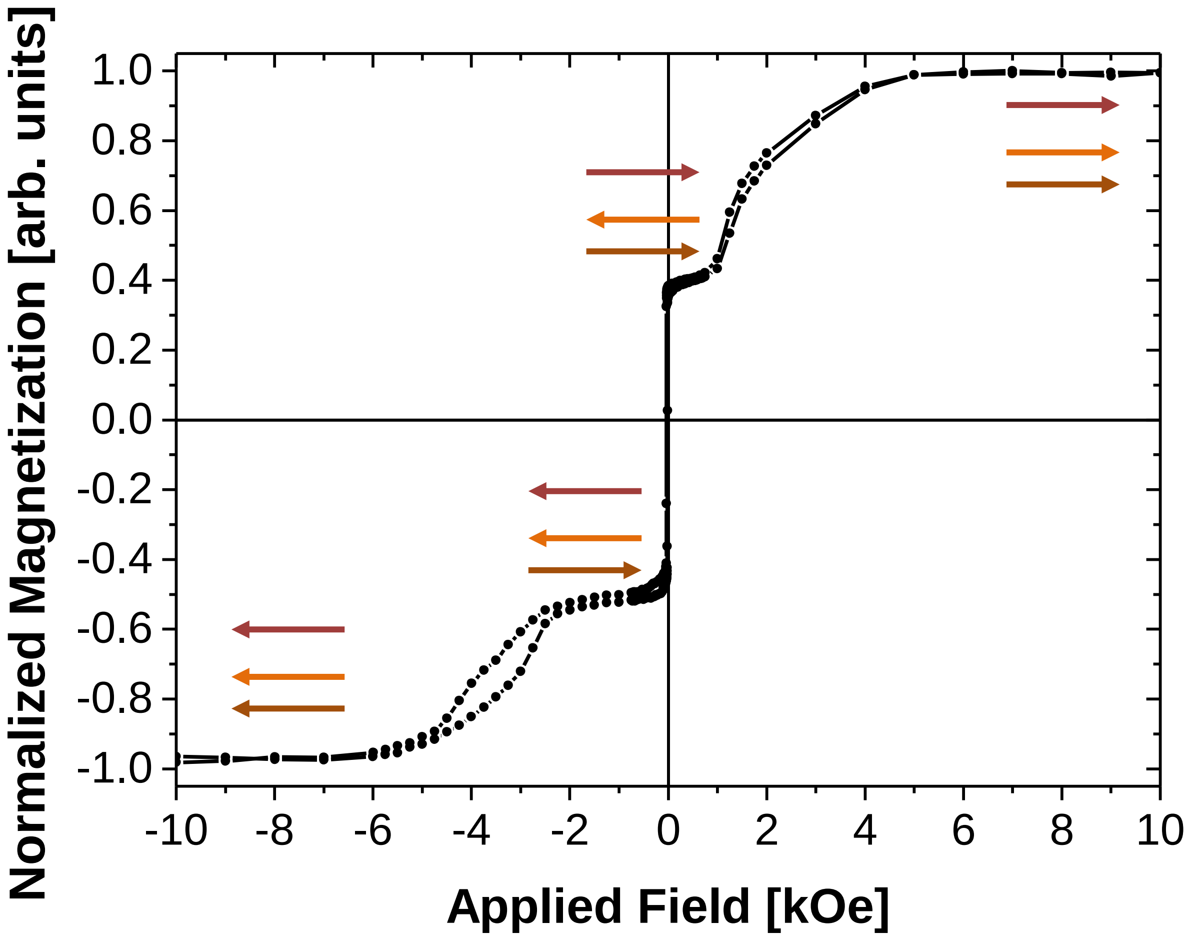

Magnetoresistive devices

Magnetic sensors

Magnetic Sensors

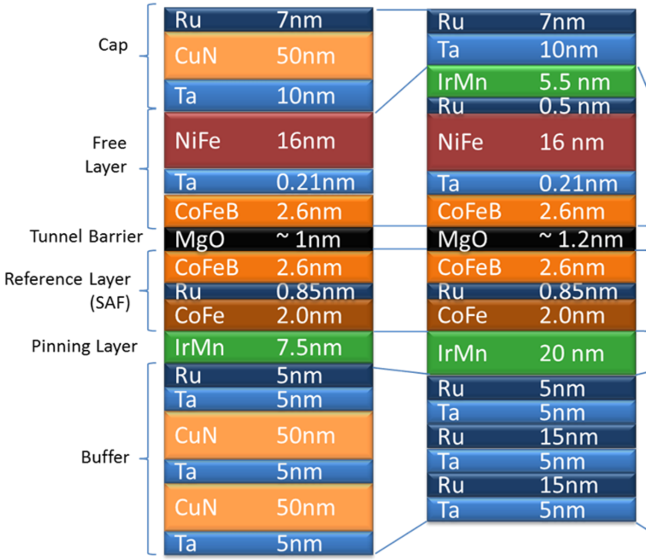

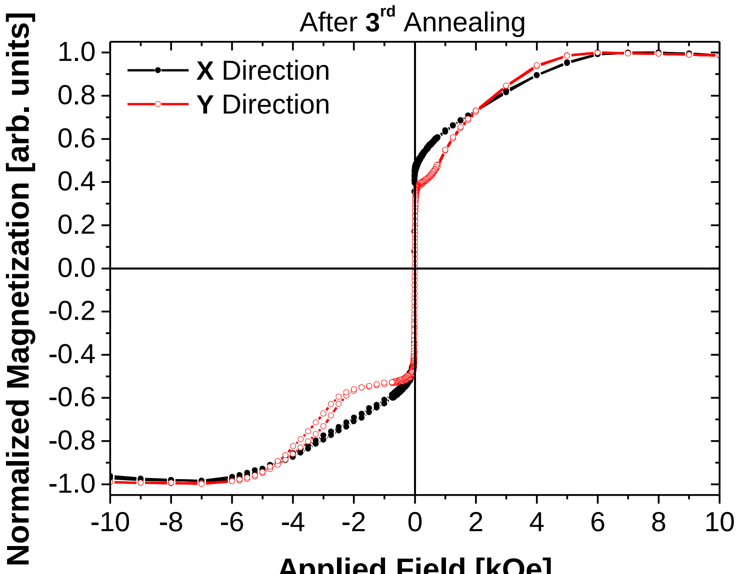

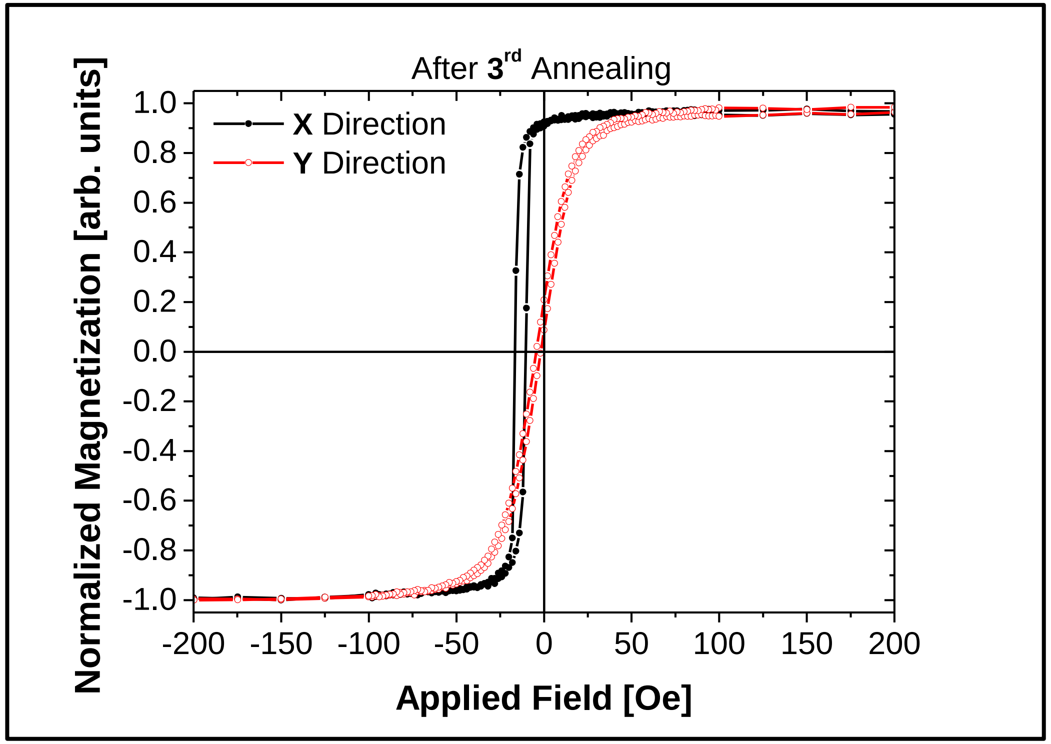

Zeeman Energy | Demagnetizing Field | Néel Coupling

$$\frac{E_f}{V} = \boxed{-\mu_0 \mathrm{H} \cdot \mathrm{M}^{\mathrm{f}}} + \boxed{K \sin^2 \theta} - \boxed{\frac{1}{2}\mu_0 \mathrm{H}_{\mathrm{d}}^{\mathrm{f}} \cdot \mathrm{M}^{\mathrm{f}}} - \boxed{\mu_0 \mathrm{H}_{\mathrm{d}}^{\mathrm{p}} \cdot \mathrm{M}^{\mathrm{f}}} - \boxed{\mu_0 \mathrm{H}_{\mathrm{N}} \cdot \mathrm{M}^{\mathrm{f}}}$$

Crystalline Anisotropy | Pinned Layer Stray Field

- **Zeeman energy** - or the external field energy, is the potential energy of a magnetised body in an external magnetic field
- **Magneto-crystalline anisotropy** - a ferromagnetic material is said to have magnetocrystalline anisotropy if it takes more energy to magnetize it in certain directions than in others
- **Demagnetizing field** - magnetic field (H-field) generated by the magnetization in a magnet. It is also called the stray field (outside the magnet)
- **Pinned Layer Stray Field** – magnetic field generated by the magnetization of the pinned layer
- **Neel coupling** - effect of the dipolar magnetic coupling (also known as or “orange-peel” coupling)

Magneto-crystalline anisotropy

Uniaxial anisotropy
Easy Axis vs. Hard Axis

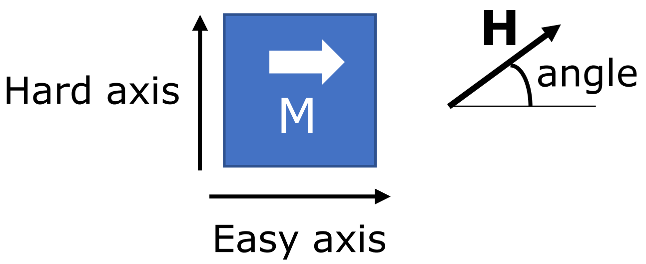

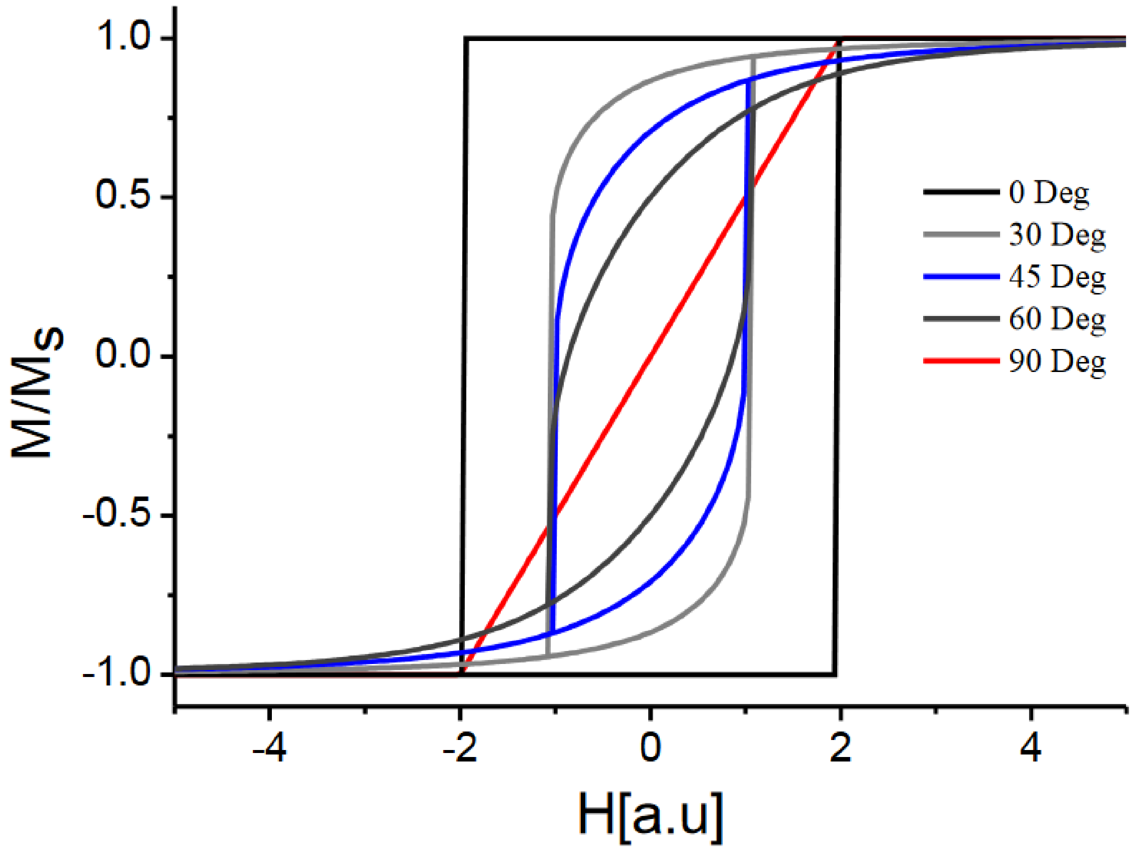

Stray and demagnitizing field

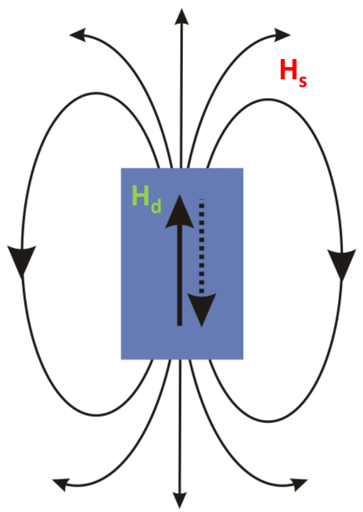

Néel coupling

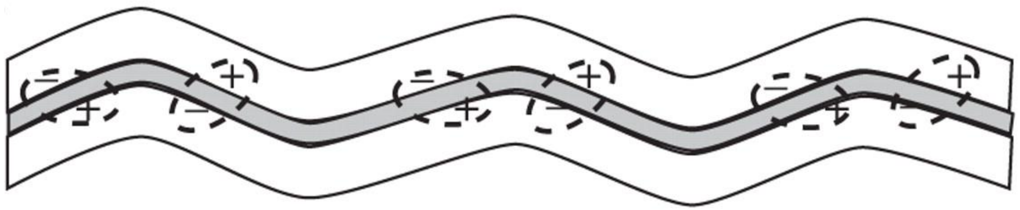

Pinned Layer Stray Field

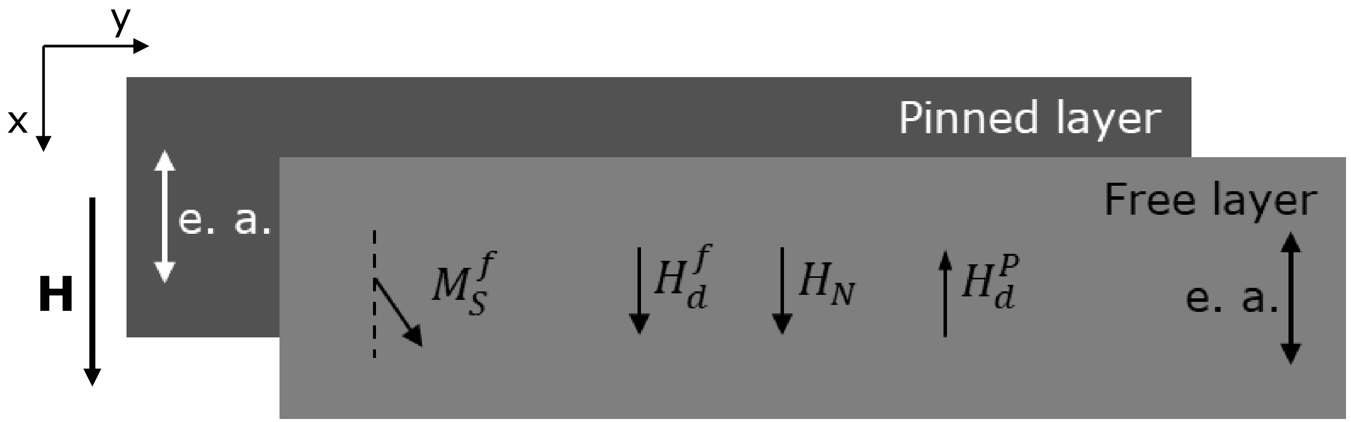

Shape anisotropy

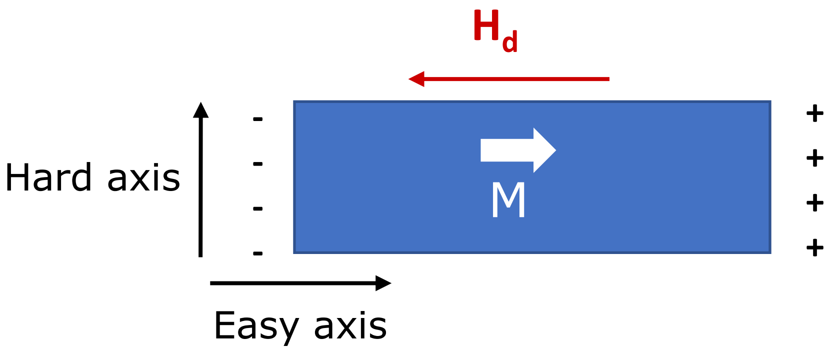

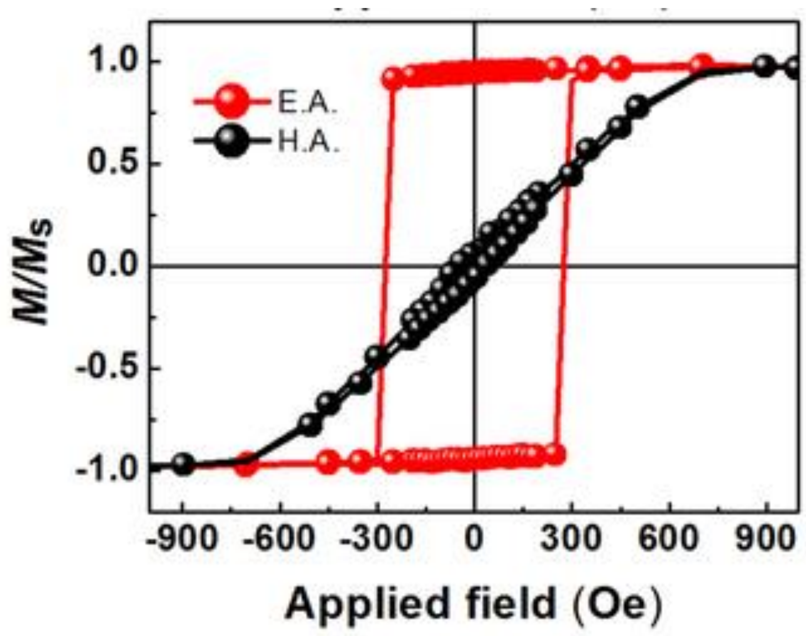

Demagnetizing Field

$$\boldsymbol{H}_d = -N\boldsymbol{M}$$

N – Demagnetizing factor

In general N is a tensor that depends on the shape of the magnetic material

Magnetostatic energy

$$\boldsymbol{E}_d = -\frac{1}{2}\mu_0 \boldsymbol{M} \cdot \boldsymbol{H}_d = -\frac{1}{2}\mu_0 N M^2$$

Linearization of an MTJ Sensor

Shape anisotropy

- The demagnetizing field can be very difficult to calculate for arbitrarily shaped objects, even in the case of a uniform magnetizing field
- For the special case of ellipsoids, long thin rods, and flat plates, H_d is linearly related to M by a geometry-dependent matrix of the demagnetizing factors N
- It can be as important as magnetocrystalline anisotropy in driving the magnetization process under many circumstances
- *Na*, *Nb*, and *Nc* are the demagnetizing factors pertaining to the three principal axes, and *Na + Nb + Nc = 1*

$$\frac{E_M}{V} = \frac{\mu_0 M_S^2}{2}\left(N_a m_x^2 + N_b m_y^2 + N_c m_z^2\right)$$ Magnetostatic energy

$$\overrightarrow{H_{Demag}} = \frac{1}{2}\mu_0 \bar{N}\,\vec{M}$$

$$\bar{N} = \begin{pmatrix} N_a & 0 & 0 \\ 0 & N_b & 0 \\ 0 & 0 & N_c \end{pmatrix}$$

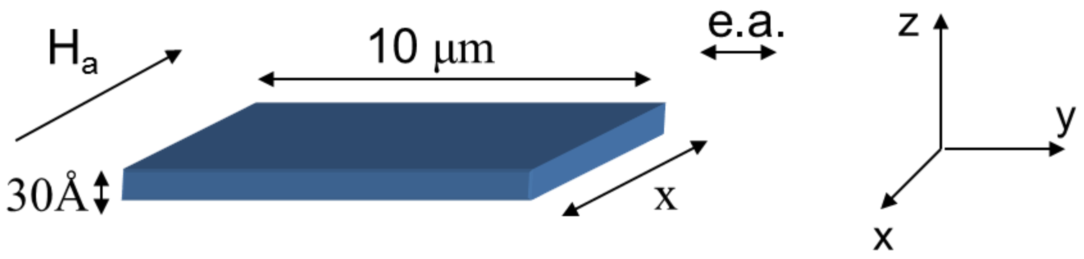

Linearization of an MJT Sensor

Shape anisotropy

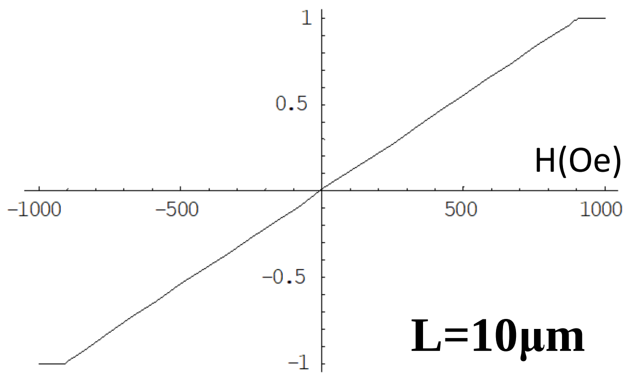

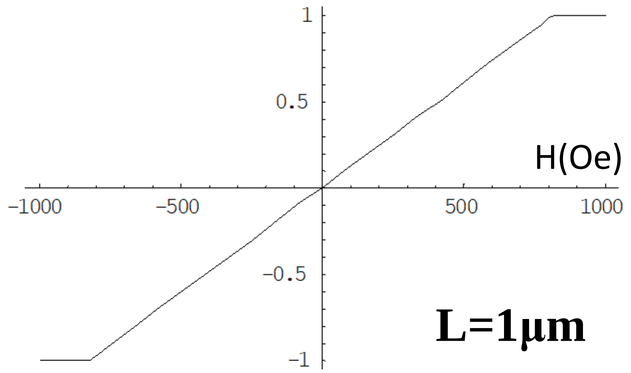

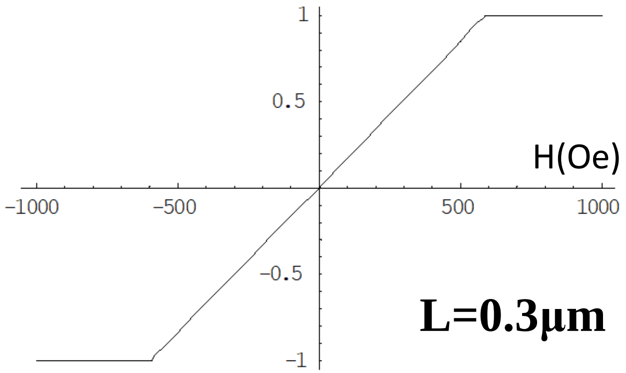

Linearization of an MTJ Sensor

Shape anisotropy

- All ferromagnetic layers have an easy axis defined during deposition/annealing

Crystalline Anisotropy **Shape Anisotropy**

- Virtual magnetic charges far apart, low energy

- Virtual magnetic charges far close, high energy

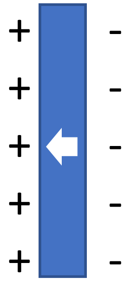

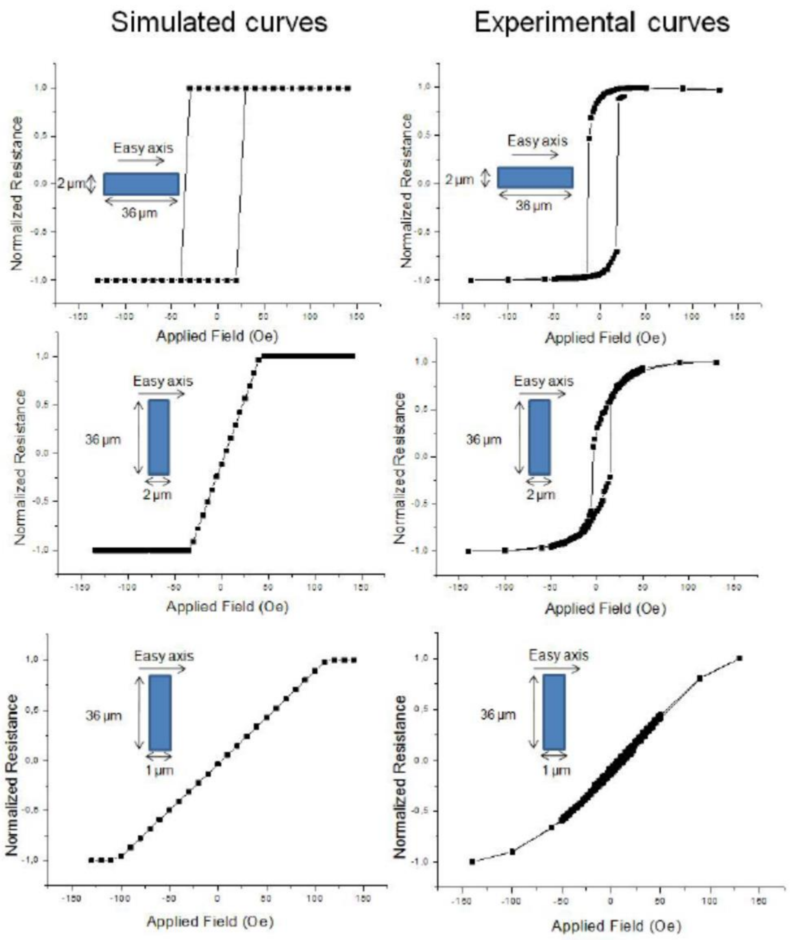

Figure 4.11: Comparison of the evolution of the experimental sensor transfer curve (right) and the modeled sensor transfer curve (left).

Linearization of an MTJ Sensor

Free layer energy

Zeeman Energy

Demagnetizing Field

Néel Coupling

$$\frac{E_f}{V} = \boxed{-\mu_0 \mathbf{H} \cdot \mathbf{M}^{\mathrm{f}}} + \boxed{K \sin^2 \theta} - \boxed{\frac{1}{2}\mu_0 \mathbf{H}_{\mathrm{d}}^{\mathrm{f}} \cdot \mathbf{M}^{\mathrm{f}}} - \boxed{\mu_0 \mathbf{H}_{\mathrm{d}}^{\mathrm{P}} \cdot \mathbf{M}^{\mathrm{f}}} - \boxed{\mu_0 \mathbf{H}_{\mathrm{N}} \cdot \mathbf{M}^{\mathrm{f}}}$$

Crystalline Anisotropy

Pinned Layer Stray Field

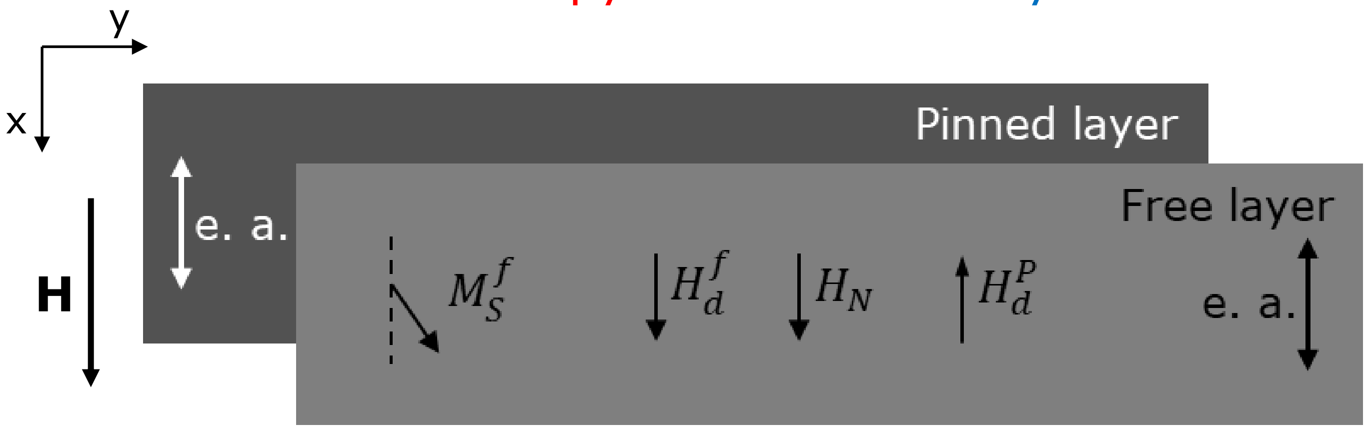

$$\mathbf{H}_{\mathrm{d}}^{\mathrm{f}} = -N_{xx} M_s^f \cos\theta$$

$$\frac{E_f}{V} = \mu_0 M_s^f \left[\frac{1}{2}\sin^2\theta (H_k - N_{xx} M_s^f) + \frac{1}{2} N_{xx} M_s^f - \cos\theta (H - H_d^p + H_N)\right]$$

Linearization of an MTJ Sensor

Free layer energy – Finding the energy minimum

$$\frac{\partial \frac{E_f}{V}}{\partial \theta} = \mu_0 M_s^f \sin\theta \left[\cos\theta (H_k - N_{xx} M_s^f) + H - H_d^p + H_N\right]$$

$$\frac{\partial \frac{E_f}{V}}{\partial \theta} = 0 \Rightarrow \sin\theta \left[\cos\theta (H_k - N_{xx} M_s^f) + H - H_d^p + H_N\right] = 0$$

There are then three possible solutions:

- **1-** $\sin\theta = 0 \Leftrightarrow \theta = 0$ or π
- **2-** $H_k - N_{xx} M_s^f = 0$ and $H - H_d^p + H_N = 0$
- **3-** $\cos\theta = \frac{H - H_d^p + H_N}{N_{xx} M_s^f - H_k}$

Linearization of an MTJ Sensor

Free layer energy – Finding the energy minimum

- 1- $\sin\theta = 0 \Leftrightarrow \theta = 0$ or π

$$\frac{\partial^2 \frac{E_f}{V}}{\partial\theta^2} > 0 \Rightarrow \begin{cases} H > H_d^p - H_N + (N_{xx}M_s^f - H_k) & \text{for } \theta = 0 \\ H < H_d^p - H_N - (N_{xx}M_s^f - H_k) & \text{for } \theta = \pi \end{cases}$$

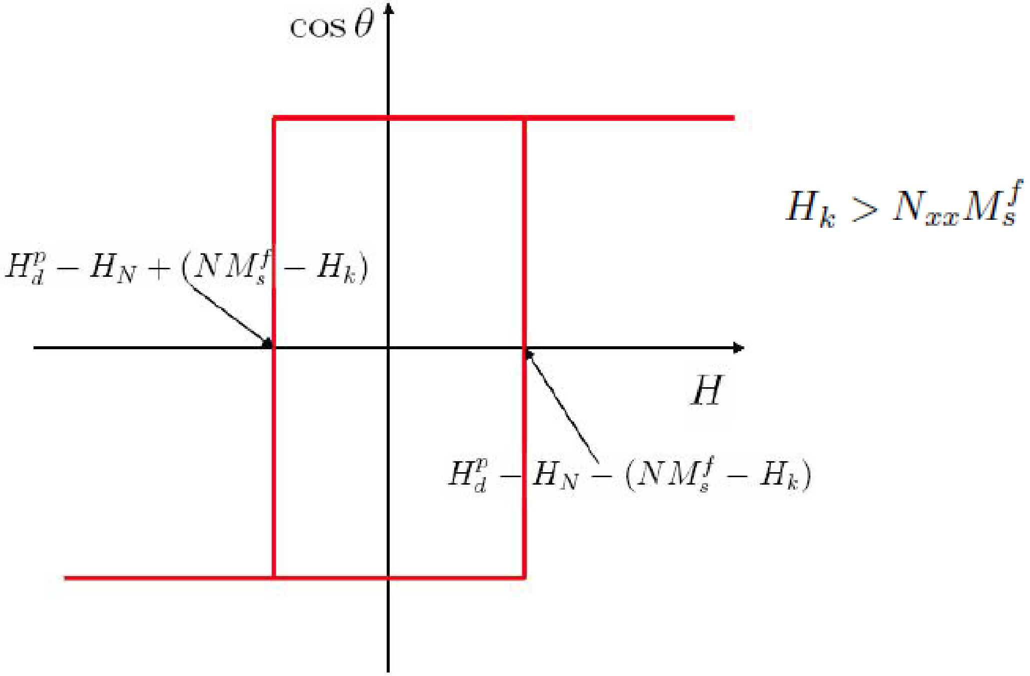

Figure 4.5: Transfer curve with hysteresis.

- 2- $H_k - N_{xx}M_s^f = 0$ and $H - H_d^p + H_N = 0$
- 3- $\cos\theta = \frac{H - H_d^p + H_N}{N_{xx}M_s^f - H_k}$

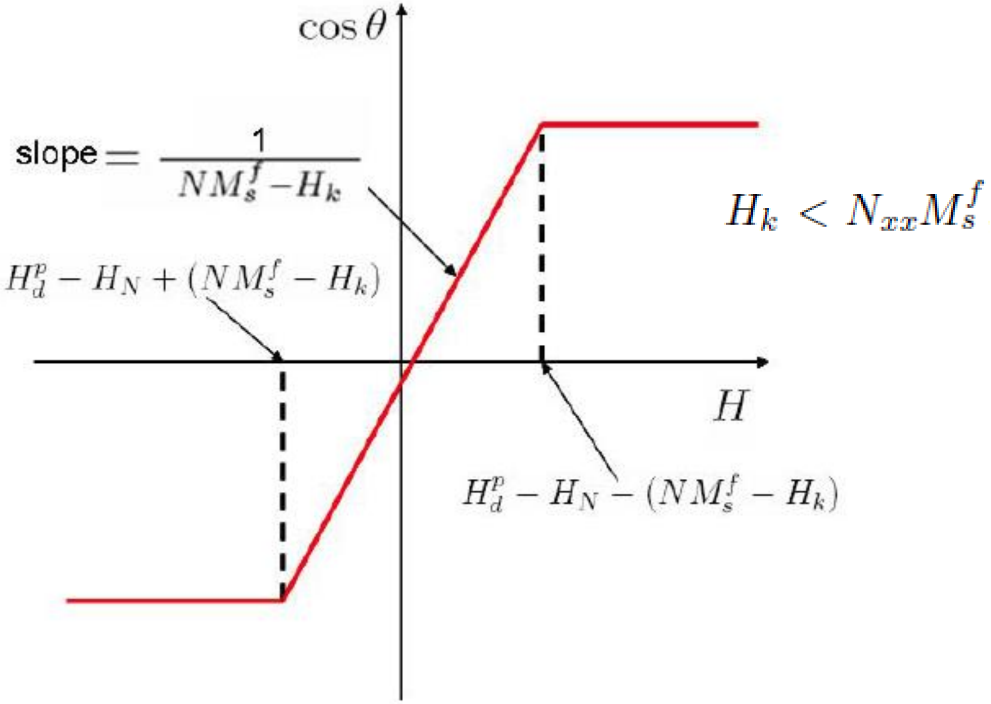

Figure 4.6: Linear transfer curve.

Part III
MTJ stack deposition and microfabrication

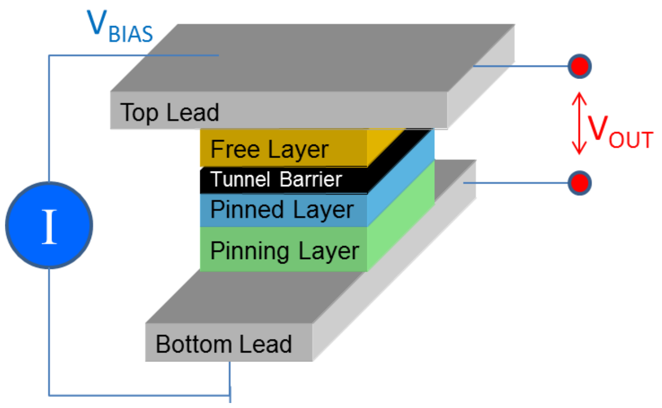

4 pillars of spintronics

- Memories
- **Sensors**
- **Oscillators**
- Logic

Magnetoresistive devices

Stack optimization

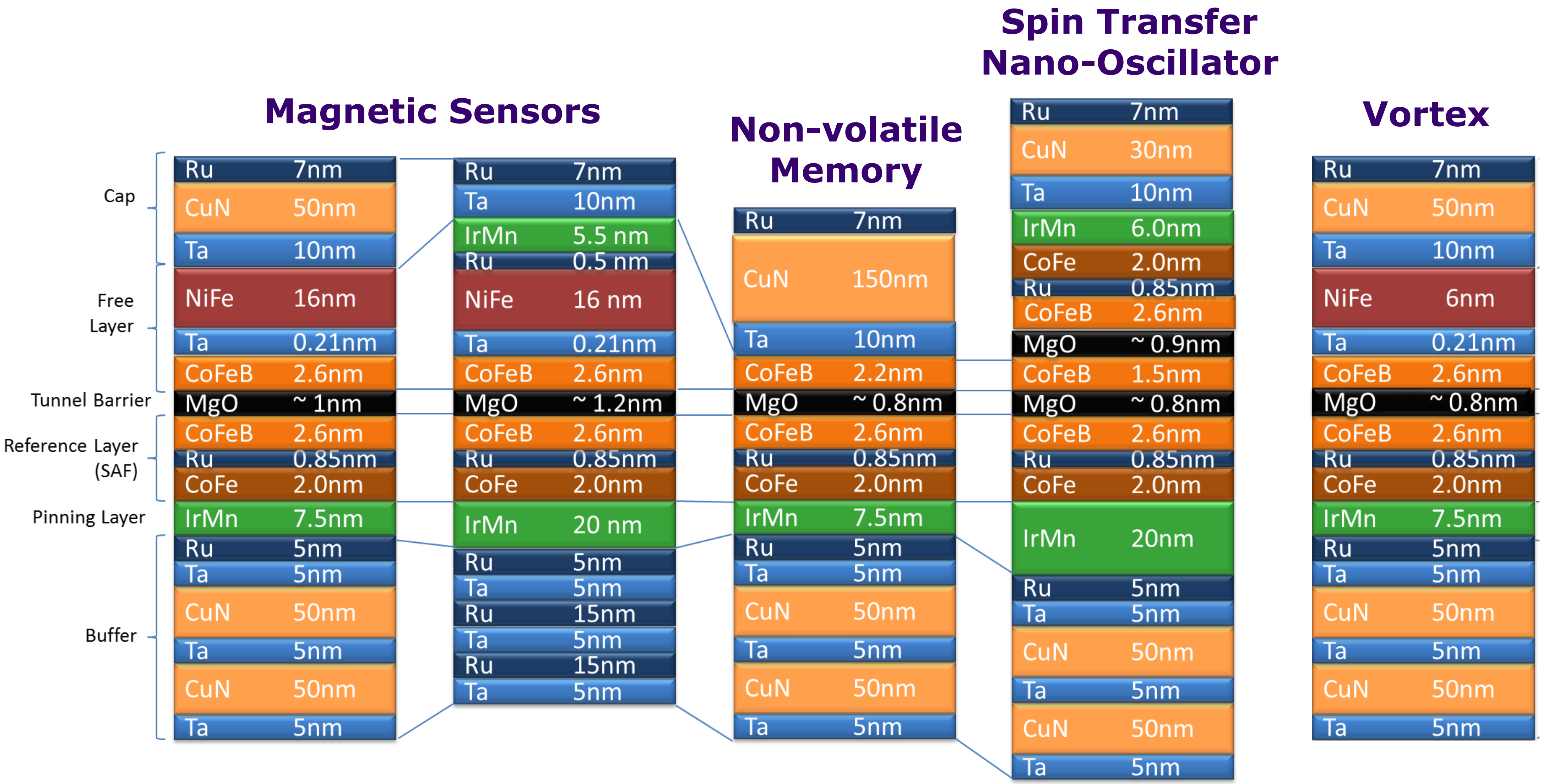

Magnetoresistive devices

Sensors

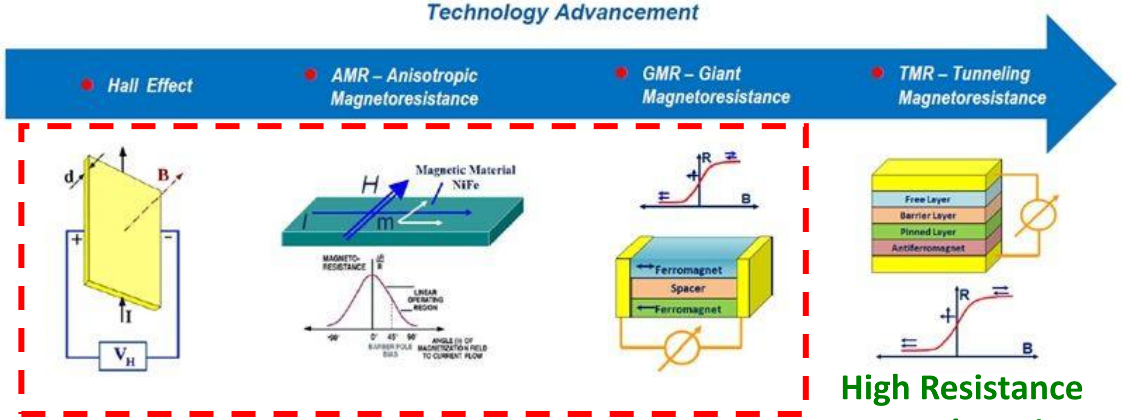

High Resistance Tunnel Barrier

Metallic Stacks (Low Resistance)

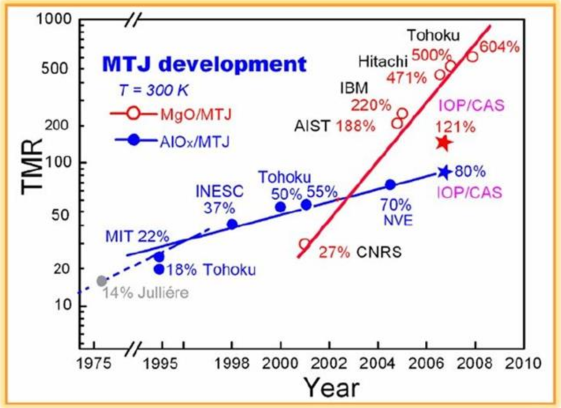

TMR sensors are being used in consummer market Hard Disk Drives since 2005

MR : ~2-3% ~8-20% ~200%

Technology	Hall Effect	AMR	GMR	TMR
Power Consumption (mA)	5 ~ 20	1 ~ 10	1 ~ 10	0.001 ~ 0.01
Die Size (mm^2)	1 × 1	1 × 1	1 × 2	0.5 × 0.5
Field Sensitivity (mV/V/Oe)	~ 0.05	~ 1	~ 3	~ 100
Dynamic Range (Oe)	~ 10000	~ 10	~ 100	~ 1000
Resolution ($nT/Hz^{1/2}$)	>100	0.1 ~ 10	1 ~ 10	0.1 ~ 10
Temperature Performance (℃)	< 150	< 150	< 150	< 200

- Lower Power Consumption
- Smaller Footprint
- Larger Sensitivity (modest amplification requiments)
- Highly Tunnable Dynamic Range
- Higher Sensitivity to weak magnetic fields
- Higher Thermal Stability (adequate for operation in Harsh Environments)

Magnetoresistive devices

Artificial neurons – Neuromorphic computing

Synapses

Simplified Neuron

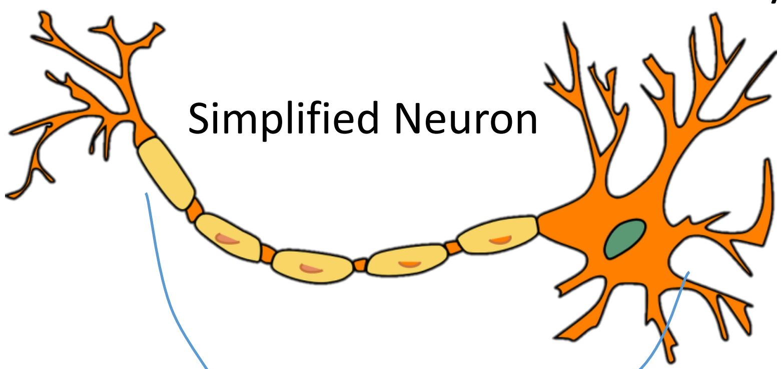

Nonlinear transfer-function

Weighted inputs

$$\text{output} = f\left(\sum_i W_i x_i\right)$$

Artificial Neuron

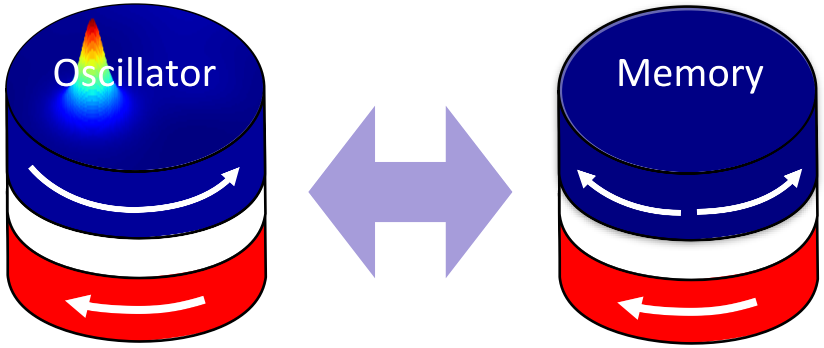

Oscillator

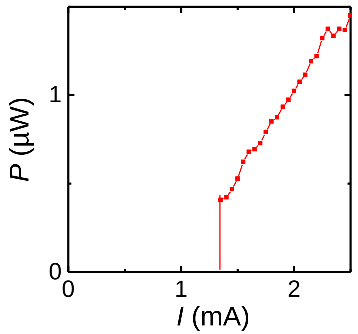

Memory

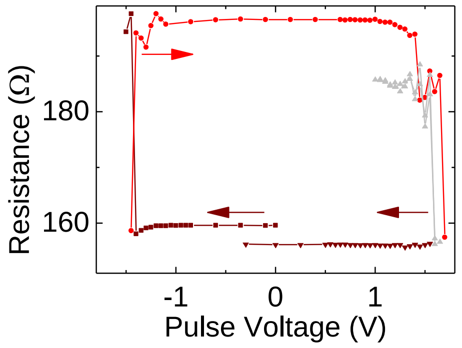

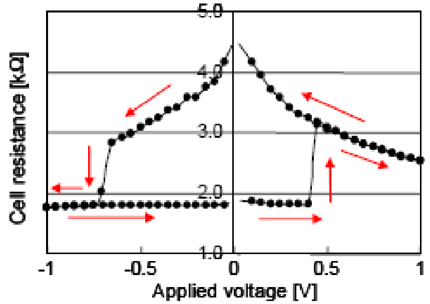

Magnetoresistive devices

Artificial neurons – Neuromorphic computing

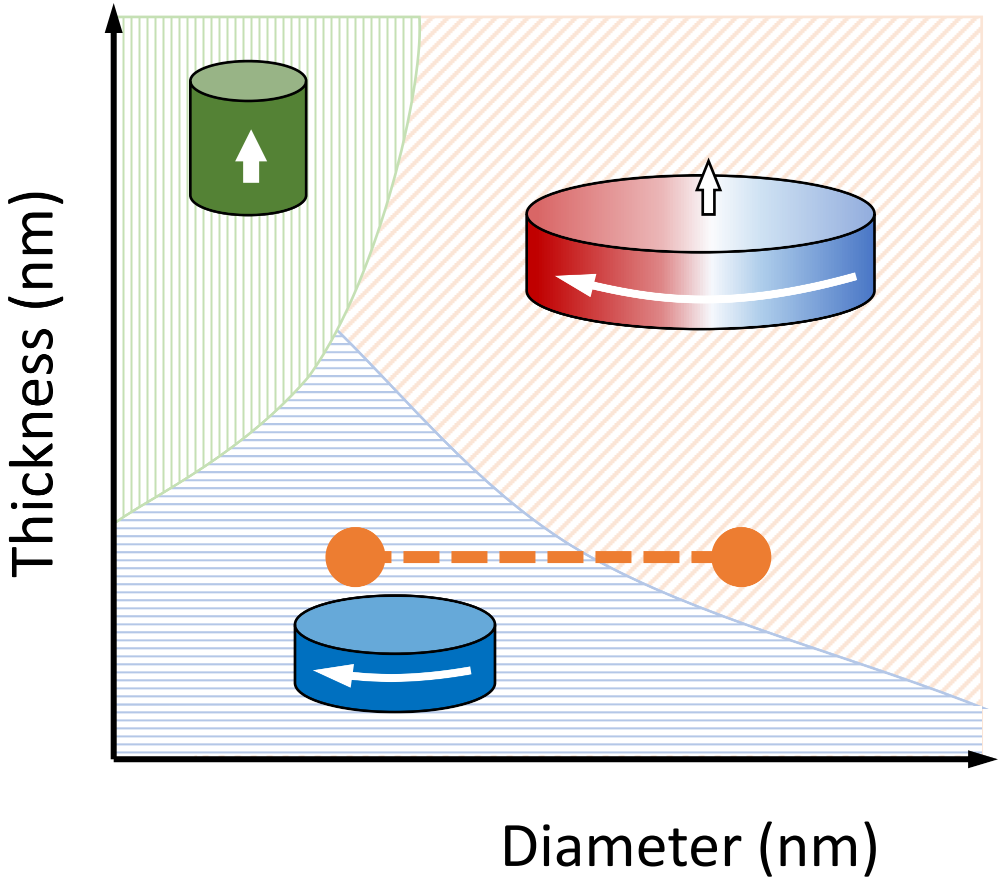

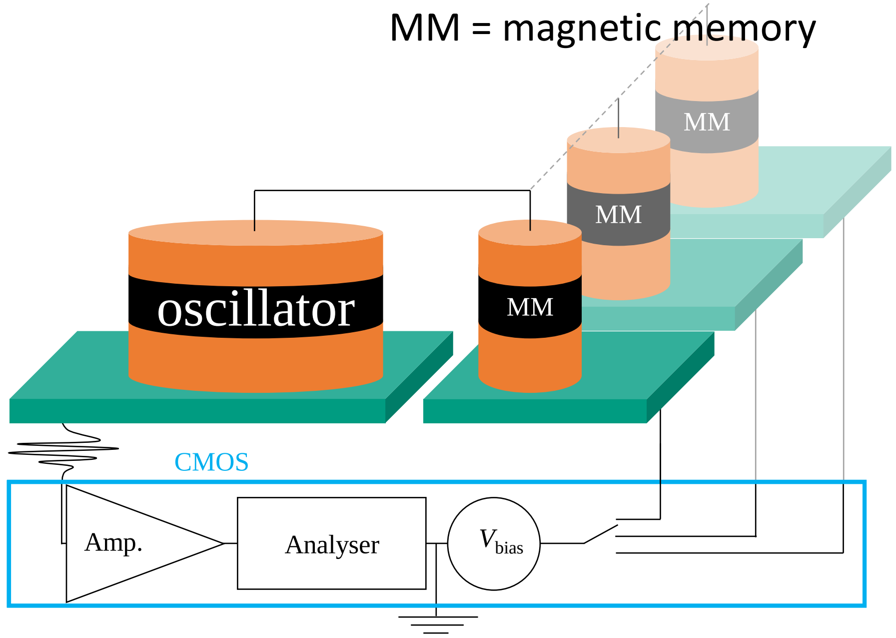

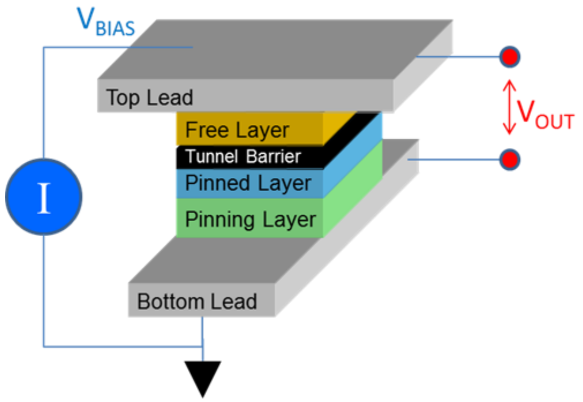

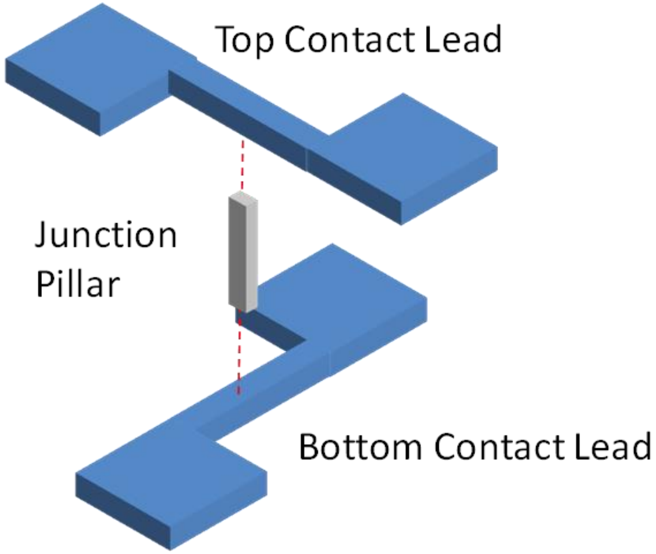

- 5 Lithography layers
- 22 processes
- 60 steps

Runsheet necessary for:

- **Smooth team work**
- **Control of the process**

Microfabrication process

Runsheet

TMR Stack:	TJ2615 - NO ETCH / [5 Ta / 15 Ru]x3 / 10 Ta / 5 Ru / 20 IrMn / 2 $CoFe_{30}$ / 0.7 Ru / 2.6 $CoFe_{40}B_{20}$ / MgO 4x90 3kW 600sccm [1.5 kOhm um2] / 2 CoFe40B20 / 0.21 Ta / 4 NiFe / 0.2 Ru / 6 IrMn / 2 Ru / 5 Ta / 10 Ru

No.	Layer	Process Step	Equipment	Conditions	Recipe Name	Specs for reference / Purpose / Comments	Date Completed:
1	Wafer Incoming			CMOS Wafer			na
2	01 - MTJ-Dep	TMR depo	MTM			Surface will end in Ru as always. Bottom contact/buffer layers will be a happy medium from previous experiences - not as thick as 6 periods (too much topography) nor 1 period (too much contact resistance). So, we will go with 3 periods (5Ta/15Ru). Purpose to have a thicker Ta in this case (10nm instead of 5nm) is to have a larger target to stop pillar etch in the Ta. We do not want to stop in the Ru because it will oxidize in atmosphere and it Ru oxide is conductive. So, during the pillar etch, we want to remove the IrMn and the 5nm Ru.	10/10/2017
3		Anneal	MRT	330C_1T_2hr, along the notch	330C_1T_2hr with CLEANZONE ON.	The idea is to crystalize the MgO and perform the higher temperature processes before we deposit the AlSiCu top metal. It is known to cause voids and grain issues when exposed to high temperatures, so therefore we plan to perform these anneals at the beginning, prior to the fabrication process.	06/11/2017
4		VSM	VSM				na
5		CIPT Test	CIPT			if possible	na

Microfabrication process

Runsheet

6	02 - Stopper	Stop Layer	FTM	15 TiWN / 10 AlSiCu / 40 TiWN w/etch		This stopping layer is meant to be 40nm in order to have enough TiWN to have at least a 5min overetch during the via opening step. Sandwich of TiWN/AlSiCU/TiWN was added to this wafer to help during the via etch. No EDX will be needed since these are relatively large pillars.	07/11/2017
7	03 - MTJ-PH	Vapor Prime	Baking	150C, HDMS coating, vacuum,30 minutes cycle	#4		07/11/2017
8		MTJ photo coating	Suss Coater	Coat AZ1505 600nm	#1		07/11/2017
9		Exposure	DWL	Mask DXF: MTJonCMOS DWL Map: MTJonCMOS Exposure Job name: MTJonCMOS Design names: MTJonCMOS_L2D CD Bias: X:-600nm Y:-600nm Focus: 50 Intensity:70 X offset: -5170.7 um Y offset: -266.275um Alignment mark: L0 No of Dies:		Alignment marks L0 (Left) = (x,y) = (5065.7, 266.275) L0 (Right)= (x,y) = (5170.7, 266.275) L1 (Left) = (x,y) = (5065.7, 757.0) L1 (Right)= (x,y) = (5170.7, 757.0) L2(Left)= (x,y) = (5065.7, 1257.0) L2(Right)= (x,y) = (5170.7, 1257.0) L3(Left)= (x,y) = (5065.7, 1757.0) L3(Right)= (x,y) = (5170.7, 1757.0) L4(Left)= (x,y) = (5065.7, 2257.0) L4(Right)= (x,y) = (5170.7, 2257.0) L5(Left)= (x,y) = (5065.7, 2757.0) L5(Right)= (x,y) = (5170.7, 2757.0)	12/11/2017
10		Develop	Suss Coater	MTJ 60s develop			13/11/2017
11		CD measure	Microscope				13/11/2017
12		Inspection	Microscope	pictures and dimension of Pillars			13/11/2017
13	04 - MTJ-ML	MTJ milling	Nordiko 7500	**Recipe: #19 MTJ HR 130deg 15s_165deg 5s** **Gun:** 400W; +XXXmA; +350V/-3000V; 40 sccm Ar **Neut:** 1x [OFF] with 4sccm, 2x [0.22A, 6 sccm] **Table:** 30 rpm; **130 deg 15sec_165 deg 5sec pan** **Stop point: 1st Bottom Ta peak and Ru** **Total time: 3100 sec**	#6	Uniformity might not be that great due to tool issues. Some parts might have ended in Ru	13/11/2017
14		Inspection	Microscope	check for spark clusters	N/A		13/11/2017

Deposition

Lithography

Etching

RESEARCH

Direct Writer Laser (DWL)

INDUSTRIAL PRODUCTION

Mask Aligner

Microfabrication process

Pillar definition - Ion milling

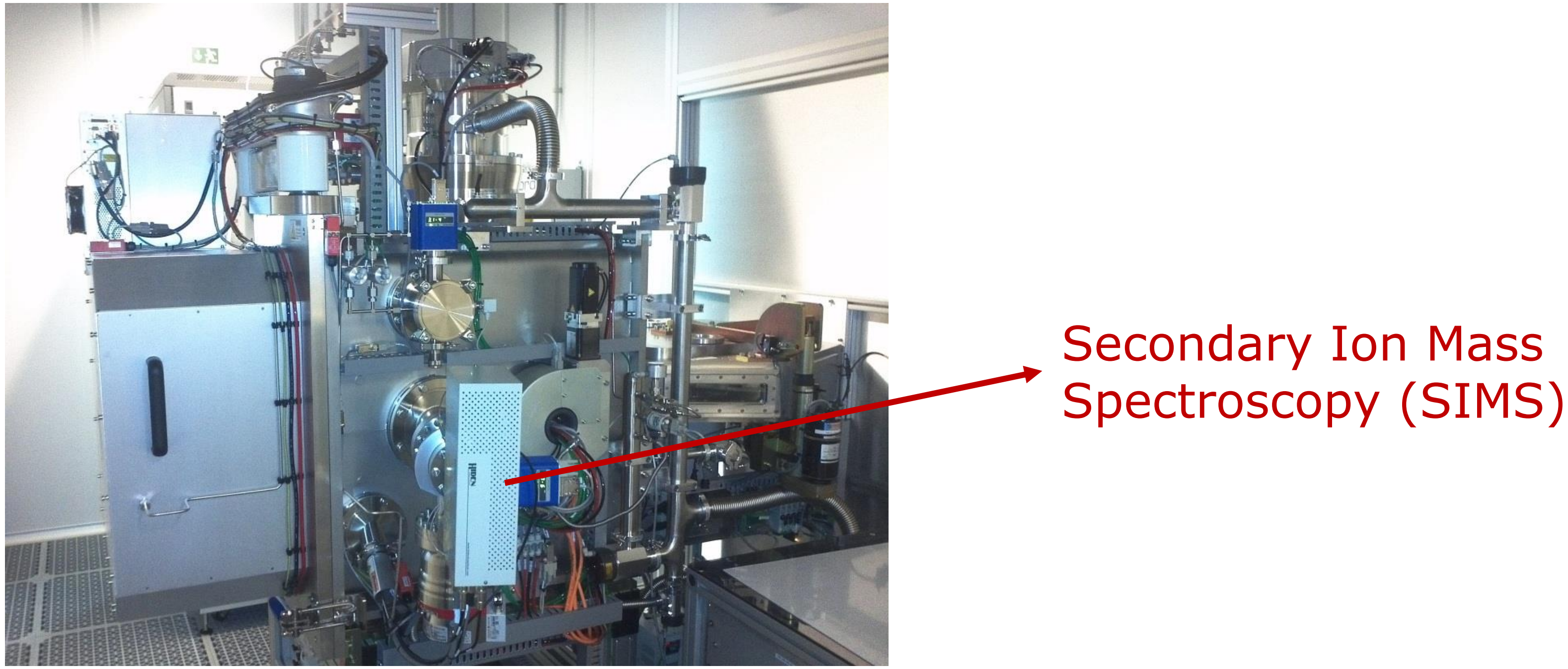

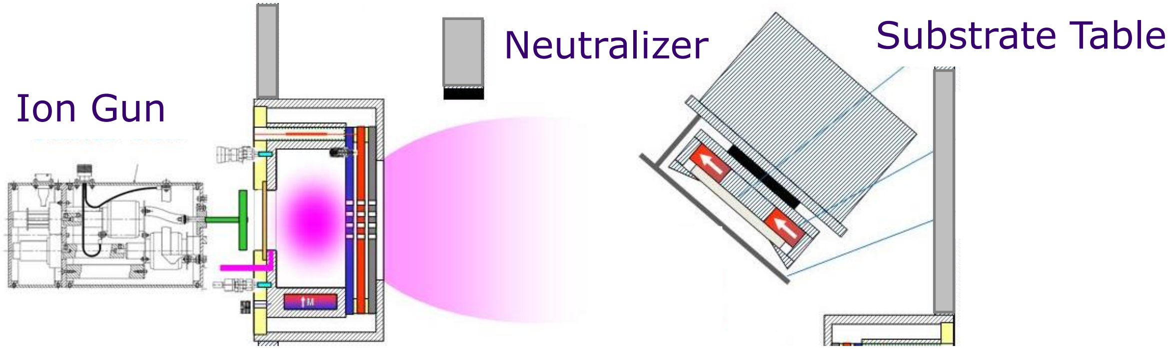

Microfabrication process

Pillar Definition - Ion beam Etching

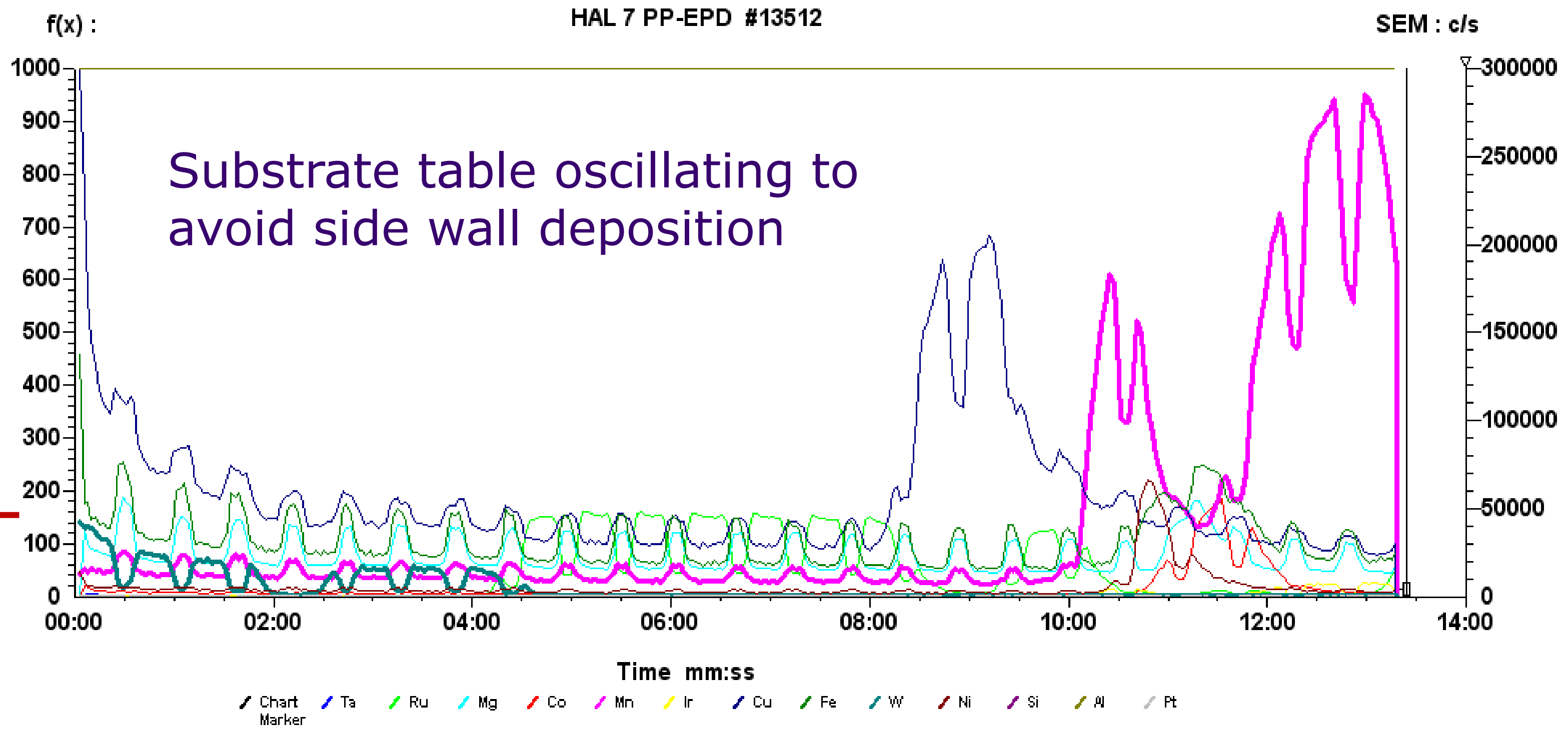

Substrate table oscillating to avoid side wall deposition

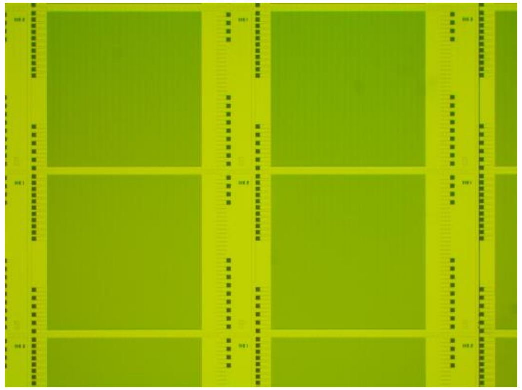

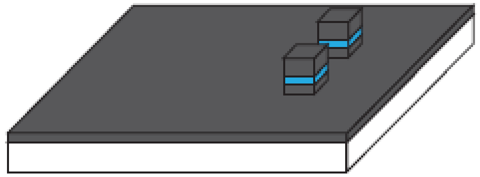

Microfabrication process

Bottom contact definition

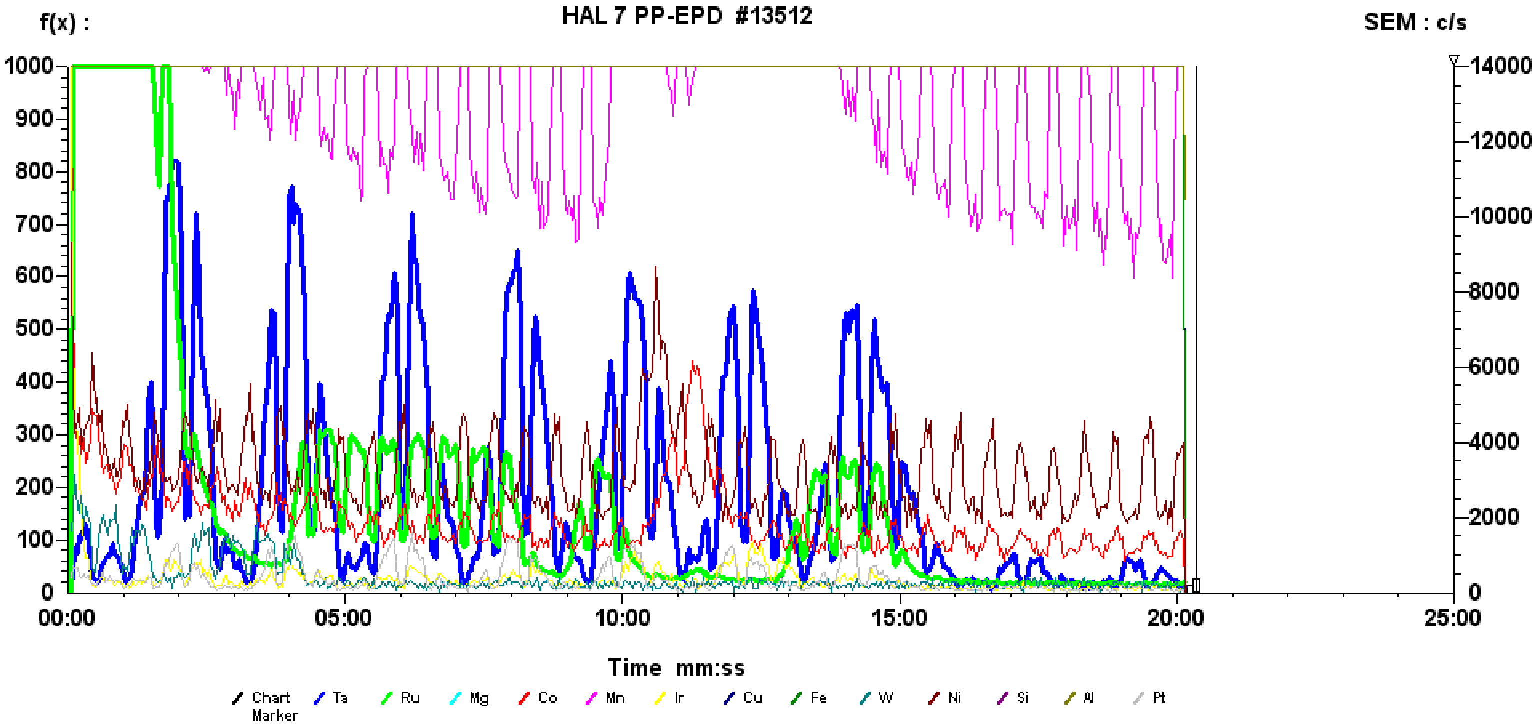

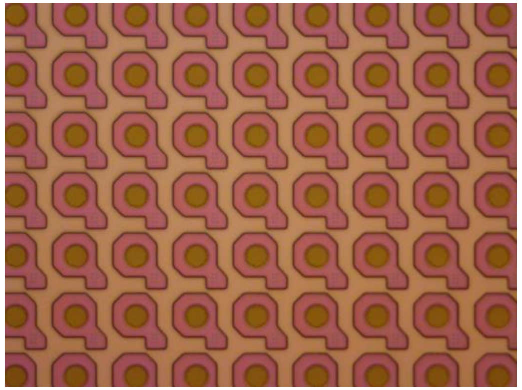

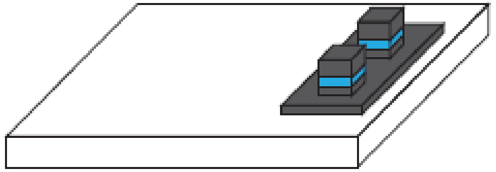

Microfabrication process

Insulating oxide deposition

RESEARCH	INDUSTRIAL PRODUCTION
RF magnetron sputtering – Al_2O_3	Plasma Enhanced Chemical Vapour Deposition (PECVD) – SiO_2

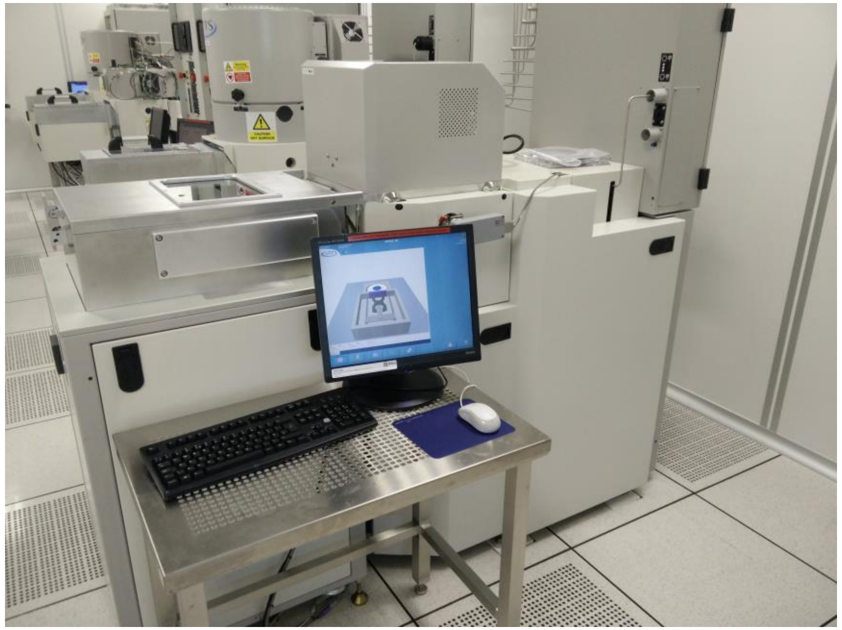

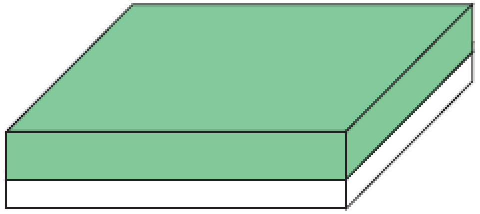

RESEARCH

Ion milling – Al_2O_3

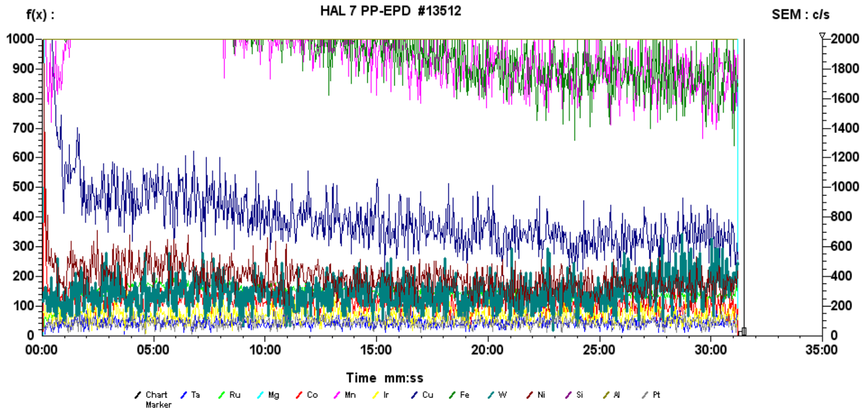

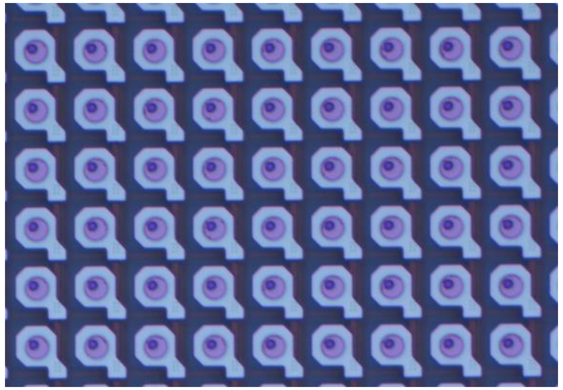

INDUSTRIAL PRODUCTION

Reactive ion etching (RIE) – SiO_2

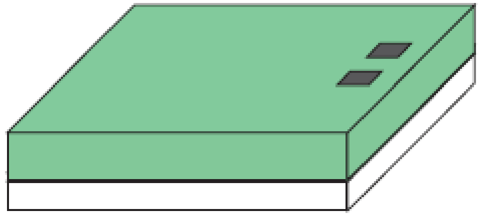

Thick metal sputtering

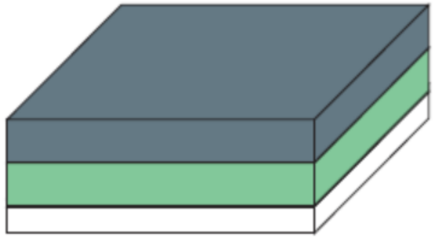

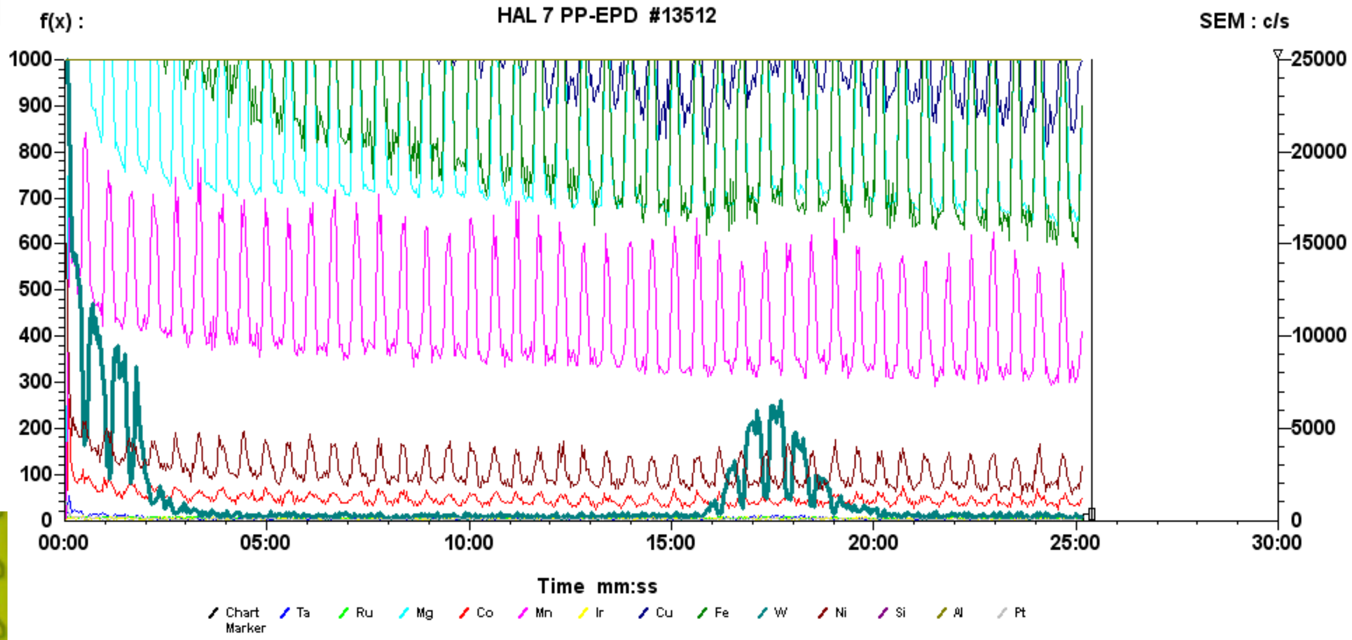

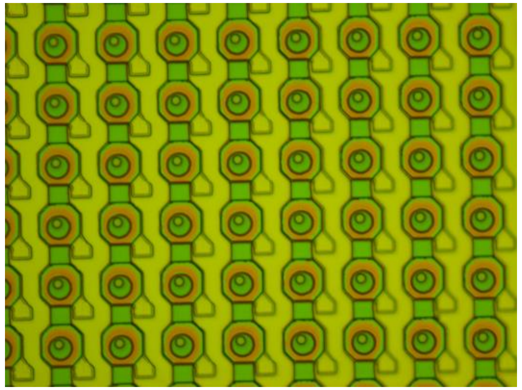

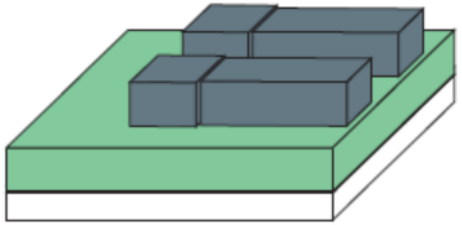

Microfabrication process

Pasivation

Oxide deposition

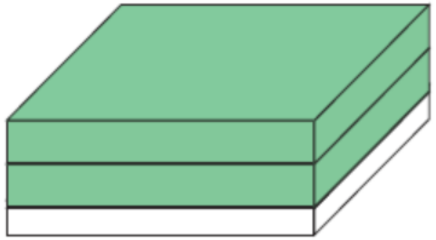

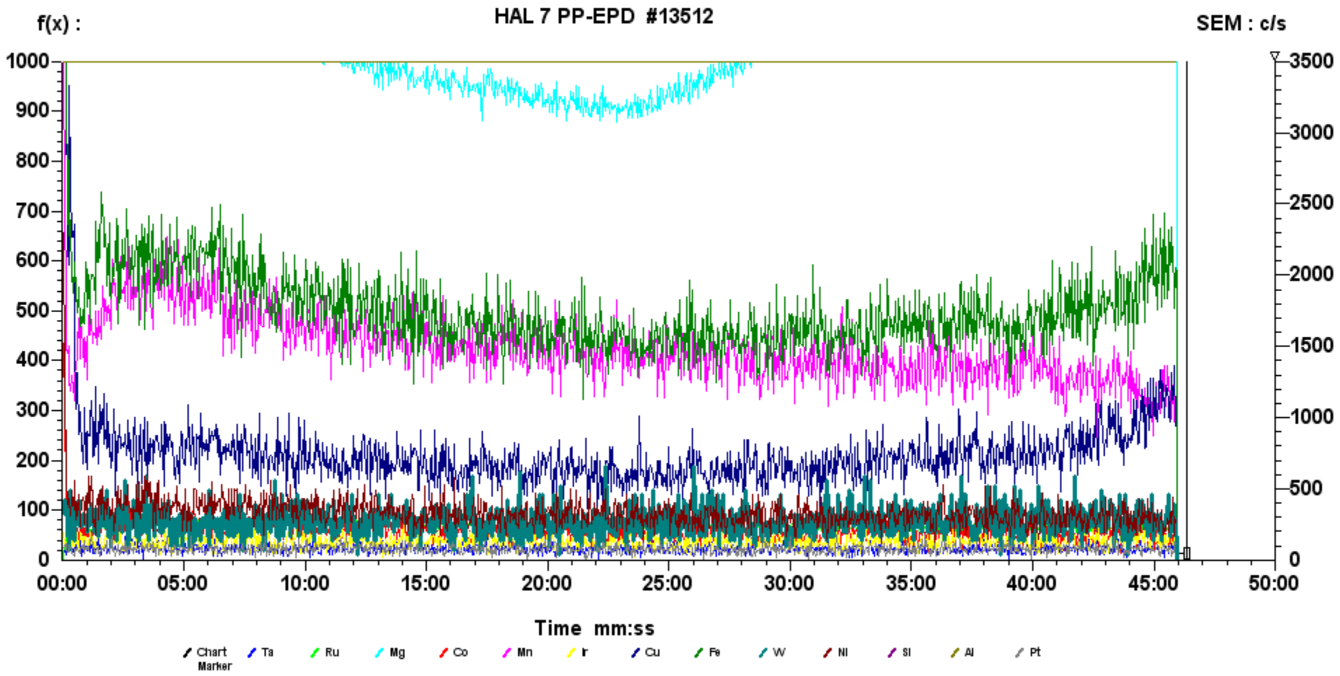

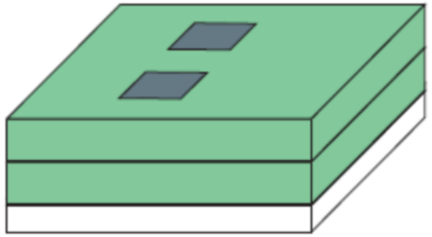

Microfabrication process

Process summary

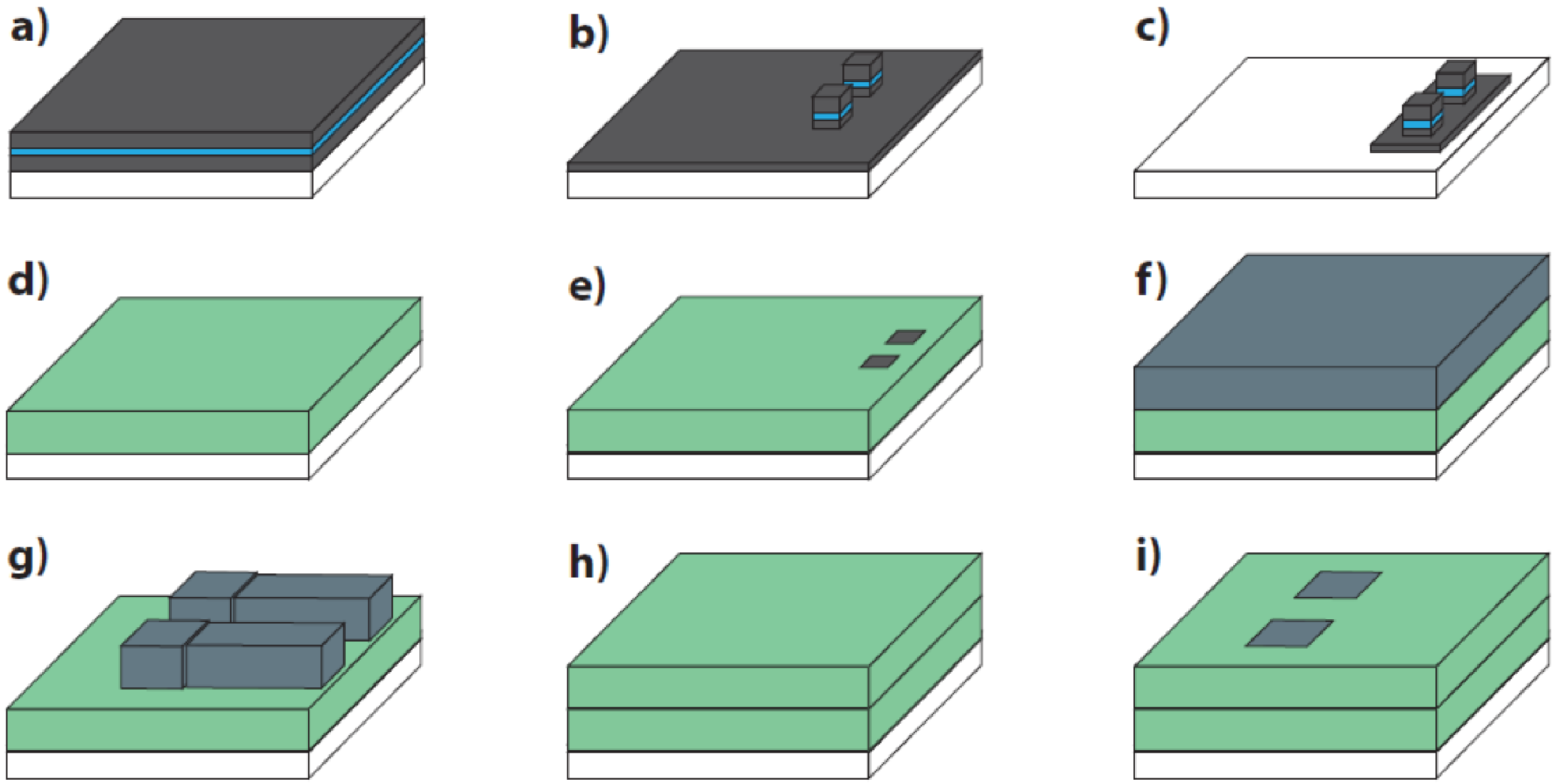

Post-process treatment

Magnetic annealing

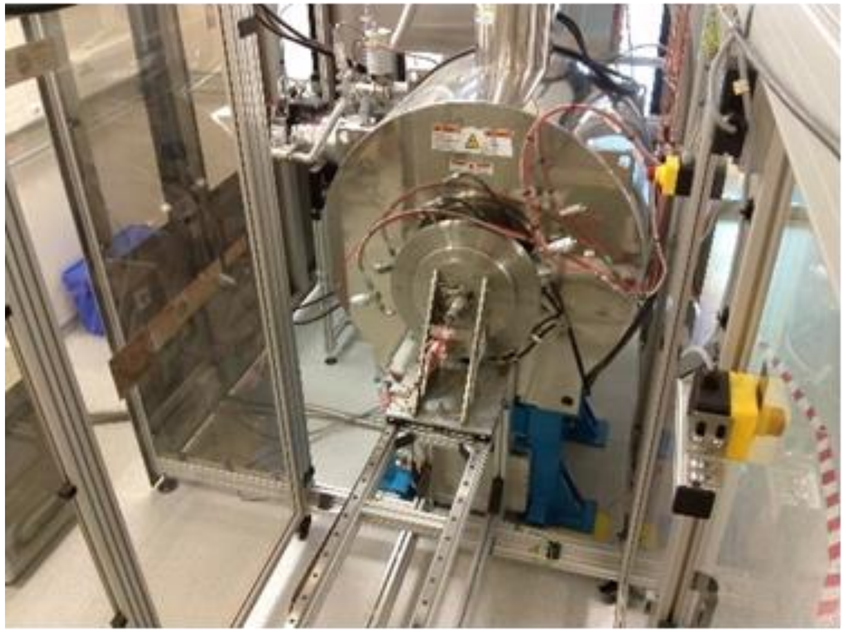

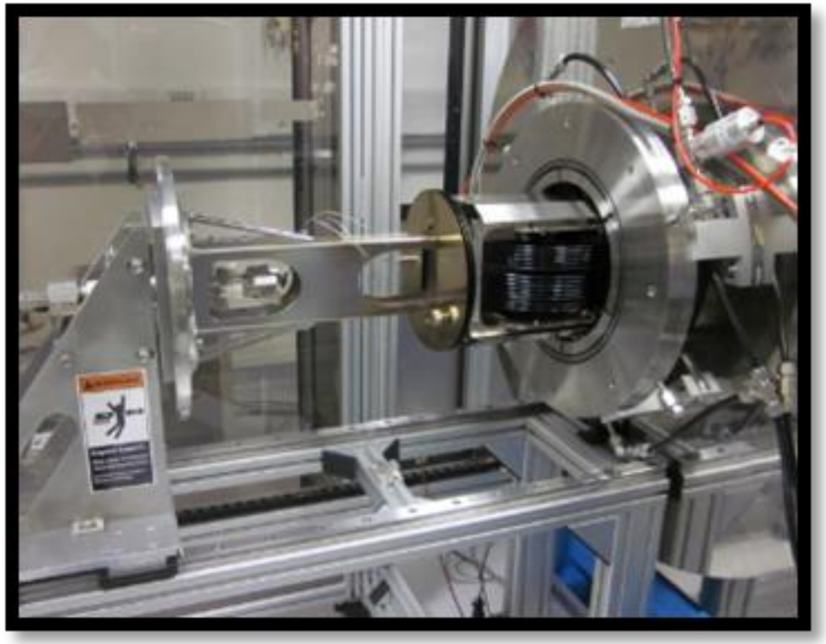

1h, 330ºC, 1T

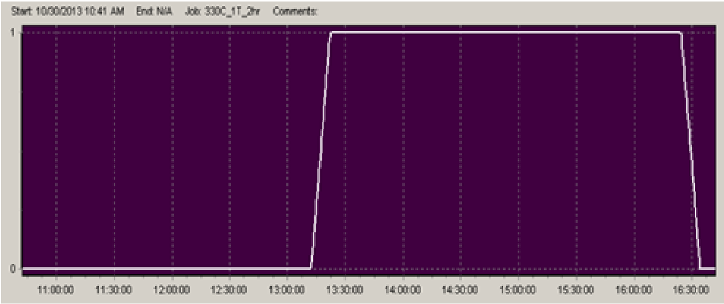

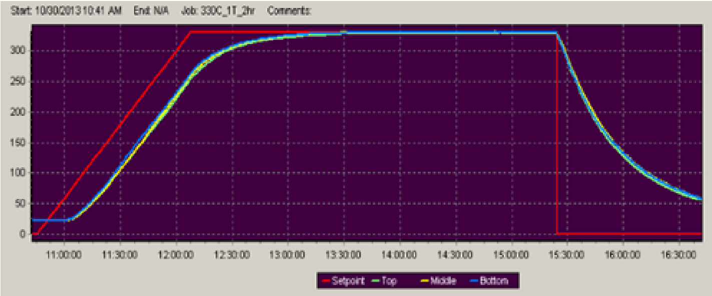

Required to:

- Set the correct crystalline structure CoFeB/MgO/CoFeB
- To control the exchange bias direction

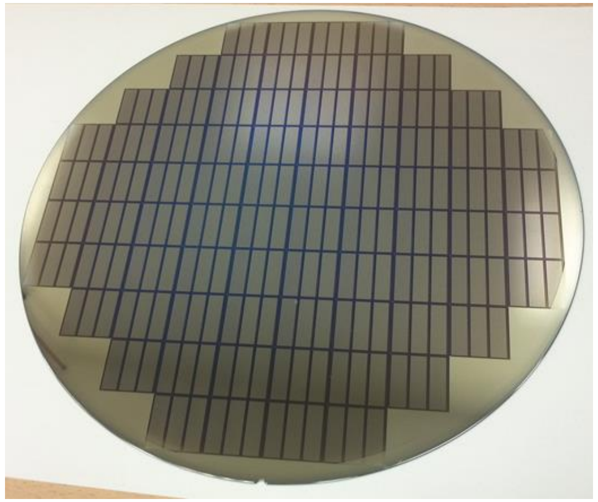

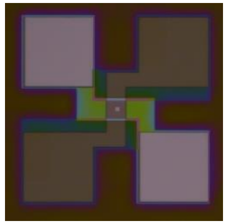

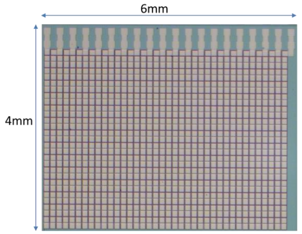

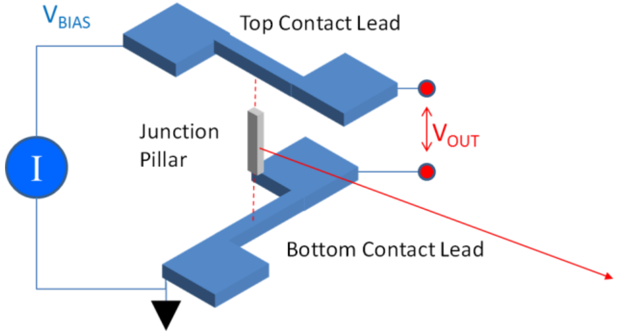

Typical MTJ stack thickness ~ 150 nm
The stack is made of 9 different alloys/materials

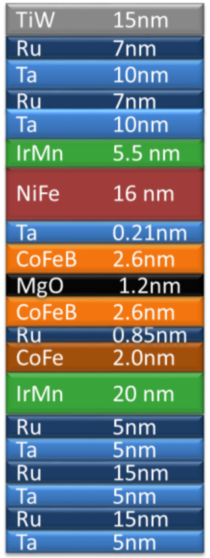

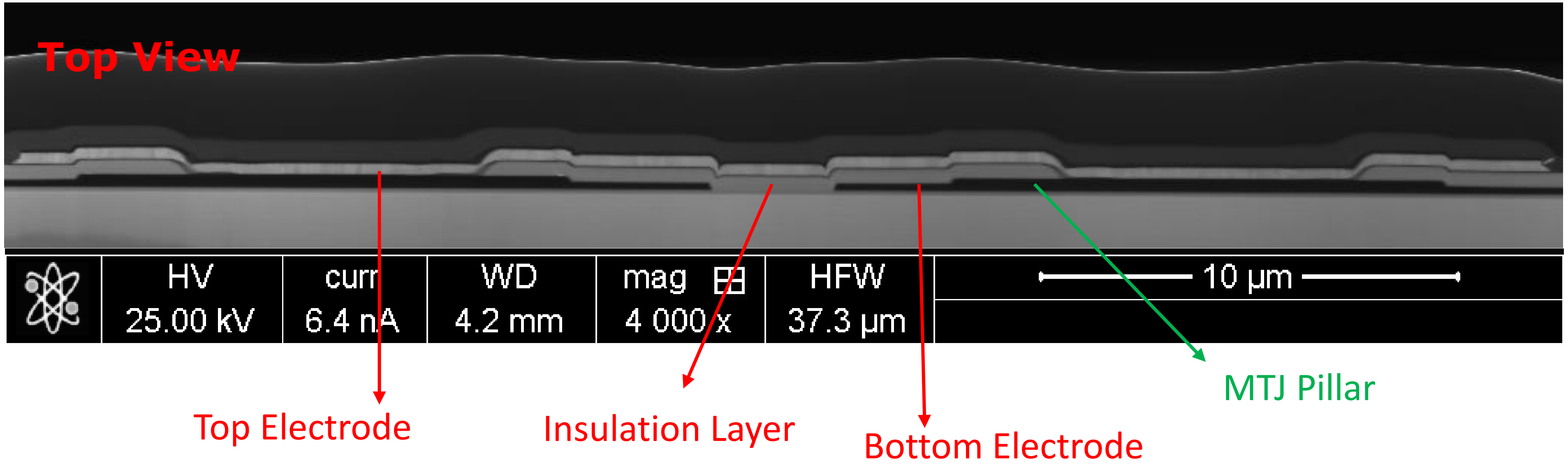

Characterization

Automatic probe station

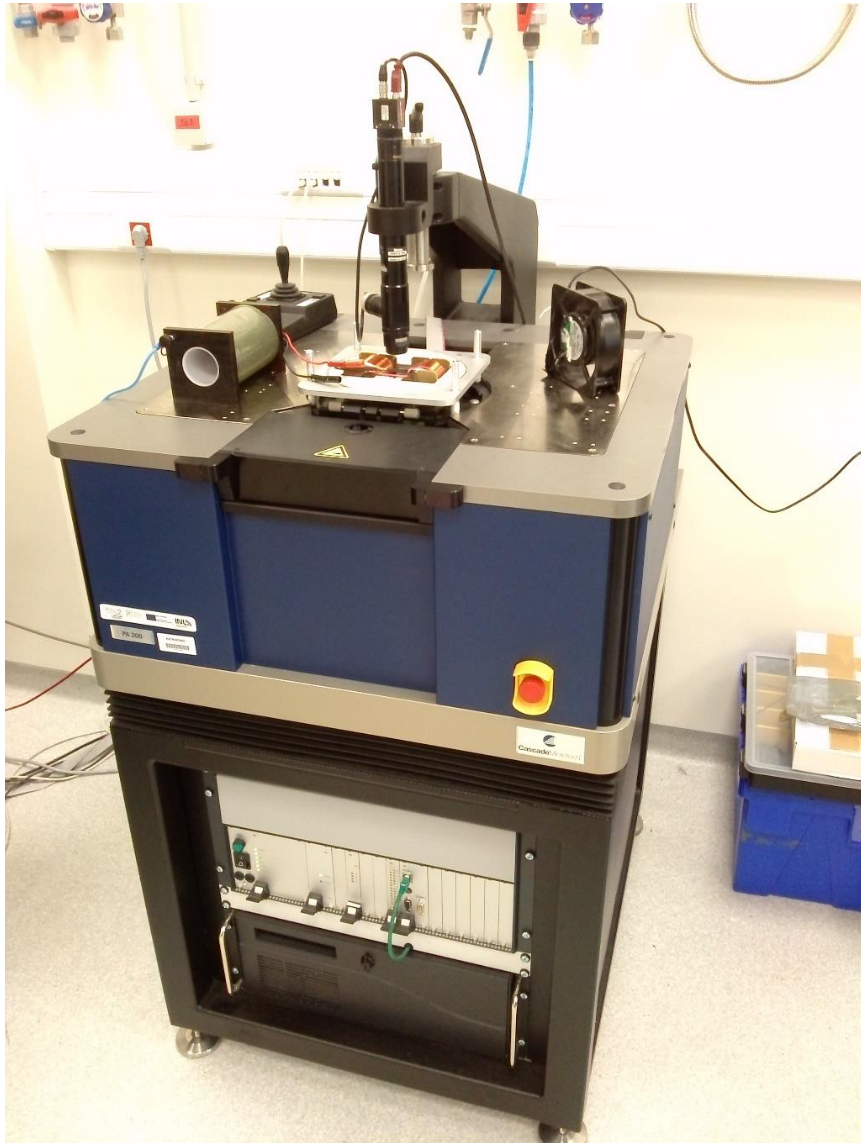

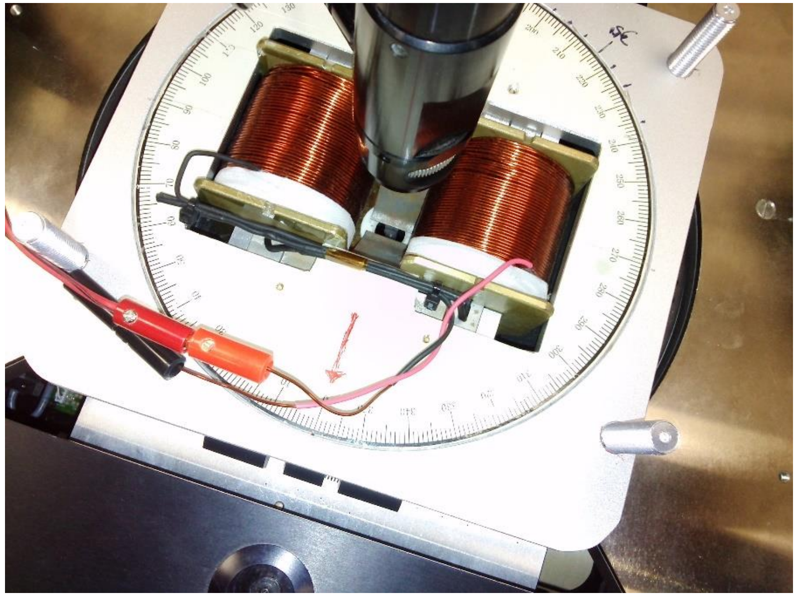

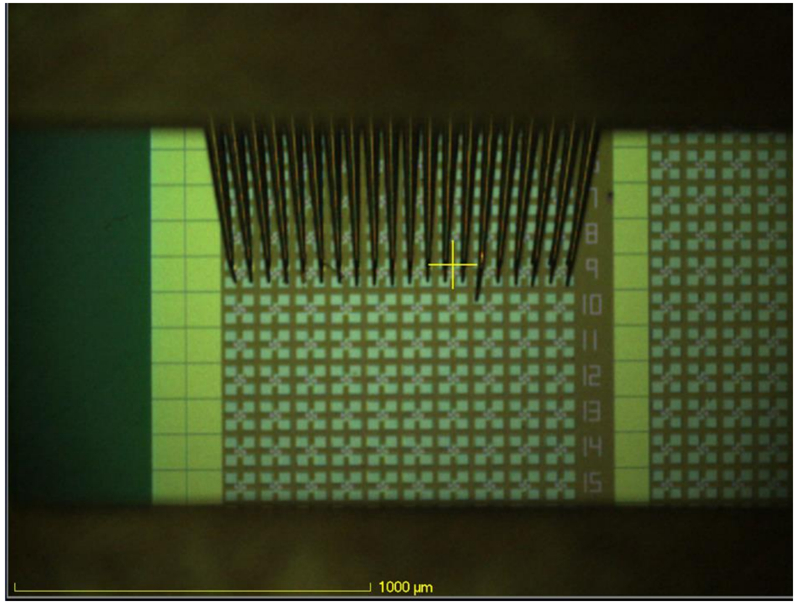

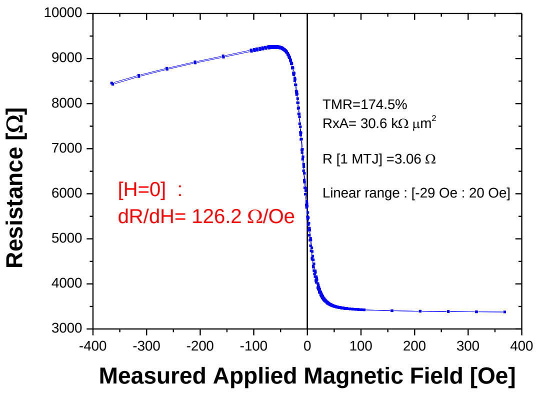

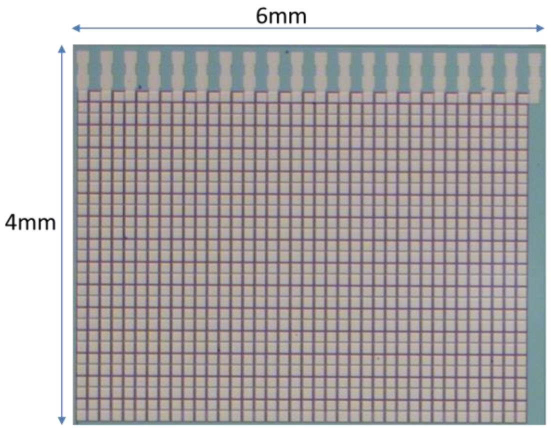

Large Series of 1102 MTJs with an area of 100x100 μm^2 each.

MTJ after process

Uniformity

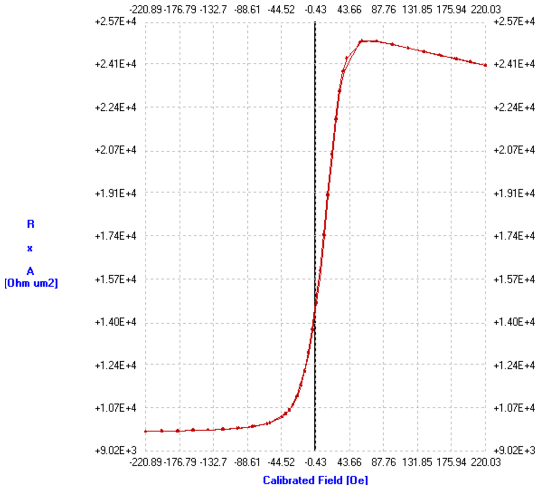

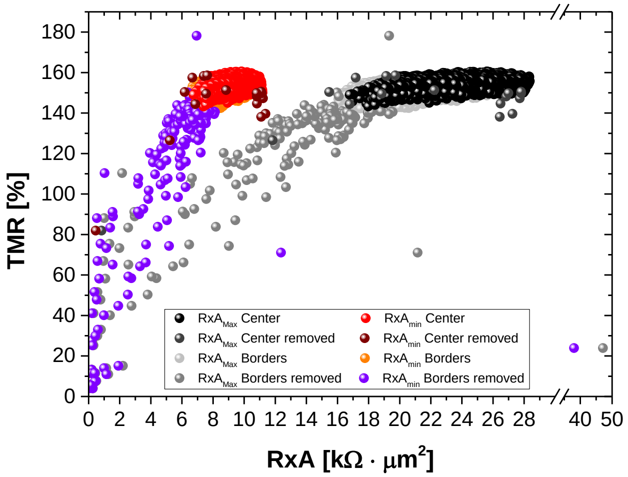

Uniformity = stdev/average * 100

1/σ Uniformity:
All 18.13%
Filtered 13.02%

1/σ Uniformity:
All 18.61%
Filtered 13.56%

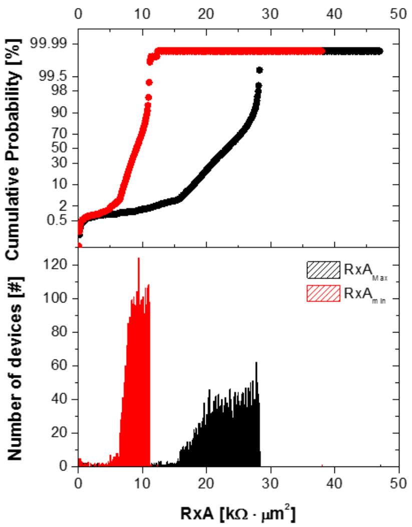

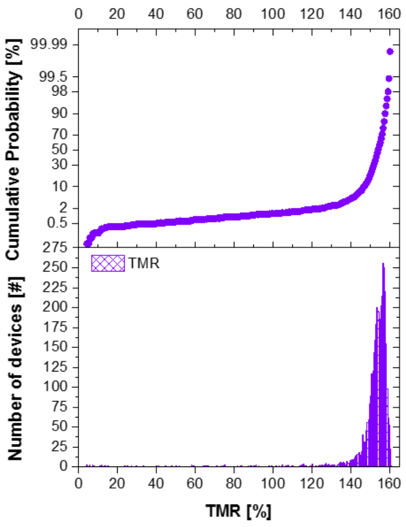

1/σ Uniformity:
All 9.85%
Filtered 2.36%

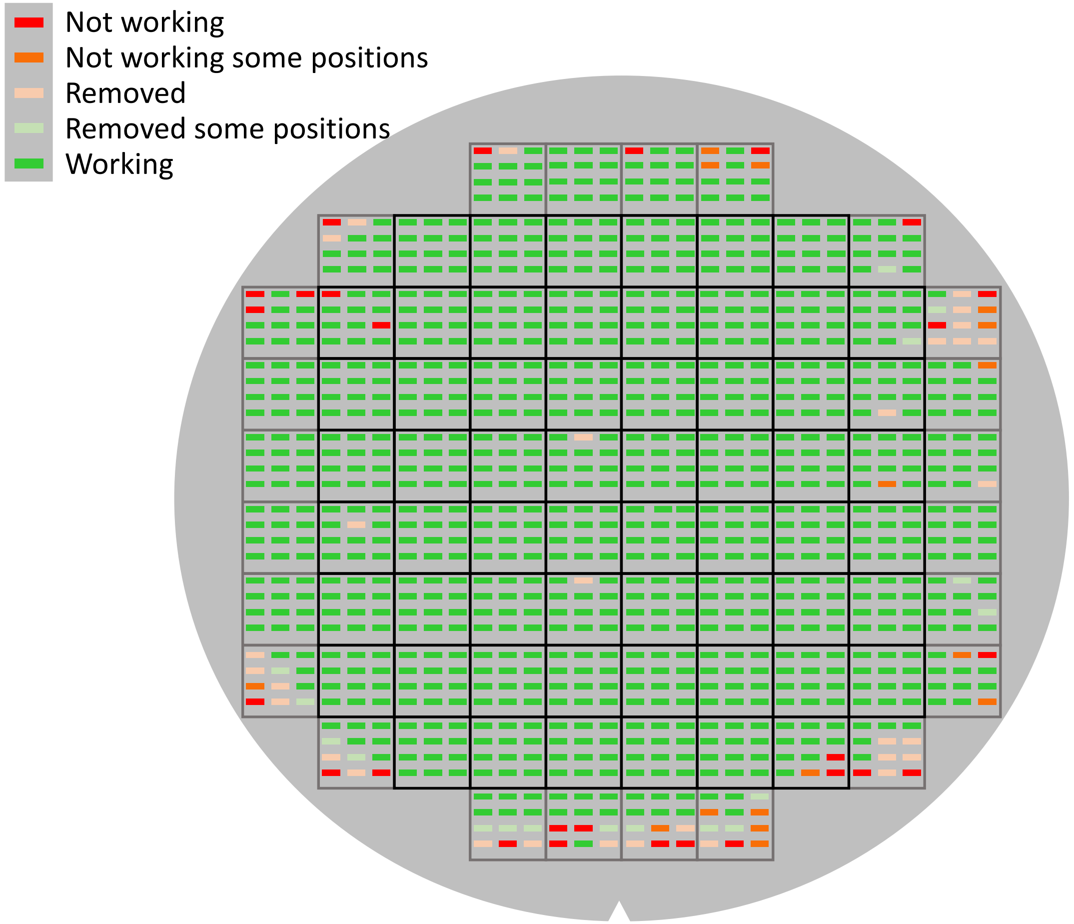

Part IV
MTJ stack linearization

Magnetic sensors

Applications

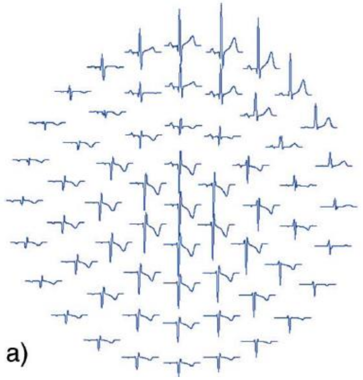

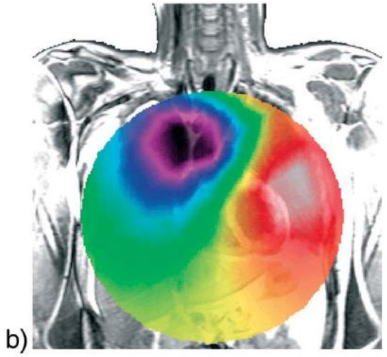

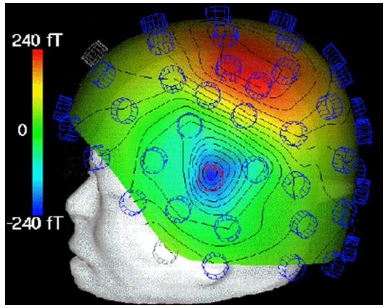

Conventional SQUID sensors

- Requires expensive cryogenic equipment
- Requires expensive shielded rooms

$$Magnetic\ Noise \propto \frac{1}{FL\ Volume}$$

Why MTJ sensors?

- They work at room temperature
- No need of expensive shielded rooms
- Low power consumption
- High output power

6x4 mm^2 array of 1102 MTJs connected in series with an individual area of 100x100 μm^2

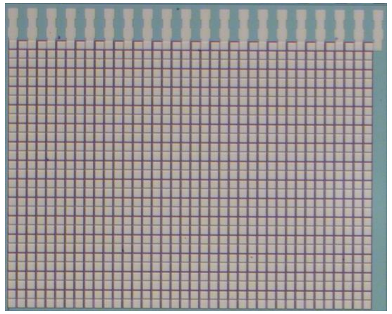

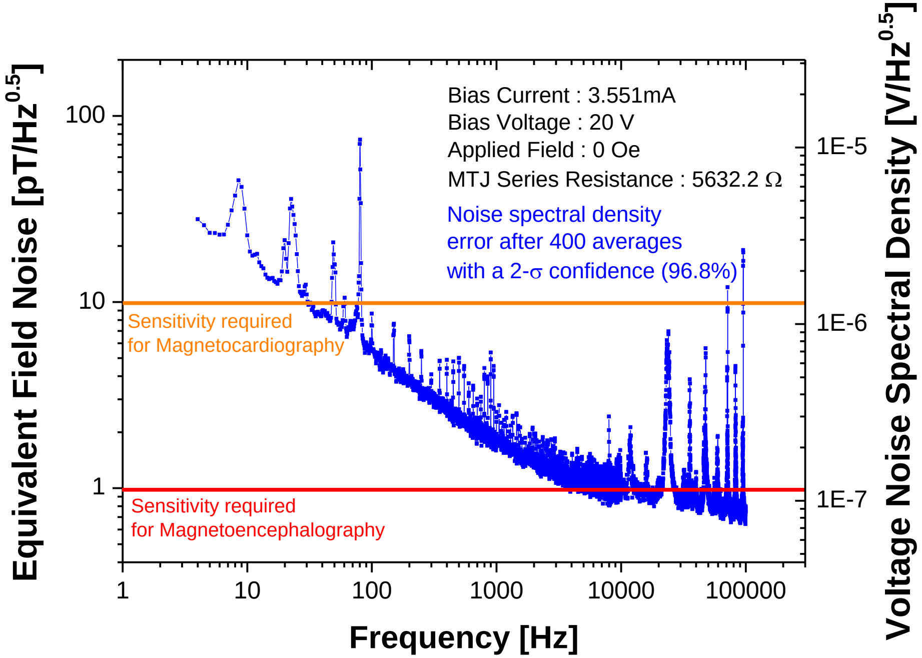

Magnetic sensors

Applications

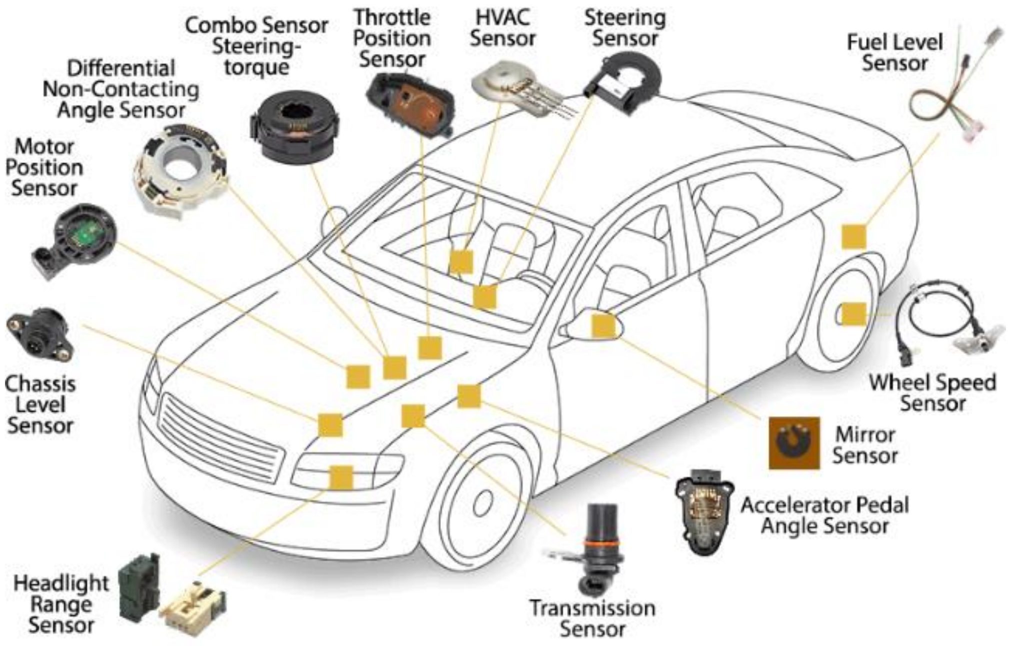

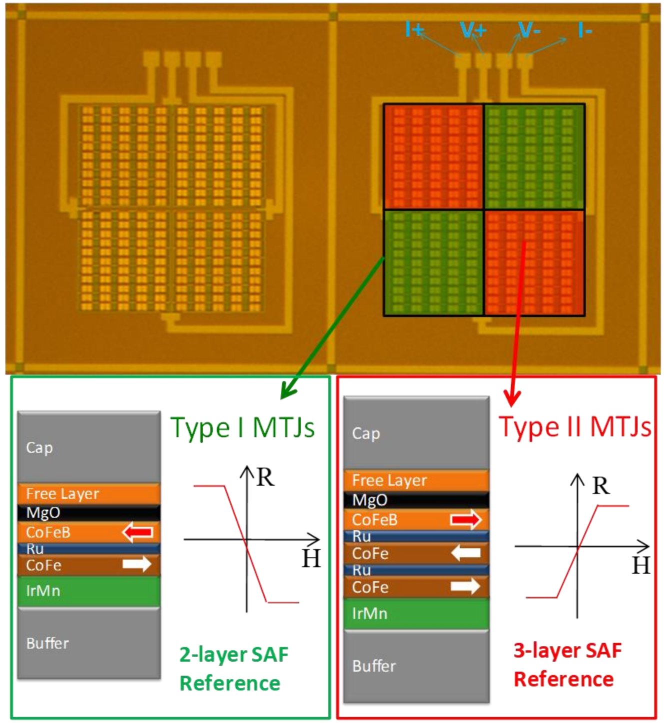

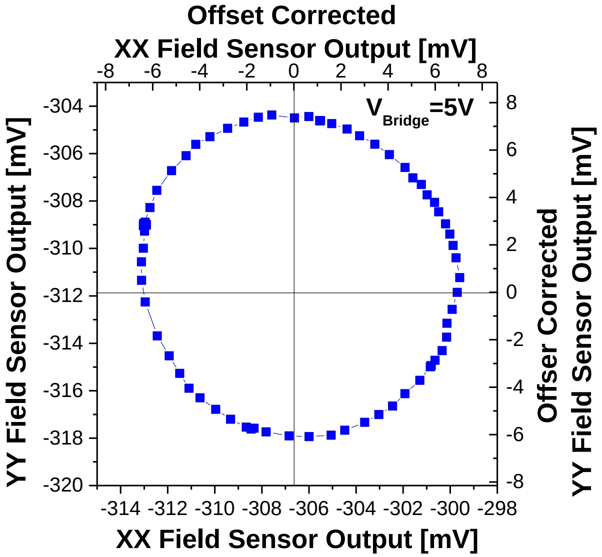

Why MTJ sensors?

- They have a good temperature stability
- They are robust and reliable devices
- Low power consumption
- High output power

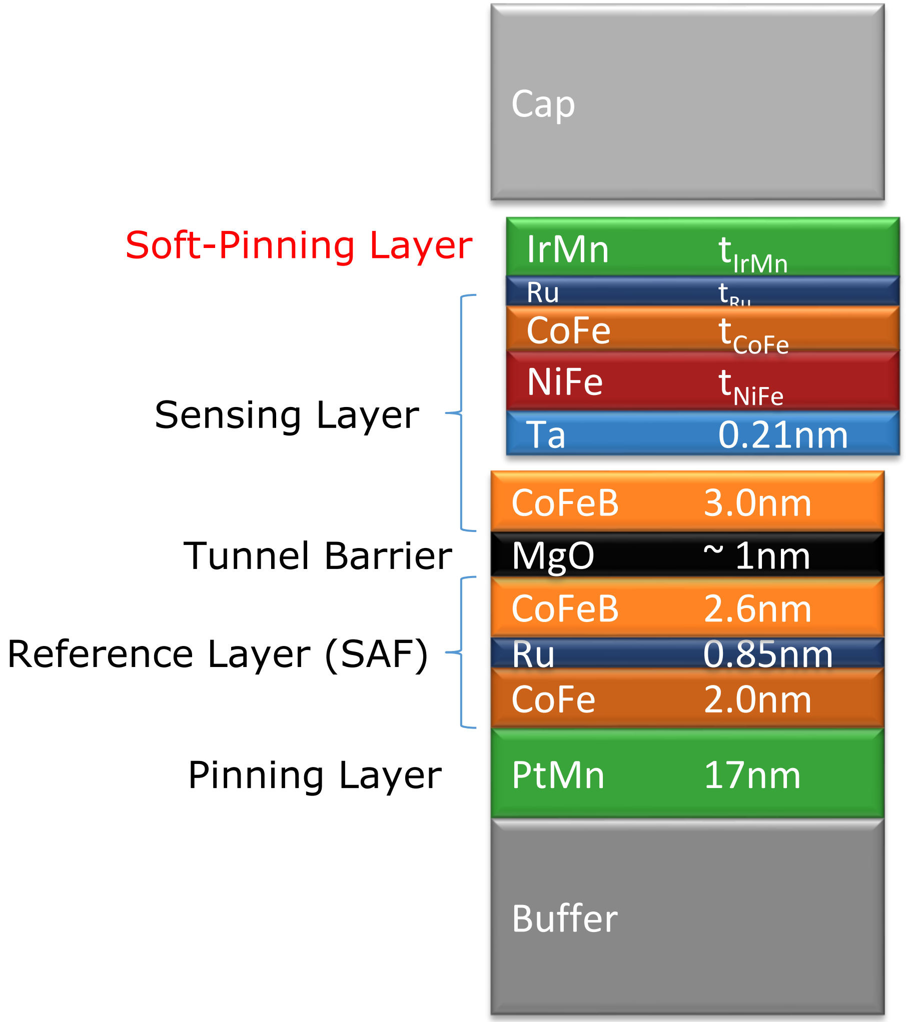

The sensing layer and the soft pinning layer thicknesses control the magnetic linear range of the sensors → Changing the thicknesses we control the sensitivity

3 Anisotropies involved:

- Magnetocrystalline: Uniaxial anisotropy (SL-Hk)
- Sensing layer soft pinning field (SL-Hex)
- Reference layer strong pinning field (RL-Hex)

Magnetic characterization

Characteristic fields

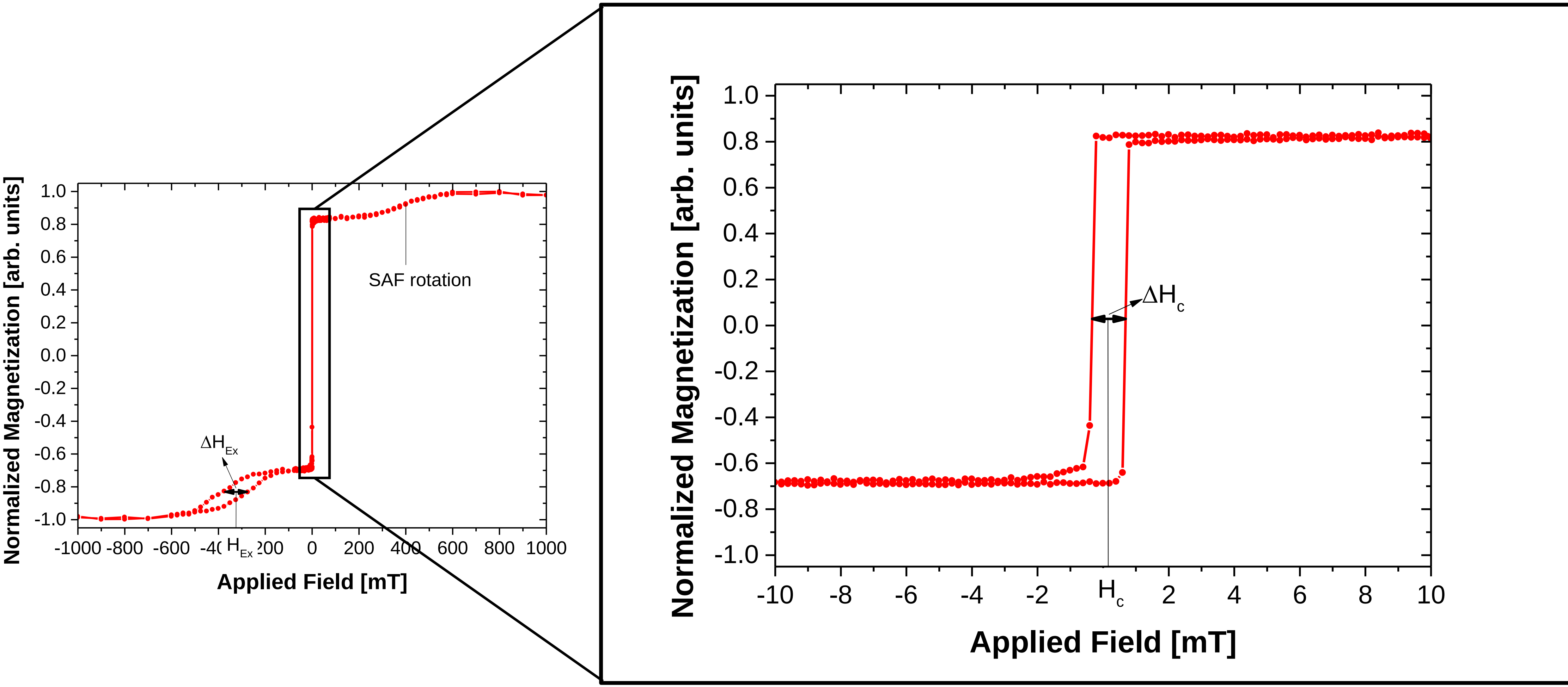

2-step annealing process

Process

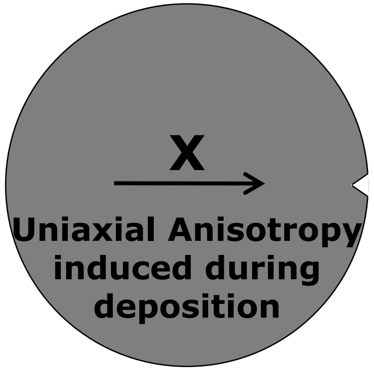

First annealing
330ºC 1T 2hr

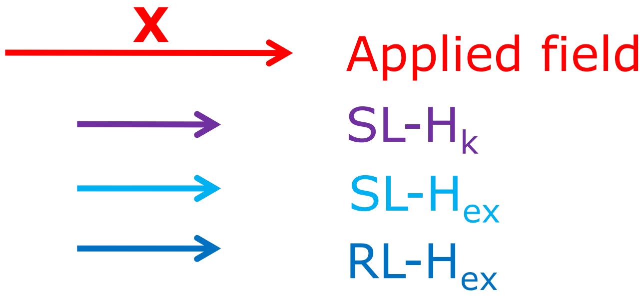

Second annealing

$T_{BlockSL\text{-}AFM} < T < T_{BlockRL\text{-}AFM}$

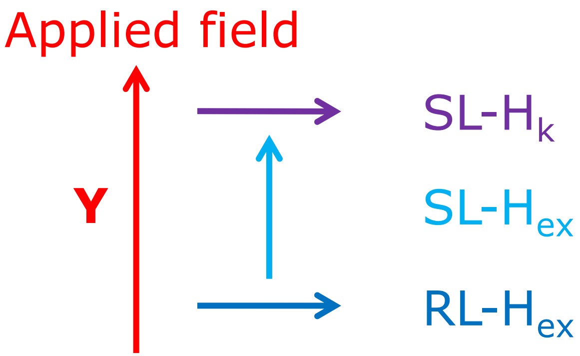

1st annealing

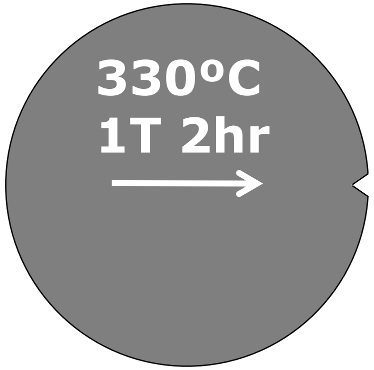

2nd annealing

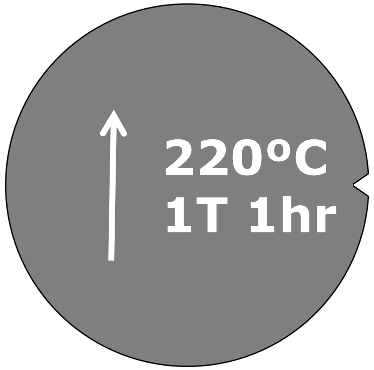

Tunable linear response of the sensing layer with respect to the external magnetic field

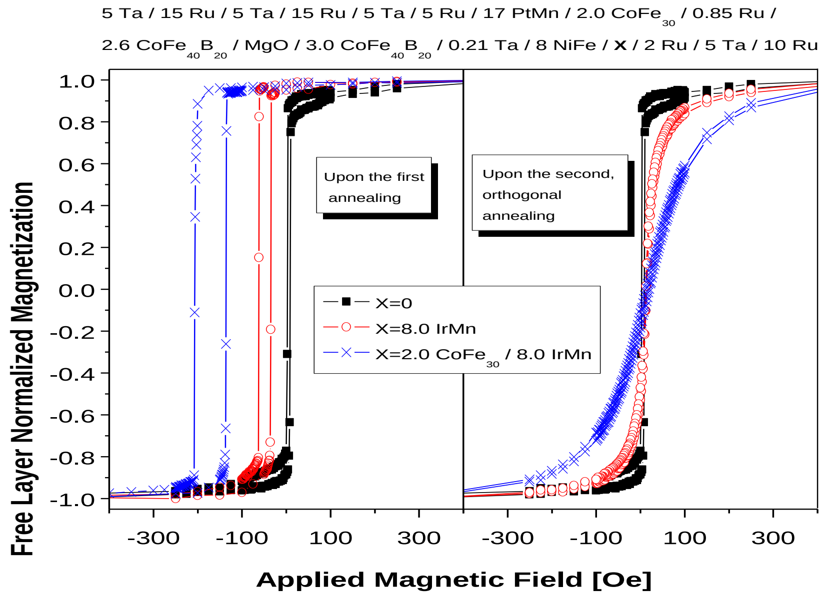

Ruthenium

5 Ta / 50 CuN / 5 Ta / 50 CuN / 5 Ta / 5 Ru / 17 PtMn / 2 $CoFe_{30}$ / 0.85 Ru / 2.6 $CoFe_{40}B_{20}$ / **MgO** / 3 $CoFe_{40}B_{20}$ / 0.21 Ta / 16 NiFe / t_{Ru} / 5.5 IrMn / 10 Ta / 30 CuN / 7 Ru

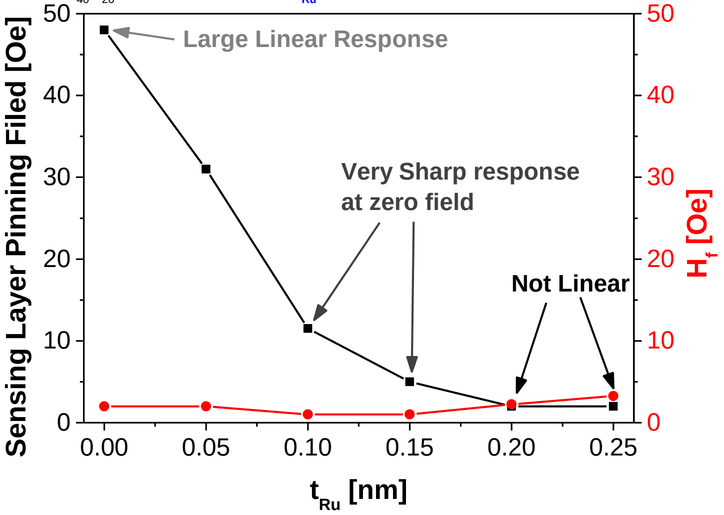

- The spacer Ru reduces the linear range.

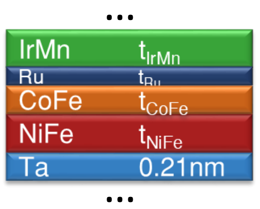

Iridium Manganese

5 Ta / 50 CuN / 5 Ta / 50 CuN / 5 Ta / 5 Ru / 17 PtMn / 2 $CoFe_{30}$ / 0.85 Ru / 2.6 $CoFe_{40}B_{20}$ / MgO / 3 $CoFe_{40}B_{20}$ / 0.21 Ta / 16 NiFe / t_{IrMn} / 10 Ta / 30 CuN / 7 Ru

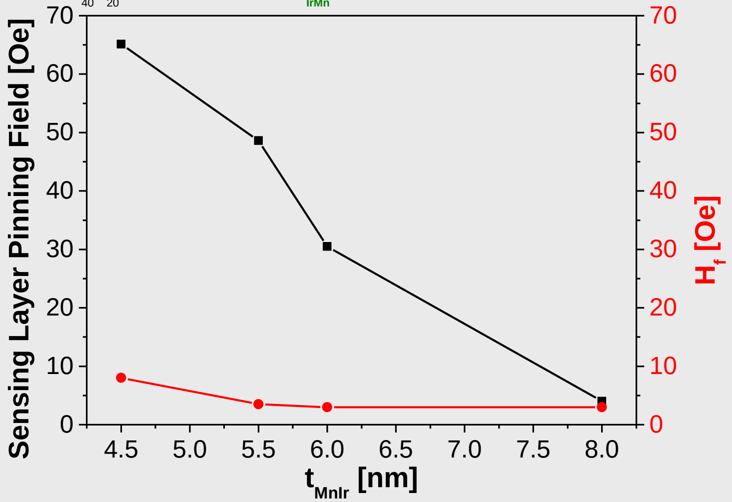

- Exchange decreases with increasing MnIr thickness.
- Thinner MnIr appears to be better textured than thicker MnIr.

Nickle Iron

5 Ta / 15 Ru / 5 Ta / 15 Ru / 5 Ta / 5 Ru / 20 PtMn / 2 $CoFe_{30}$ / 0.85 Ru / 2.6 $CoFe_{40}B_{20}$ / **MgO** / 3 $CoFe_{40}B_{20}$ / 0.21 Ta / t_{NiFe} / 6 IrMn / 2 Ru / 5 Ta / 10 Ru

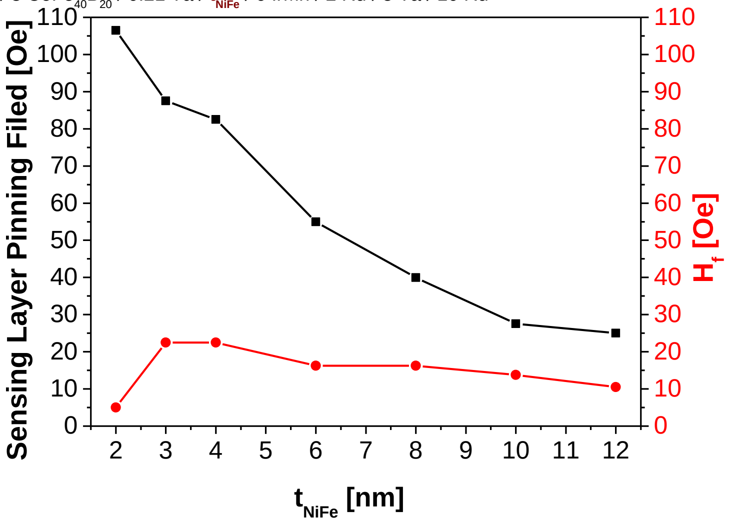

- Changing the thicknesses of NiFe and CoFe allows the sensing layer slope to be tuned over a large range.

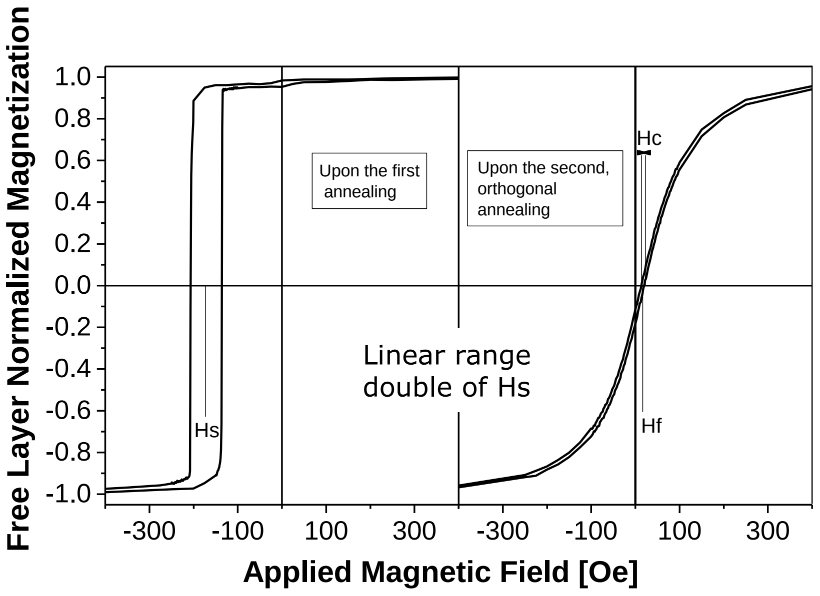

- Successfully lineared MTJs with linear ranges > 60-100 Oe

Most demanding requirements
Hs < 30 Oe
Hc < 1 Oe
Hf < 1 Oe

- Usually fails to meet the most demanding requirements for sensing applications

- With the 2 annealing process we are not taking into account the magnetocrystalline anisotropy.
- We try to linearize with a 3 annealing process to control the 3 anisotropies independently

European patent: EP15171162.9

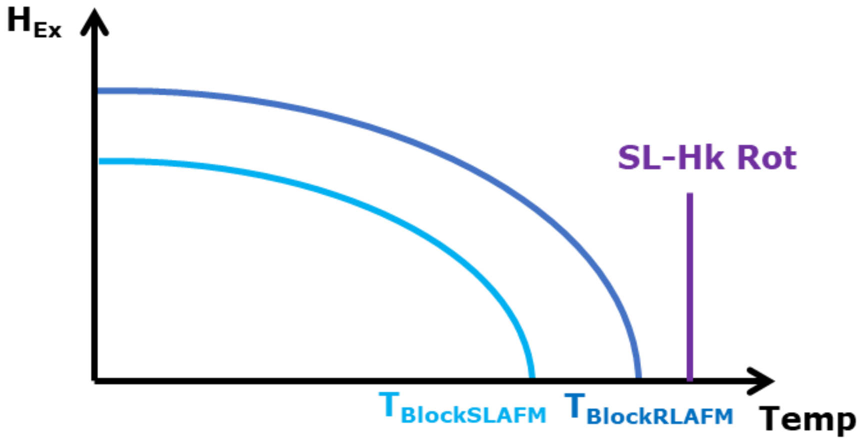

3-step annealing process

Process

- Different times, temperatures and directions can be used to control all the anisotropies of the stack

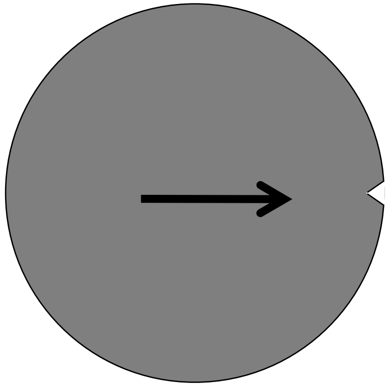

Uniaxial Anisotropy induced during deposition

First annealing

Applied field

Uniaxial Anisotropy

Top AFM

Bottom AFM

Second annealing ($T_{BlockBAFM}<T$)

Applied field

Uniaxial Anisotropy

Top AFM

Bottom AFM

Third annealing ($T_{BlockTAFM}<T< T_{BlockIBAFM}$)

Applied field

Uniaxial Anisotropy

Top AFM

Bottom AFM

1st Annealing

330ºC 1T 2hr

- To crystallize the CoFeB/MgO/CoFeB
- To achieve a large TMR ratio

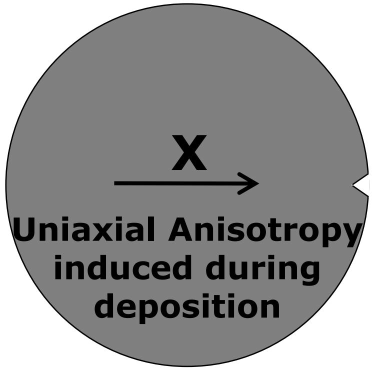

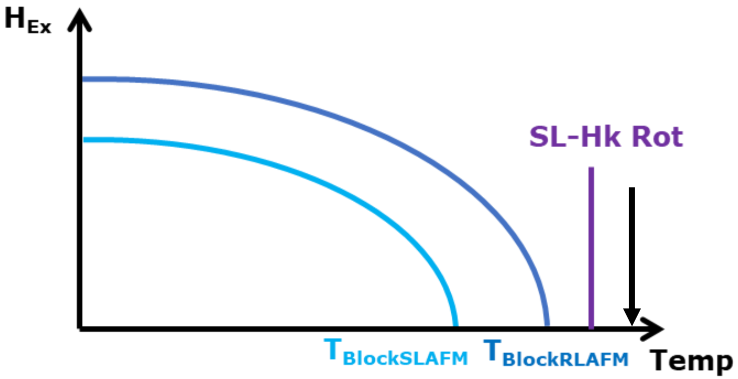

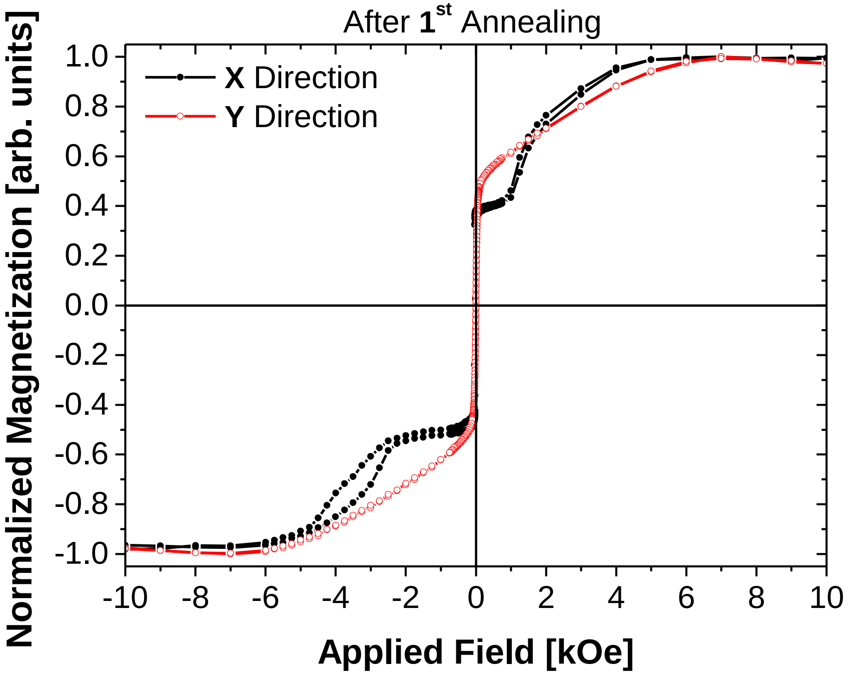

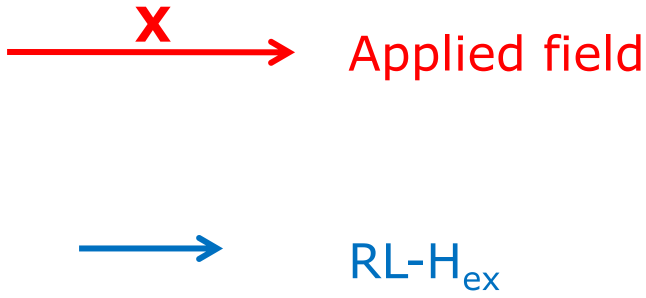

3-step annealing process

1st Annealing

330ºC 1T 2hr

- To crystallize the CoFeB/MgO/CoFeB
- To achieve a large TMR ratio

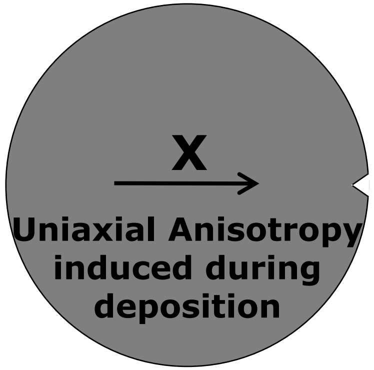

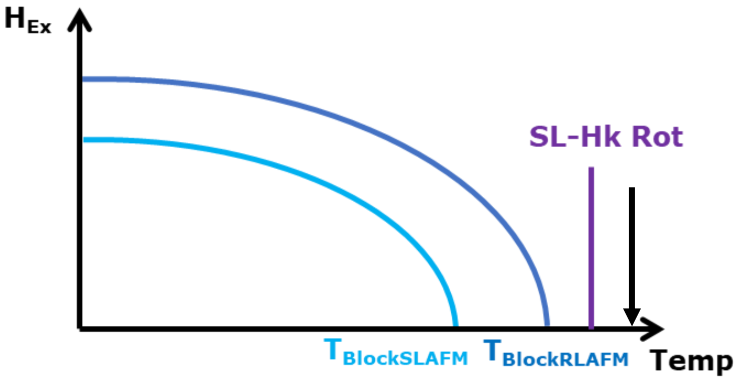

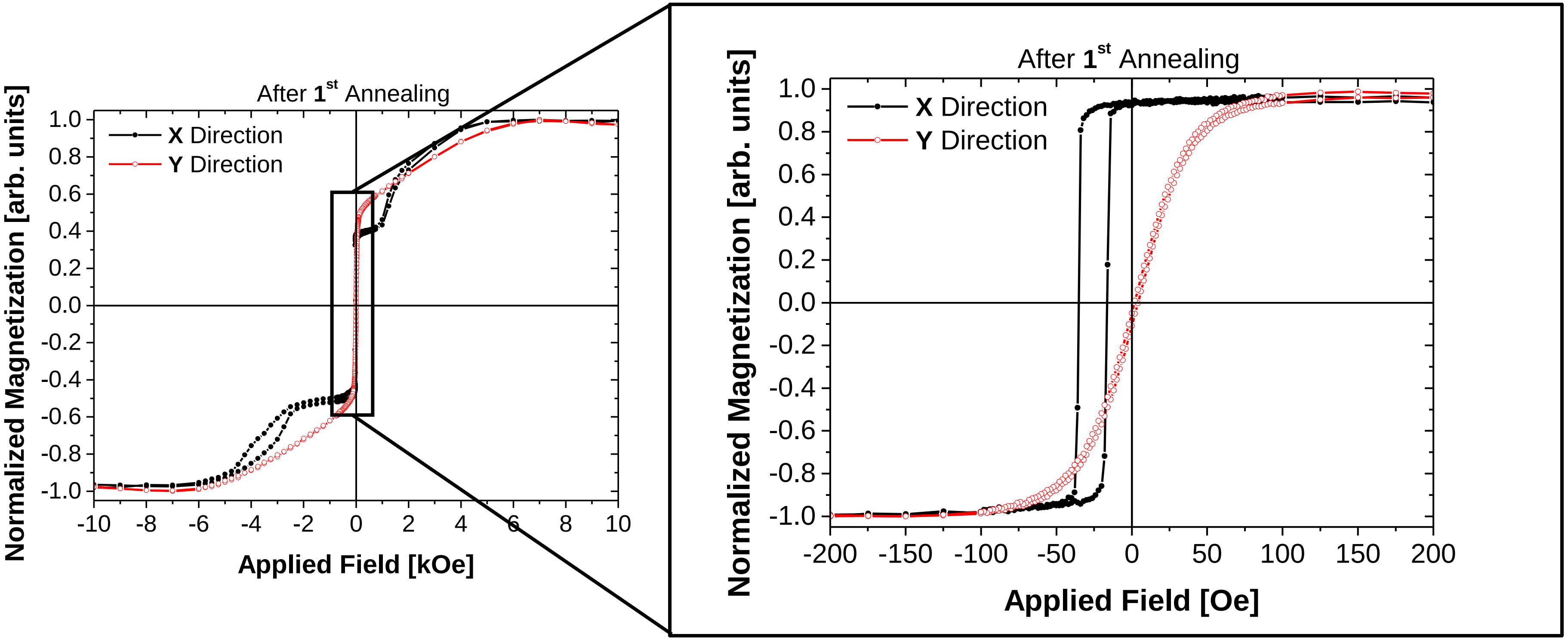

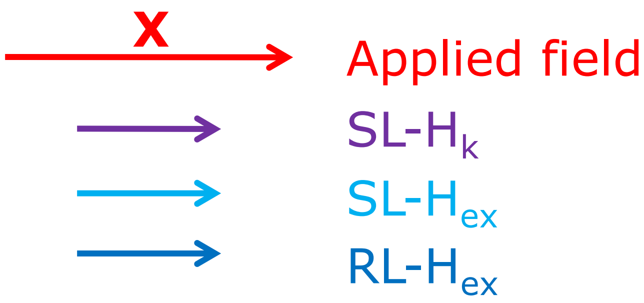

$T_{BlockRL-AFM}$ < T < 275ºC (270ºC 1T 2hr)

- To rotate both AFM without rotating the SL-Hk
- Temp: - Above the block temperature of the reference layer AFM
  - Below 275ºC at which the magnetocrystalline anisotropy rotates

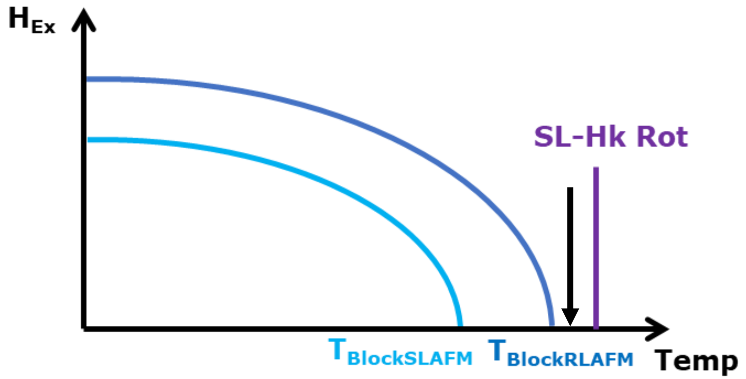

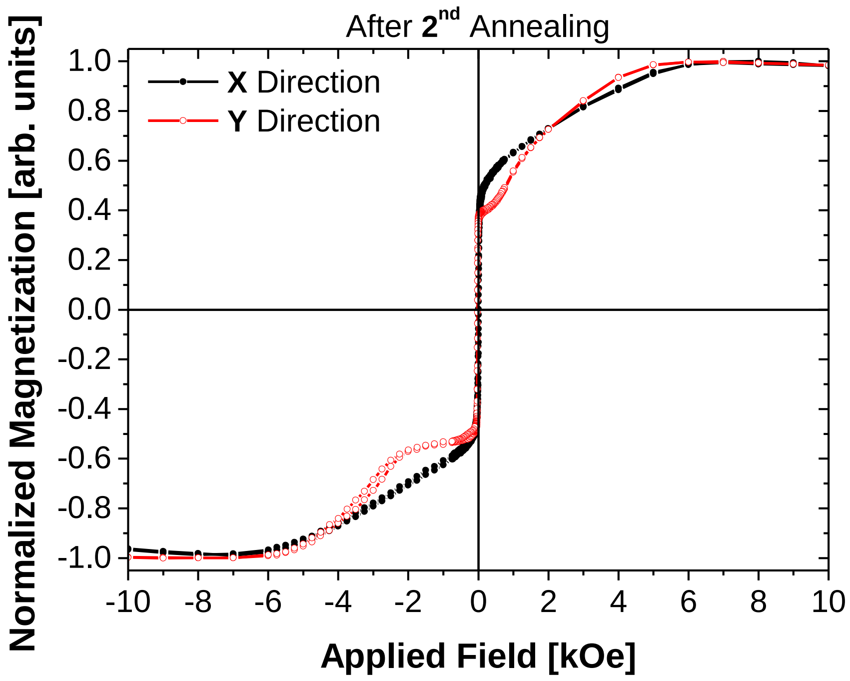

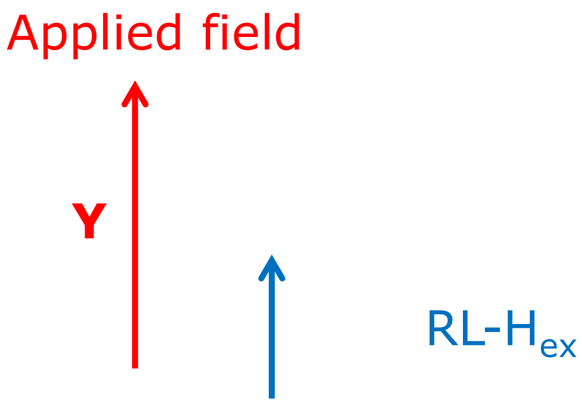

$T_{BlockRL\text{-}AFM} < T < 275^{o}C$ (270ºC 1T 2hr)

- To rotate both AFM without rotating the SL-Hk
- Temp: - Above the block temperature of the reference layer AFM
  - Below 275ºC at which the magnetocrystalline anisotropy rotates

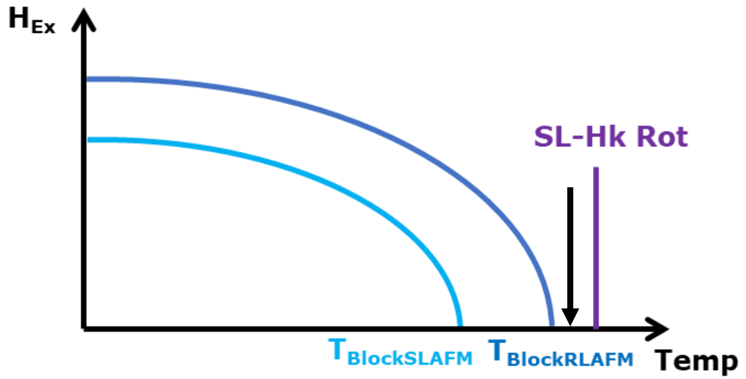

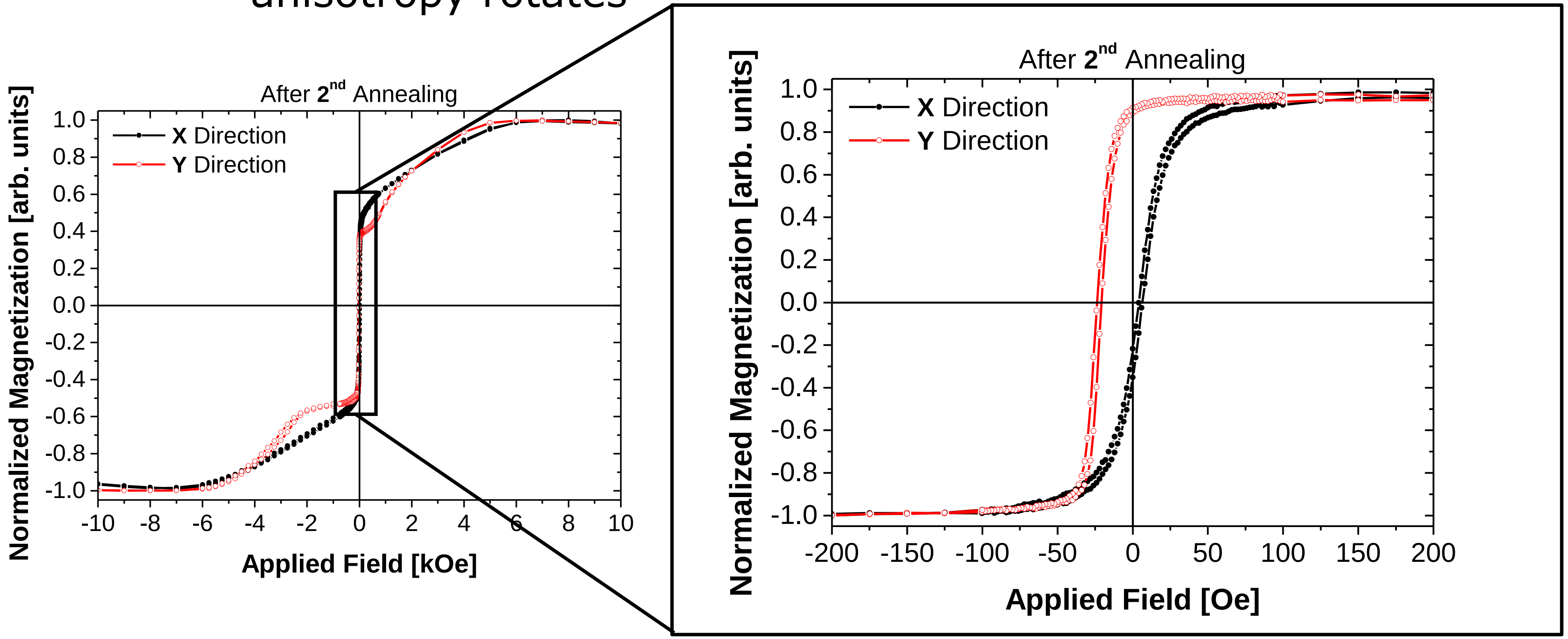

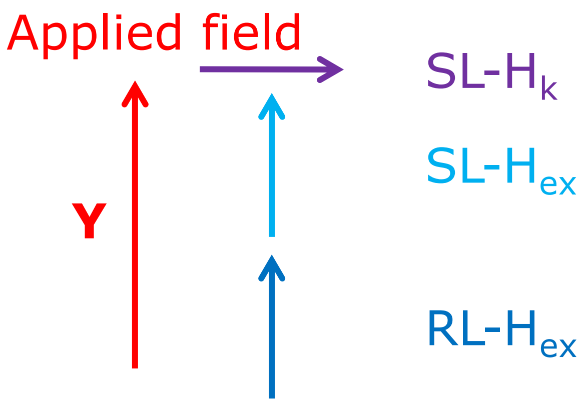

3-step annealing process

3rd Annealing

$T_{BlockSL\text{-}AFM}$ < T < $T_{BlockRL\text{-}AFM}$ (150ºC 0.02T 1hr)

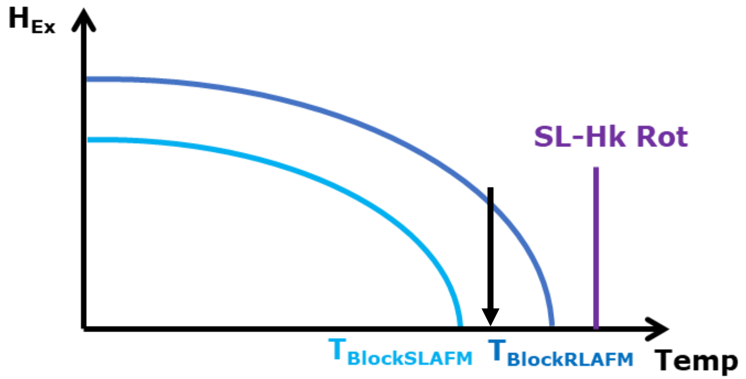

- To rotate SL AFM without rotating nothing else
- Temp: - Below the block temperature of the reference layer AFM
  - Above the block temperature of the sensing layer AFM
- Field: Enough to rotate the sensing layer

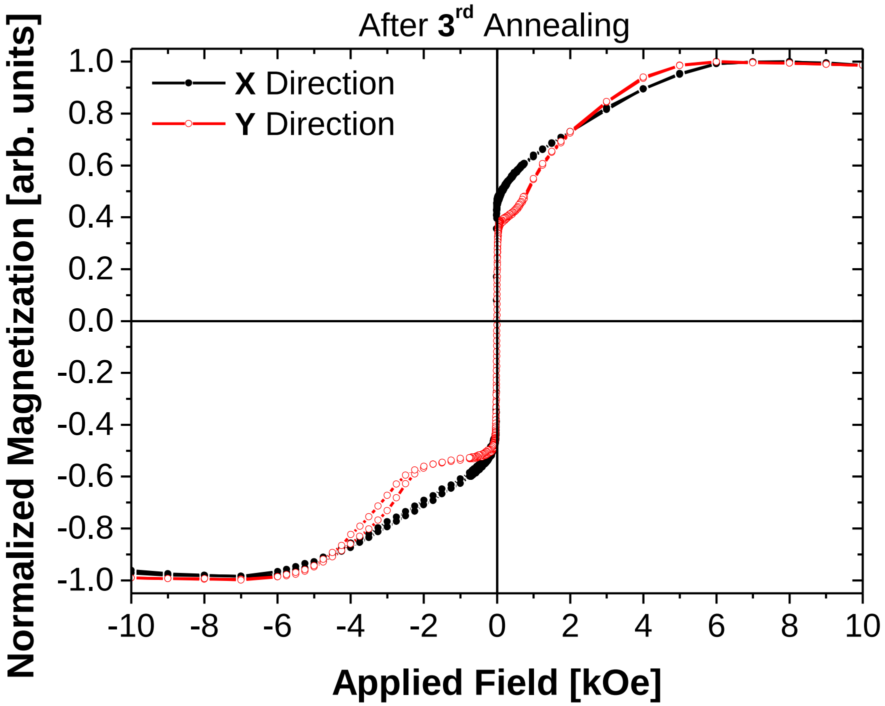

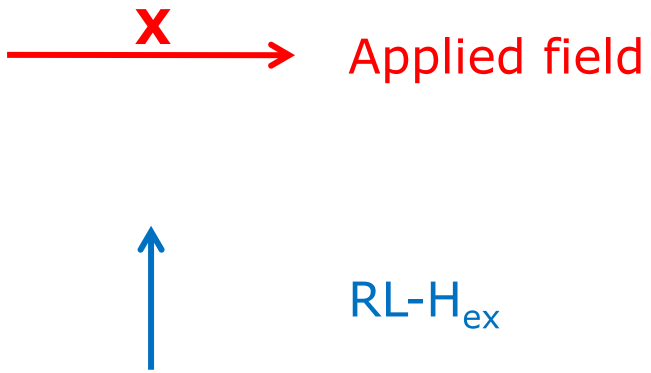

3-step annealing process

3rd Annealing

$T_{BlockSL\text{-}AFM} < T < T_{BlockRL\text{-}AFM}$ (150ºC 0.02T 1hr)

- To rotate SL AFM without rotating nothing else
- Temp: - Below the block temperature of the reference layer AFM
  - Above the block temperature of the sensing layer AFM
- Field: Enough to rotate the sensing layer

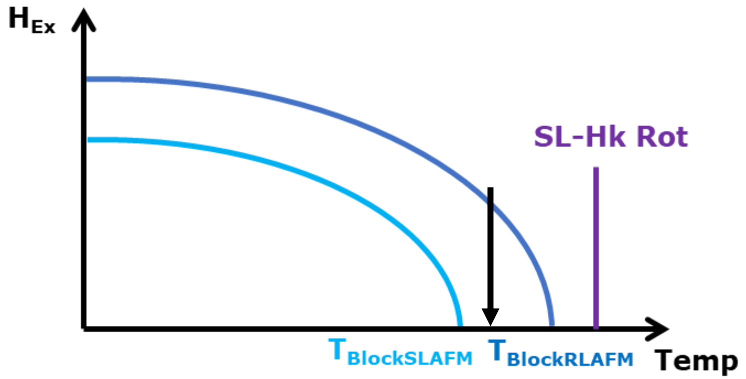

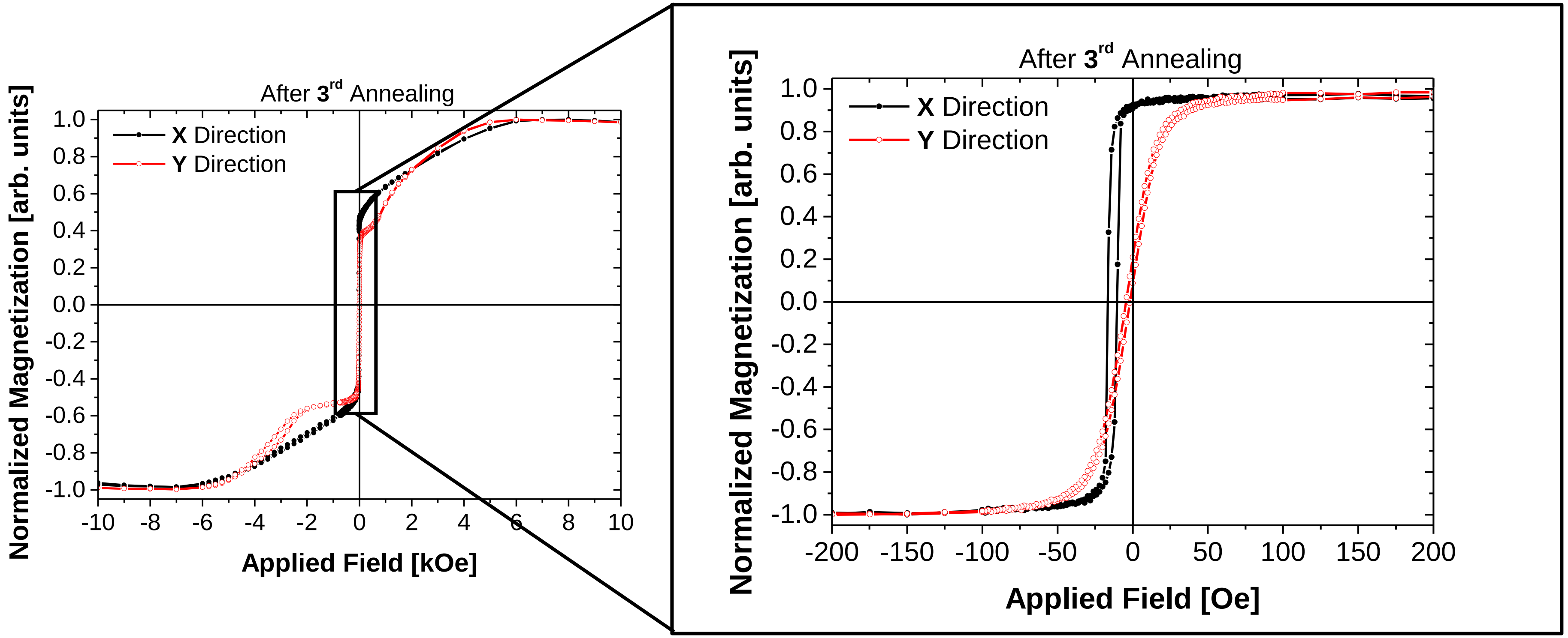

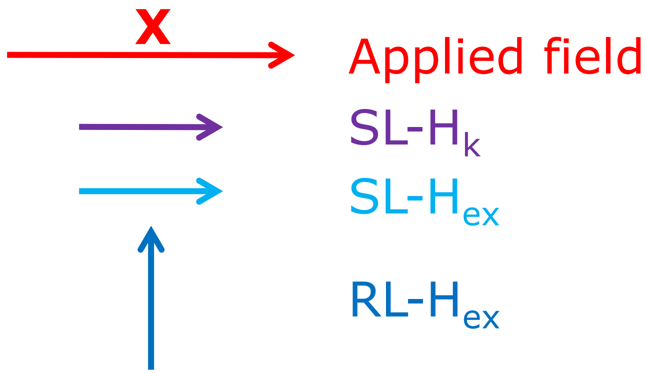

2-step vs 3-step annealing process

Magnetic behaviour

SAME STACK

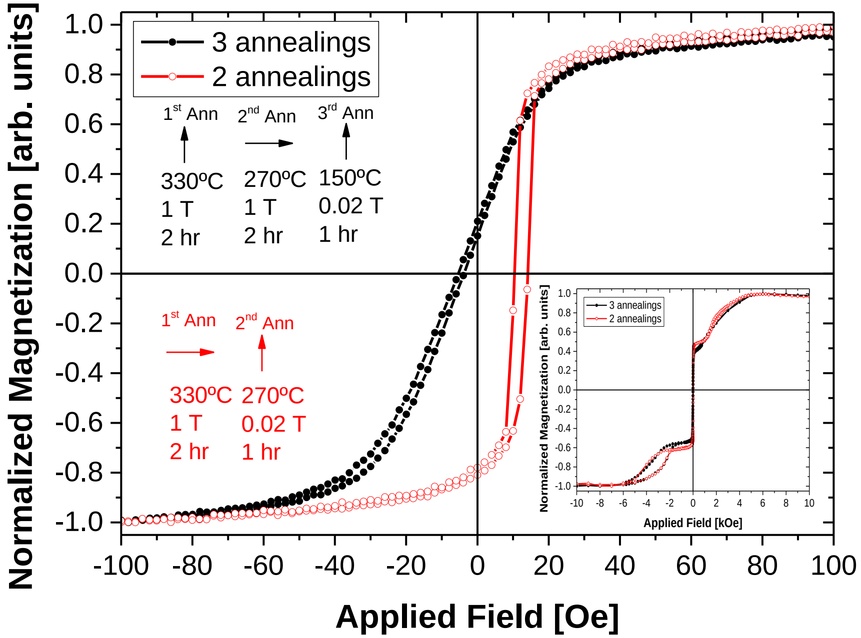

SAME LINEAR RANGE

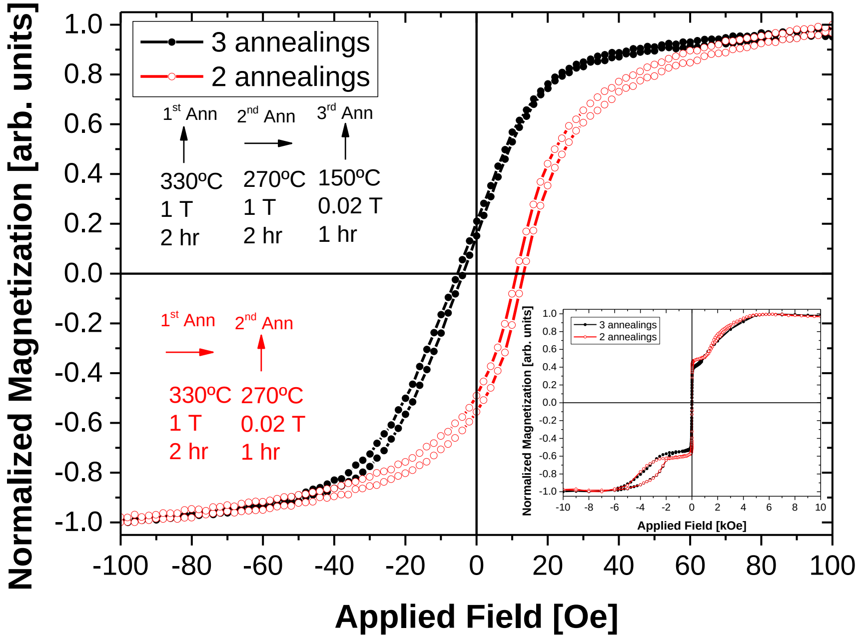

Same stack:

	3 Annealings	2 Annealings
t_{NiFe}	4 nm	4 nm
t_{Ru}	0.2 nm	0.2 nm

$SL\text{-}H_K > SL\text{-}H_{ex}$

Impossible to linearize with 2 annealings

Same linear range:

	3 Annealings	2 Annealings
t_{NiFe}	4 nm	8 nm
t_{Ru}	0.2 nm	0 nm

$SL\text{-}H_K < SL\text{-}H_{ex}$

Better linearization with 3 than with 2 annealings (Better H_c and H_f)

2-step vs 3-step annealing process

Temperature behavior

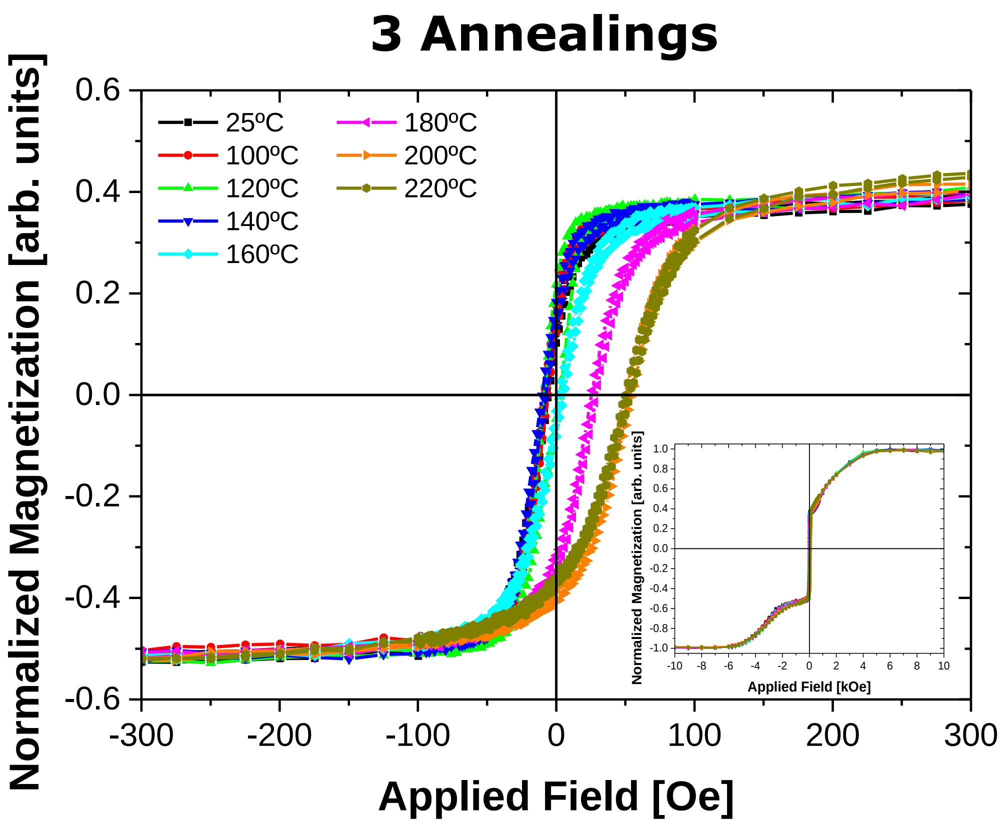

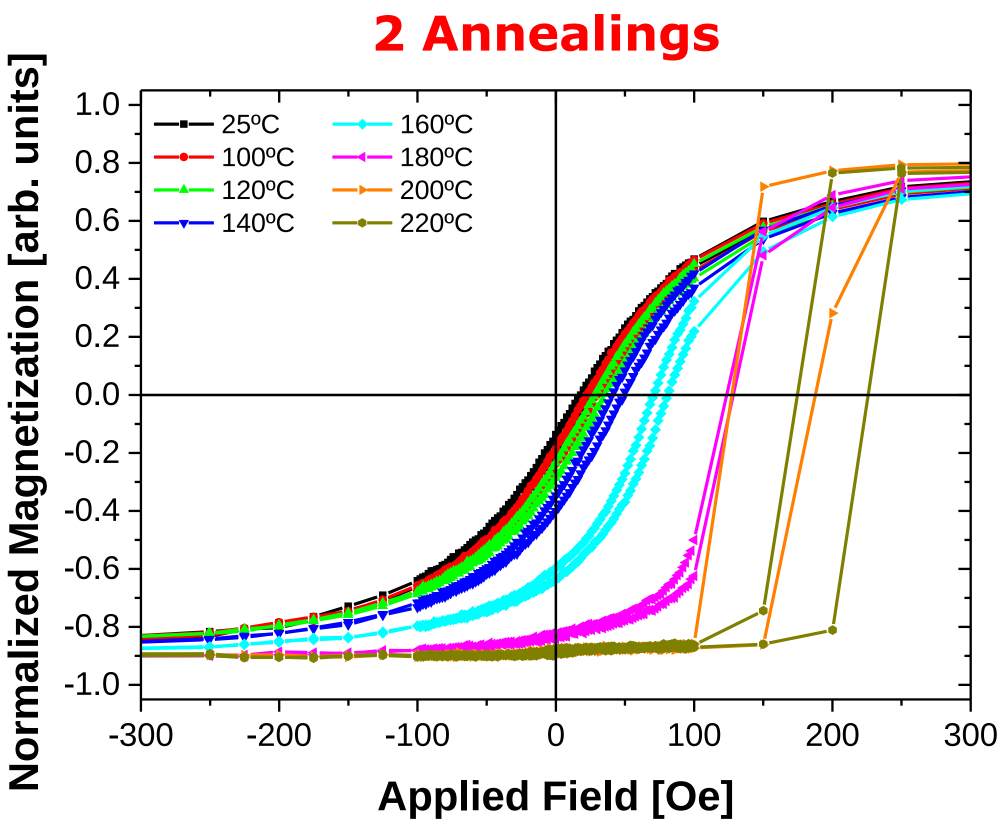

	3 Annealings	2 Annealings
STABLE UP TO:	160ºC	140ºC
LINEAR UP TO:	220ºC	180ºC

2-step vs 3-step annealing process

Transfer curves

	3 Annealings	**2 Annealings**
t_{NiFe}	4 nm	8 nm
t_{Ru}	0.2 nm	0 nm

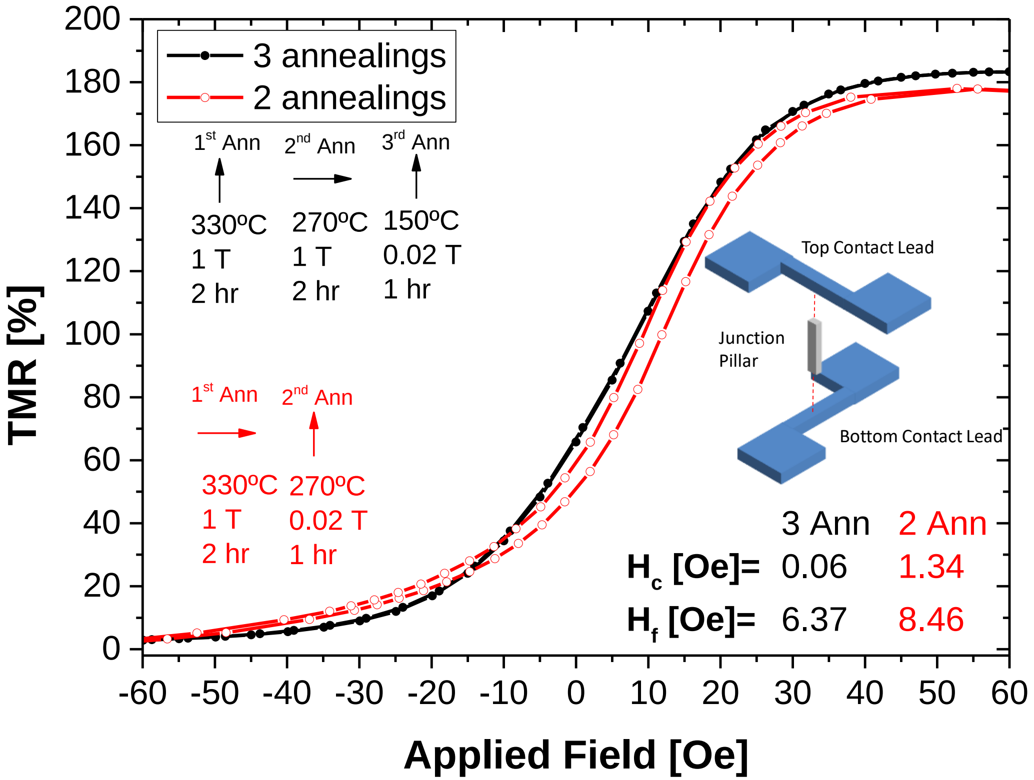

Good linear response from micron to nano devices

Journal of Applied Physics, 115, 17E501 (2014)
Nanotechnology, 27, 045510 (2016)

Part V
Noise

MTJ stack

Description

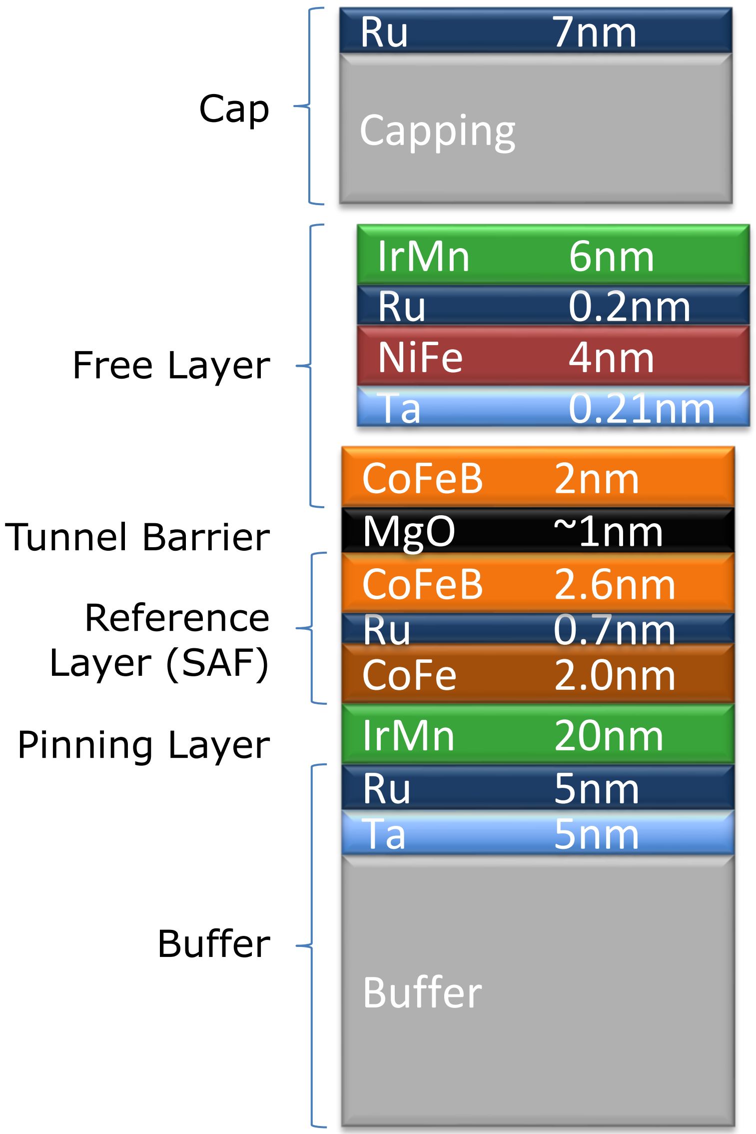

3-annealing process, linearization of bulk sample

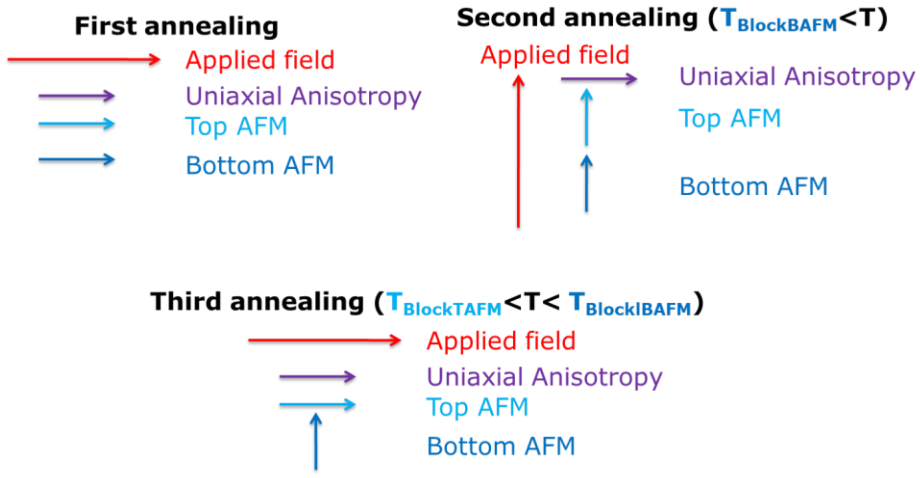

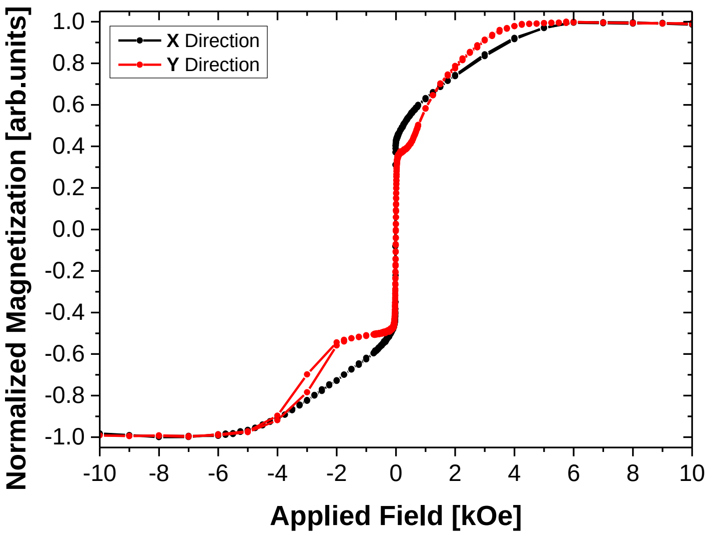

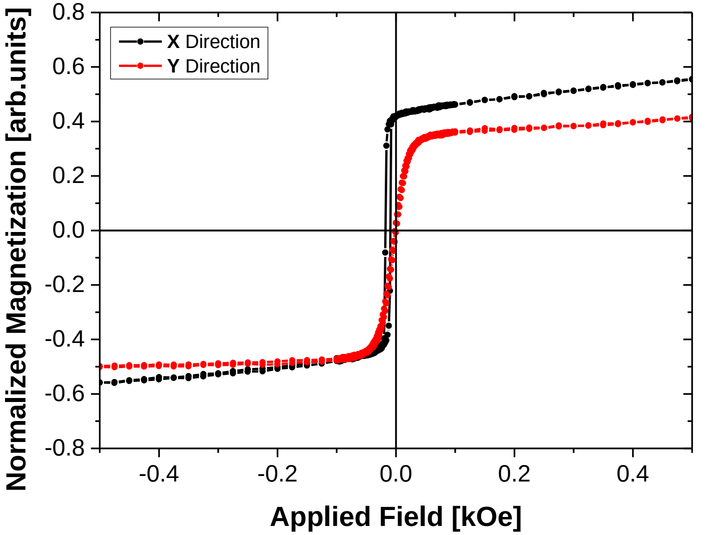

Gauss Probe

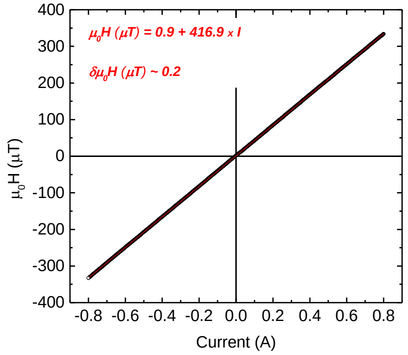

MTJ Series

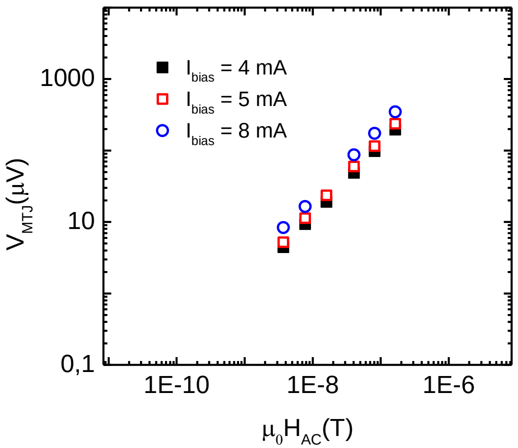

Gauss Probe *vs* MTJ Series

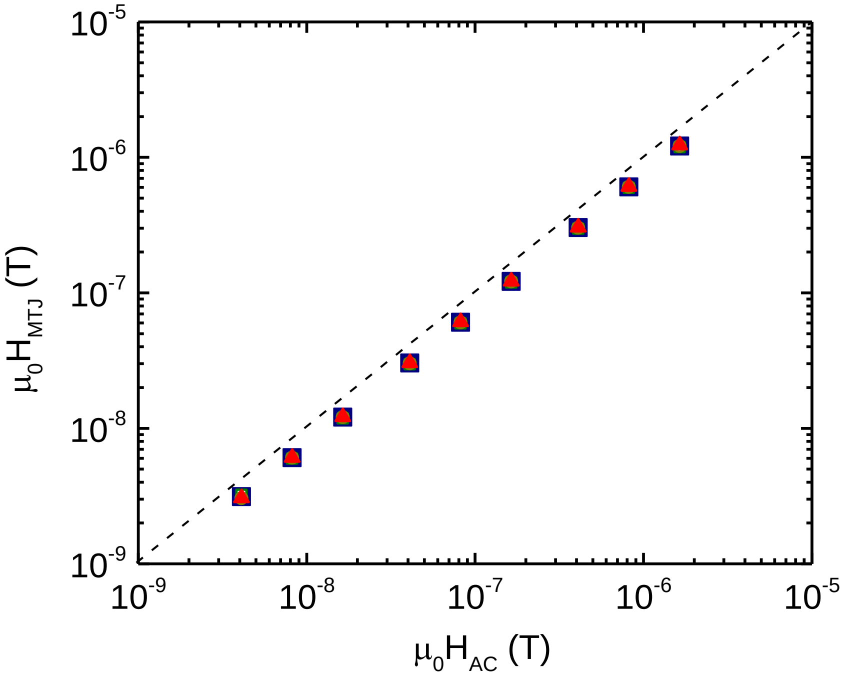

Difference between magnetic field measured by the gauss probe and by the series is of the order of 25%, due to:

- Uniformity of the field
- The positioning and area of the MTJ series is not exactly the same as that of the gauss probe

TMR = 170%

$RxA \sim 30\ k\Omega \cdot \mu m^2$

The TMR dependence with bias voltage is negligible up to V_{bias} = 50 V (I_{bias} = 10 mA)

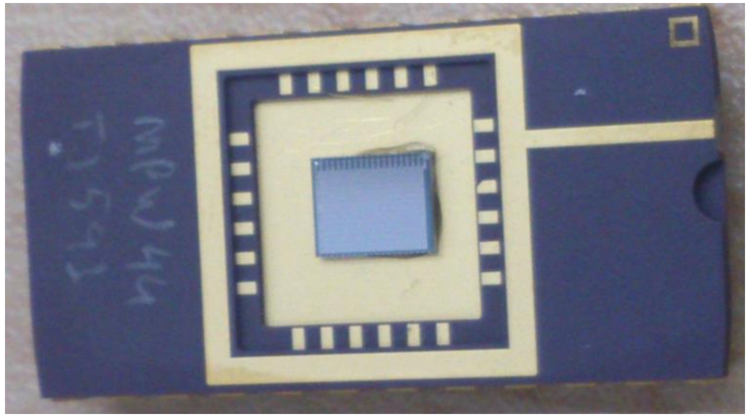

Linear response of the sensing layer with respect to the external magnetic field

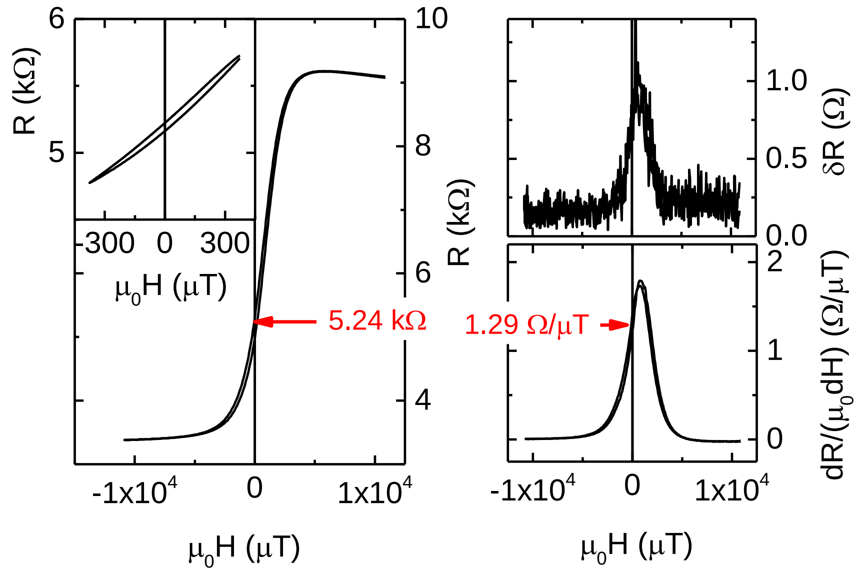

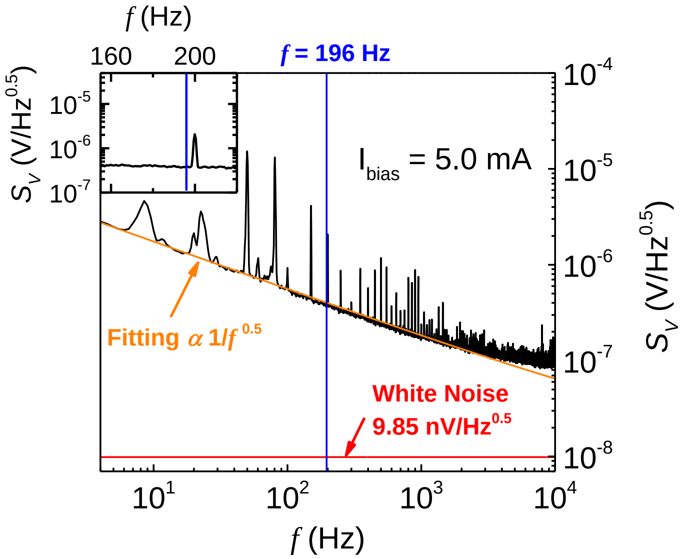

$$S_V^2(f) = \frac{2eIR^2}{N} coth\left(\frac{eV_{bias}}{2Nk_BT}\right) + \frac{\propto V_{bias}^2}{NA}\frac{1}{f}$$

$\alpha(H=0)=8.32 \cdot 10^{-7}\ \mu m^2$

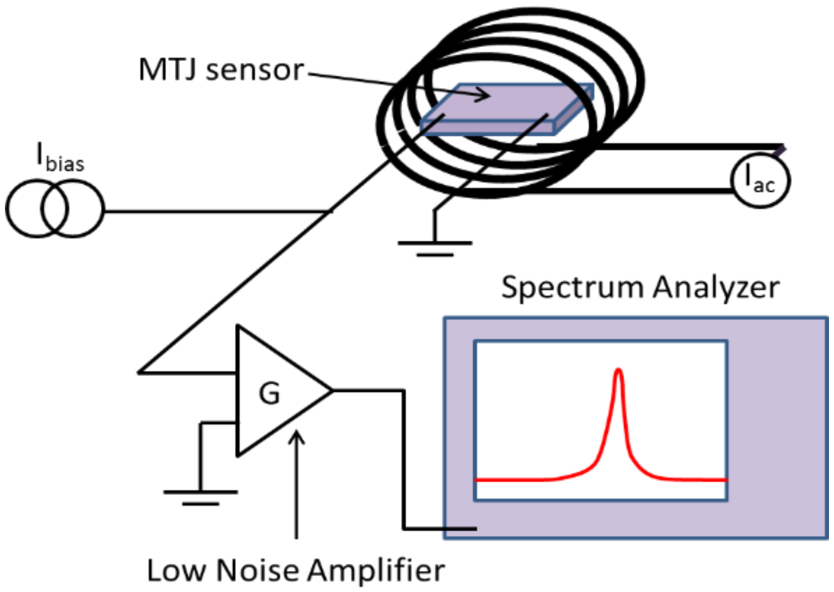

- An AC magnetic field induces an AC magnetic excitation ➡ R_{ac}
- DC bias current (I_{bias}) through the MTJ to measure the AC V_{out} :

$$\mathbf{V_{out}\ (\mathit{f}\ ,\ H) = R_{ac} \cdot I_{bias}}$$

- Reference measurement is acquired without AC field applied
- Electrical noise from the circuit is substracted

- The Spectrum analyzer input must be protected from the large sensor V_{bias}
- AC Coupling, only AC components of the sensor output reach the spectrum analyzer
- No amplification: G = 1

MTJ after process

Noise measurements

- Zero static fields (H_{DC}=0)
- 0.1 mA < I_{bias} < 10 mA
- AC magnetic field at a frequency of 196 Hz
- 4.1 nT < m_0H_{AC} < 1.6 µT

Dependence of the minimum detectable field on I_{bias}:

- I_{bias}<4 mA the noise is dominated by the noise of the acquisition system
- I_{bias}>4 mA the noise of the system becomes dominated by the MTJ series *1/f* noise

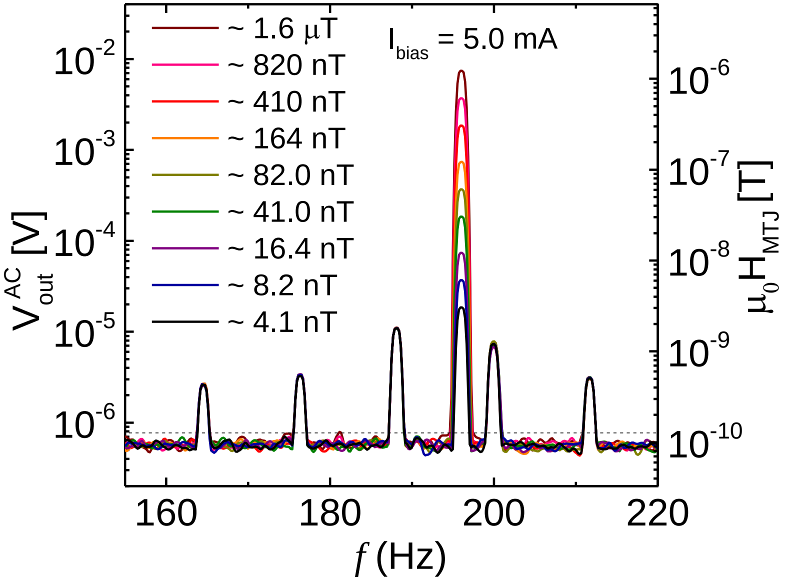

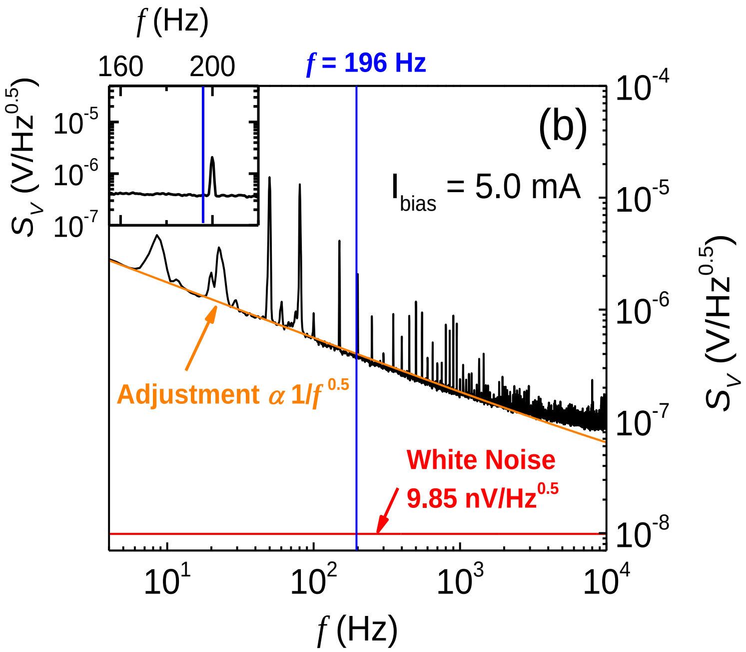

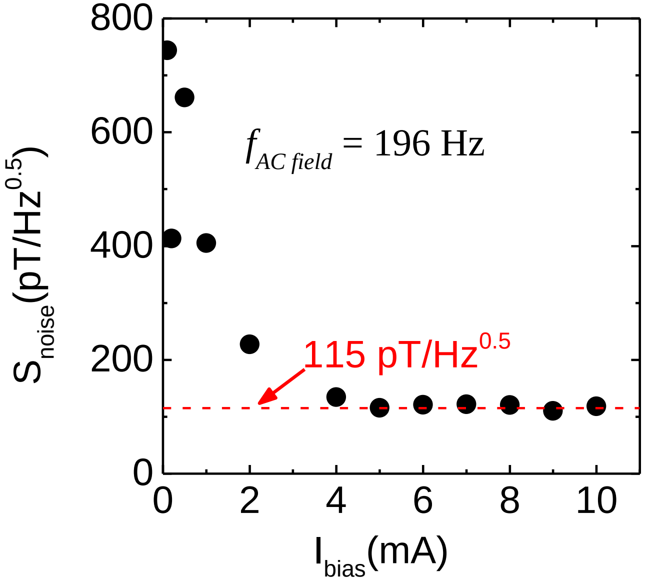

Thank you for listening!